Mammalian Esterase Activity: Implications for Peptide Prodrugs

Yana D. Petri,[†] Ruben Verresen,[‡,§] Clair S. Gutierrez,[†] Volga Kojasoy,[†] Erika Zhang,[†] Nile S. Abularrage,[†] Evans C. Wralstad,[†] Kaya R. Weiser,[#] and Ronald T. Raines*[,†,⊥]
[†]Department of Chemistry, [‡]Department of Physics, and [#]Department of Chemical Engineering, Massachusetts Institute of Technology, Cambridge, Massachusetts 02139, United States
[§]Department of Physics, Harvard University, Cambridge, Massachusetts 02138, United States
[⊥]Broad Institute of MIT and Harvard, Cambridge, Massachusetts 02142, United States

*E-mail: rtraines@mit.edu

Content	Page

I. General Information

Abbreviations

CES	carboxylesterase
CI	confidence interval
Dabcyl	4-(dimethylaminoazo)benzene-4-carboxylic acid
DCM	dichloromethane
DIC	*N*,*N*′-diisopropylcarbodiimide
DIPEA	*N*,*N*-diisopropylethylamine
DMF	dimethylformamide
DODT	2,2-(ethylenedioxy)diethanethiol
Edans	5-((2-aminoethyl)amino)naphthalene-1-sulfonic acid
ESI	electrospray ionization
Fmoc	fluorenylmethoxycarbonyl
FRET	Förster resonance energy transfer
HATU	hexafluorophosphate azabenzotriazole tetramethyl uronium
HEPES	2-[4-(2-hydroxyethyl)piperazin-1-yl]ethanesulfonic acid
HMBC	heteronuclear multiple bond correlation
HRMS	high resolution mass spectroscopy
HSQC	heteronuclear single quantum coherence
LC-MS	liquid chromatography-mass spectrometry
MALDI-TOF	matrix-assisted laser desorption ionization time-of-flight
MES	2-(*N*-morpholino)ethanesulfonic acid
MS	mass spectroscopy
o/n	overnight
Oxyma	ethyl cyano(hydroxyimino)acetate
Pbf	2,2,4,6,7-pentamethyldihydrobenzofuran-5-sulfonyl
PBS	phosphate-buffered saline
PCR	polymerase chain reaction
PLE	pig liver esterase
Q-TOF	quadrupole time-of-flight
RFU	relative fluorescence unit
rt	room temperature
SD	standard deviation
SIP	substrate → product → intermediate
SPPS	solid-phase peptide synthesis
PTFE	polytetrafluoroethylene
TFA	trifluoreoacetic acid
THF	tetrahydrofuran
TLC	thin-layer chromatography
TMS–Cl	trimethylsilyl chloride
UV	ultraviolet

Conditions

All procedures were performed at ambient temperature (~22 °C) and pressure (1.0 atm) unless indicated otherwise.

Solvent Removal

The phrase "concentrated under reduced pressure" refers to the removal of solvents and other volatile materials with a rotary evaporator at water-aspirator pressure of <20 Torr and a water bath at <25 °C. Residual solvents were removed from compounds by vacuum (<0.1 Torr) achieved by using a mechanical belt-drive oil pump.

Synthesis and Purification of Diazo Compounds

Pd(0)-mediated cross-coupling reactions were performed under positive pressure of N_2(g) using standard Schlenk-line techniques. All other reactions were performed under ambient atmosphere. Reactions carried out at low temperature were cooled in a Dewar vessel (water-ice bath at 0 °C), and reactions performed above rt were heated on the IKA RCT basic plate. All reactions were magnetically stirred and monitored by analytical thin-layer chromatography (TLC). Organic solutions were concentrated in vacuo using a Buchi rotary evaporator (model R-210). Purification of all diazo compounds was performed with flash column chromatography with Silicycle 40−63 Å silica (230−400 mesh). *All diazo compounds were purified by a hand column to avoid exposure to UV light from UV detectors.*

Microplate Reader Assays

Note that, since low μM concentrations of peptides were employed in the assay, the use of low-binding Eppendorf tubes, low-binding plates, and buffered solutions containing solubilizing detergent Triton X-100 were crucial to ensure reproducibility and adequate sample fluorescence.

Safety

Caution Although we have not encountered problems, diazo compounds are potentially explosive upon exposure to heat, light, pressure, and shock. They should be stored at ≤0 °C in the dark. *N*-Succinimidyl 2-diazoacetate (**S1**) is an exception, as it has been reported to be bench-stable and can be isolated in gram amounts as a crystalline solid.[1] α-Aryl-α-diazoesters structurally similar to **S1** have been shown to have T_{onset}, which reports on thermostability, ranging from 80 °C (*p*-OMe) to 130 °C (*p*-NO_2), depending on the aryl substituents.[2] Our synthetic routes (see "Chemical Synthesis of Small Molecules") do not require any heat and are done on a small scale (<200 mg). Still, a blast shield should be placed around reaction vessels containing large amounts of potentially dangerous material.

Caution Iodomethyl isopropyl carbonate, chloromethyl cyclobutanecarboxylate, and iodomethyl cyclobutanecarboxylate have structural resemblance to chloromethyl methyl ether (commonly referred to as MOM chloride), which is a known human carcinogen classified as an extremely hazardous substance by the Environmental Protection Agency. In this light, the three above-mentioned compounds could also be carcinogenic. Care must be taken to avoid exposure by wearing appropriate personal protective equipment, double gloving, and always working in a well-ventilated hood (including while weighing out these compounds and concentrating them under reduced pressure).

Chemical Reagents and Supplies

Reagents and solvents were from Sigma-Aldrich (Milwaukee, WI) and were used without further purification unless indicated otherwise. Water was obtained from a Milli-Q IQ 7000 purification system from MilliporeSigma (Burlington, MA) and had a resistivity of 18.2×10^6 Ω cm. Iodomethyl isopropyl carbonate was from AmBeed (Arlington Heights, IL). Chloromethyl cyclobutanecarboxylate was from Enamine (Kyiv, Ukraine). Reagent-grade solvents (DCM, THF, and Et_3N) were dried over a column of alumina and removed from a dry still under an inert atmosphere. Anhydrous EtOAc was from ACROS Organics (Geel, Belgium). $CDCl_3$ was from Cambridge Isotope Laboratories (Tewksbury, MA). TLC was performed with EMD 250 μm silica gel 60 F254 plates. DIC and 4-methylpiperidine were from Oakwood Chemical (Tampa, FL). Rink Amide ProTide Resin (LL) (0.2 mmol/g), Cl-TCP(Cl) ProTide Resin (0.45 mmol/g), and Oxyma were from CEM (Matthews, NC). Fmoc-L-Glu(Edans)-OH (CAS: 193475-66-0) was from AmBeed. Fmoc-D-Arg(Pbf)-OH (CAS: 187618-60-6) was from Aapptec (Louisville, KY). Fmoc-L-Lys(Dabcyl)-OH was from Aapptec.

Protein Accession Codes

The accession codes listed here are from UniProtKB. CES1: P23141; CES2: O00748; Glu-C: Q6GI34; PLE: Q29550.

Proteins, Intestinal Fraction, and Supplies

Lyophilized bacteria-derived V8 protease Glu-C (product number: IBCTV8LY, 1 mg) was from Innovative Research (Novi, Michigan). Low protein binding microcentrifuge tubes (product number: 90410) from Thermo Scientific (Waltham, MA) or 0.2 mL polymerase chain reaction (PCR) snapsrtip II 8-strip tubes with flat cap, clear (product number: 490003-706) from GeneMate were used in manipulations with purified peptides. 96-well, half area, black, flat bottom polystyrene nonbinding surface microplates (product number: 3993) from Corning (Corning, NY) were used in fluorescence assays. Thermomixer F1.5 from Eppendorf (Hamburg, Germany) equilibrated to 37 °C was used to shake (300 rpm) peptide solutions during prolonged incubations with Glu-C or hydrolysis assays. Lyophilized PLE (product number: 46058-10MG-F, ≥50 U/mg) with lot number BCCJ5320 (lot activity result: 62.6 U/mg) was from Sigma–Aldrich (St. Louis, MO). Lyophilized human (HEK293, C-His) recombinant CES1 (product number: 30105-H08H) with specific activity >10,000 pmol/min/μg was from Sino Biological (Wayne, PA). Lyophilized human (HEK293, C-His) recombinant CES2 (product number: HY-P76192) with specific activity >20000 pmols/min/μg was from MedChemExpress (South Brunswick Township, NJ). Suspension of human intestine S9 fraction (4 mg protein/mL), phenylmethylsulfonyl fluoride-free, mixed gender, pool of 4, was from XenoTech (Kansas City, KS).

Error Analysis

In brief, one standard deviation, (SD, ~68% confidence interval) was used to depict error bars in plotted datasets. Experimentally determined constants were reported with error corresponding to

95% confidence interval. See “Statistical Analysis: Computing Errors” for details on error propagation and error analysis.

II. Instrumentation

NMR Spectroscopy

^{1}H and ^{13}C NMR spectra were acquired with Bruker Avance Neo 400 MHz or 500 MHz spectrometers at the Department of Chemistry Instrumentation Facility (DCIF) at MIT. Proton chemical shifts are reported in parts per million (ppm, δ scale) and are relative to residual protons in the deuterated solvent ($CDCl_3$: δ 7.26; CD_3CN: δ 1.94). Carbon chemical shifts are reported in parts per million (ppm, δ scale) and are relative to the carbon resonance of the solvent ($CDCl_3$: δ 77.16; CD_3CN: δ 118.26). Multiplicities are abbreviated as: s (singlet), br (broad), d (doublet), t (triplet), q (quartet), p (pentet), sept (septet), and m (multiplet). ^{13}C signal from the diazo carbon (C=N=N) is low in 1D spectra, possibly due to a T1 relaxation effect.[3] The chemical shift of diazo carbon is generally in the 55–65 ppm range.[3] 2D HMBC and HSQC experiments were used to validate the ppm shifts of diazo carbons.

Automated Peptide Synthesizer and HPLC

Automated solid-phase peptide synthesis was performed with a Liberty Blue™ Automated Microwave Peptide Synthesizer from CEM. Purification was carried out using a 1260 Infinity II Preparative LC System from Agilent Technologies. All unesterified peptides were purified on a prep XSelect Peptide CSH C18 OBD column (pore size 130 Å, 5 µm particle size, 19 mm × 250 mm of inner diameter × length) from Waters (Milford, MA). All esterified peptides were purified on a semi-prep XSelect Peptide CSH C18 OBD column (pore size 130 Å, 5 µm particle size, 10 mm × 150 mm of inner diameter × length) from Waters. The purity of peptides was accessed on an analytical XSelect CSH C18 column (pore size 130 Å, 5 µm particle size, 4.6 mm × 100 mm of inner diameter × length) from Waters. Various gradients with solvent A (95:5:0.1 water/MeCN/TFA) and solvent B (95:5:0.1 MeCN/water/TFA) were applied for purification and purity analysis.

Intact Mass Spectroscopy (MS) for Compound Characterization

For compound characterization purposes, intact high resolution mass spectroscopy (HRMS) of small molecules and peptides was performed with a 6545 quadrupole time-of-flight (Q-TOF) mass spectrometer in ESI mode coupled to an Infinity 1260 liquid chromatography (LC) system from Agilent Technologies (Santa Clara, CA). Pooled chromatography fractions of purified peptides were also analyzed by matrix-assisted laser desorption ionization time-of-flight (MALDI-TOF) MS with a microflex LRF instrument from Bruker (Billerica, MA) on α-cyano-4-hydroxycinnamic acid matrix.

Absorbance-Based Concentration Measurements

Concentrations of synthesized peptide stocks (see respective experimental sections for detailed procedures) were typically determined using Beer–Lambert law and absorbance values measured on DS-11 UV–vis spectrophotometer from DeNovix (Wilmington, DE). See "Preparation of Stock Solutions of Glu-C and Peptides" for more details. Specifically, concentrations of **Std** stocks were

calculated using the reported extinction coefficient of Edans ($\varepsilon_{336\ nm}$ = 5438 M^{-1} cm^{-1}),[4] and the concentrations of **Opt**, **Opt**-Et, **Opt**–**1**, **Opt**–**2**, and **Opt**–**3** stocks were calculated using the reported extinction coefficient of Dabcyl ($\varepsilon_{472\ nm}$ = 15,100 M^{-1} cm^{-1}).[4] Concentrations of PLE stocks were also determined using Beer–Lambert law and absorbance values measured on DS-11 UV–vis spectrophotometer. Note that PLE was handled on ice until use in the assay. The extinction coefficient of PLE ($\varepsilon_{280\ nm}$ = 87,000 M^{-1} cm^{-1}) used in concentration calculations was found with the Expasy ProtParam online tool[5] and the amino acid sequence of EST1_PIG (accession code: Q29550) available in UniProt.

LC-MS Analysis (336 nm and 472 nm) of Peptide Transformations

For reaction monitoring purposes (*e.g.,* analysis of Glu-C cleavage products or ester hydrolysis products), intact masses of compounds were accessed with a Q-TOF 6530C mass spectrometer in ESI positive mode, equipped with a Poroshell 120 EC-C18 column (pore size 120 Å, 2.7-µm particle size, 150 mm × 3.0 mm of length × inner diameter) from Agilent Technologies. Before analysis on the Q-TOF 6530C, samples were diluted (see respective experimental sections for clarification) and passed through Advantage polytetrafluoroethylene (PTFE) MicroSpin Centrifuge Filters with Polypropylene Housing, Pore size 0.2 µm from Analytical Sales and Services (Flanders, New Jersey). Absorbance was monitored with a 1290 Infinity II diode array detector (DAD) FS (G7117A) from Agilent Technologies. Edans absorbance was monitored at 336 nm[4] and Dabcyl absorbance was monitored at 472 nm,[4] with the reference wavelength set to 0. The following gradient with solvent C (100:0.1 water/formic acid) and solvent D (100:0.1 MeCN/formic acid) was applied for elution: 20% v/v D in C for 0–2 min (sent to waste), 20–80% v/v D in C for 2–17 min, and 95% v/v D in C for 17–19 min.

LC-MS Analysis (210 nm) of Esterification Progress

The progress of esterification reactions was monitored at 210 nm (peptide backbone absorbance) by looking at the changes in the ratio between areas of peaks that correspond to the unesterified starting material and esterified product. LC-MS traces of the peptides were acquired on an LCT ESI 1260 Infinity II instrument from Agilent Technologies equipped with a Poroshell 120 SB C18-reversed-phase column (pore size 120 Å, 2.7-µm particle size, 50 mm × 2.1 mm of length × internal diameter) instrument from Agilent Technologies. A gradient of 10–95% of solvent D in C for 0–10 min was applied for elution. Sample volumes of 3–4 µL were injected into the sample loop. Prior to analysis, samples were dissolved in 50:50 water/MeCN and filtered through 0.2-µm PTFE filters.

Fluorescence Measurements with Microplate Reader

Fluorescence measurements were made with the Spark multimode microplate reader from Tecan (Männedorf, Switzerland). The plate reader was pre-equilibrated to 37 °C before plate insertion (measurements were made at 37 °C). The plate was shaken for 15 s before the first fluorescence measurement was recorded. Readings were made from the top of the plate at λ_{ex} = 340 nm (bandwidth, 20 nm) and λ_{em} = 490 nm (bandwidth, 20 nm) of Edans (using the reported λ_{ex} and

λ_{em})[4,6] typically every 20 s for continuous measurements. Gain was calculated from 90% of maximal fluorescence intensity of 10-μM **Std** sample in 10 mM HEPES–NaOH buffer, pH 7.4, containing 0.1% w/v Triton X-100 (not 0.8% w/v) and set to 63. The volume of sample pipetted into each well was 100 μL. The *z*-position based on this volume was set to 18547 μm. Fluorescence intensities are reported in relative fluorescence units (RFUs). The settle time was set to 50 ms, the lag time to 0 μs, the integration time to 40 μs, and the number of flashes to 30. The mirror was set to "automatic" (50% mirror).

III. Computational Modeling of Glu-C in Complex with a Peptide Substrate

Structure of the Model Glu-C Substrate

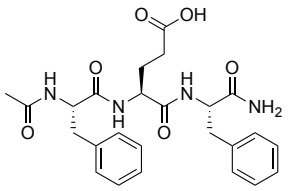

Computational Methods

To gain insights into the binding mode of Glu-C and a peptide substrate of the sequence Ac-Phe-Glu-Phe-NH_2 (deprotonated at the Glu residue) bound to the active site, we performed molecular docking studies using Autodock Vina.[7] The conformation of the Glu-C substrate was optimized by using density functional theory (DFT) at the M06-2X/6-31+g(d,p) level of theory[8,9] with Gaussian 16.[10] The optimized structure was then subjected to molecular docking into the active site of Glu-C (PDB entry 1qy6[11]), which was kept rigid during docking.

Atomic Coordinates of the Glu-C Substrate

C	3.11804000	−2.93112800	−1.35101700
C	3.75627900	−3.42688100	−2.63232100
H	3.89620700	−4.50580800	−2.55591500
H	3.17122500	−3.19117500	−3.52396400
H	4.74251300	−2.96178800	−2.71866300
O	3.48414600	−3.32617900	−0.25410400
N	2.13540200	−2.00225300	−1.50894800
H	1.82046100	−1.71596800	−2.42695500
C	1.48587400	−1.36712000	−0.38382700
H	1.57305700	−2.04246100	0.47319000
C	2.12260300	0.00281200	−0.05519400
H	1.98698600	0.64642300	−0.93163000
H	1.56509200	0.45852100	0.77058500
C	3.58167900	−0.10813800	0.29376700
C	4.56457600	0.04293600	−0.68734700
C	3.97938000	−0.40854000	1.59956700
C	5.91467300	−0.11540100	−0.37588700
H	4.26463300	0.28475200	−1.70460400
C	5.32492700	−0.56689000	1.91673200
H	3.22129300	−0.52614500	2.37106100
C	6.29812100	−0.42343700	0.92753000
H	6.66621200	0.00260000	−1.15125100
H	5.61542900	−0.80903000	2.93457000
H	7.34809300	−0.55124900	1.17241100

C	0.03525700	−1.10509800	−0.77215900
O	−0.21417700	−0.65535000	−1.89590700
N	−0.90106700	−1.31201400	0.16606100
H	−0.63877900	−1.74614500	1.04147800
C	−2.33822800	−1.11934800	−0.07539600
H	−2.50115700	−1.32507900	−1.14094700
C	−2.69065300	0.35733100	0.16880300
O	−3.46349000	0.73426700	1.04350800
N	−2.06489900	1.23320500	−0.65967900
H	−1.46498500	0.86505400	−1.39479100
C	−2.22710200	2.66790900	−0.51179800
H	−2.58262700	2.83522800	0.51058900
C	−3.34666000	3.17110600	−1.43706100
O	−3.15295400	3.95827300	−2.35095700
N	−4.56059200	2.65599100	−1.12507400
H	−5.34084400	2.85198800	−1.73273100
H	−4.66221700	1.98052400	−0.37519300
C	−0.91251000	3.39451200	−0.74388600
H	−0.53804200	3.15238700	−1.74597200
H	−1.11816000	4.47065900	−0.76225500
C	0.15514500	3.09946300	0.29281000
C	1.48278100	3.44856000	0.01274800
C	−0.12652600	2.53045900	1.54014000
C	2.49592400	3.25591100	0.94790500
H	1.72174200	3.87381800	−0.95979700
C	0.88474100	2.34914000	2.48673400
H	−1.13495900	2.21099200	1.78854100
C	2.19778200	2.71160100	2.19747900
H	3.52020800	3.51711000	0.69886800
H	0.63966200	1.90880300	3.44889900
H	2.98681100	2.55262700	2.92604200
C	−3.16138400	−2.07651000	0.77408100
H	−2.73941500	−3.08357200	0.69073600
H	−3.09265700	−1.78280200	1.82850000
C	−4.62489000	−2.15605800	0.35620500
H	−5.16795500	−1.24265800	0.61379300
H	−4.69971300	−2.27983200	−0.73409600
C	−5.37487100	−3.37519100	0.99621900
O	−4.64949600	−4.22996600	1.55754300
O	−6.61524900	−3.35407800	0.84666800

IV. Chemical Synthesis of Small Molecules

IV-1. Synthesis of *N*-Succinimidyl 2-Diazoacetate (S1)

Scheme S1. Synthetic Route to Compound S1

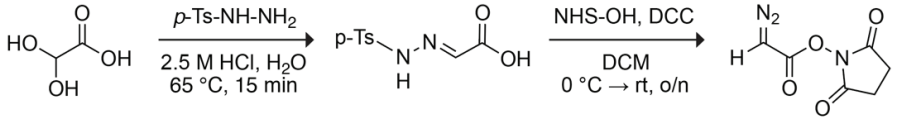

S1

***N*-Succinimidyl 2-diazoacetate** (**S1**). Compound **S1** was synthesized by following a reported synthetic route[3] (see also Wulff and coworkers[12] and Badet and coworkers[1]). **^{1}H NMR** (400 MHz, $CDCl_3$, δ): 5.11 (s, 1H), 2.85 (s, 4H). Note: The ^{1}H NMR spectrum of compound **S1** matched with that reported in the literature.[3]

IV-2. Synthesis of Diazo Compound 1

Scheme S2. Synthetic Route to Compound 1

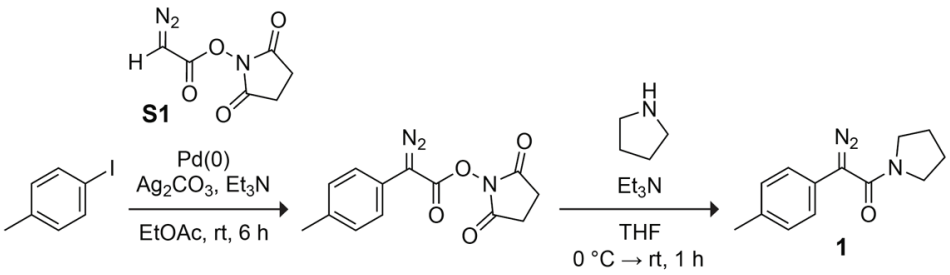

2-Diazo-1-(pyrrolidin-1-yl)-2-(*p*-tolyl)ethan-1-one (**1**). Diazo compound **1** was synthesized by following a reported synthetic route (the scale was kept to <200 mg).[3] **^{1}H NMR** (500 MHz, CD_3CN, δ): 7.23–7.19 (m, 4H), 3.41–3.31 (m, 4H), 2.32 (s, 3H), 1.88–1.83 (m, 4 H). Note: The ^{1}H NMR spectrum of diazo compound **1** matched with that reported in the literature.[3]

IV-3. Synthesis of Diazo Compound 2

Scheme S3. Synthetic Route to Compound 2

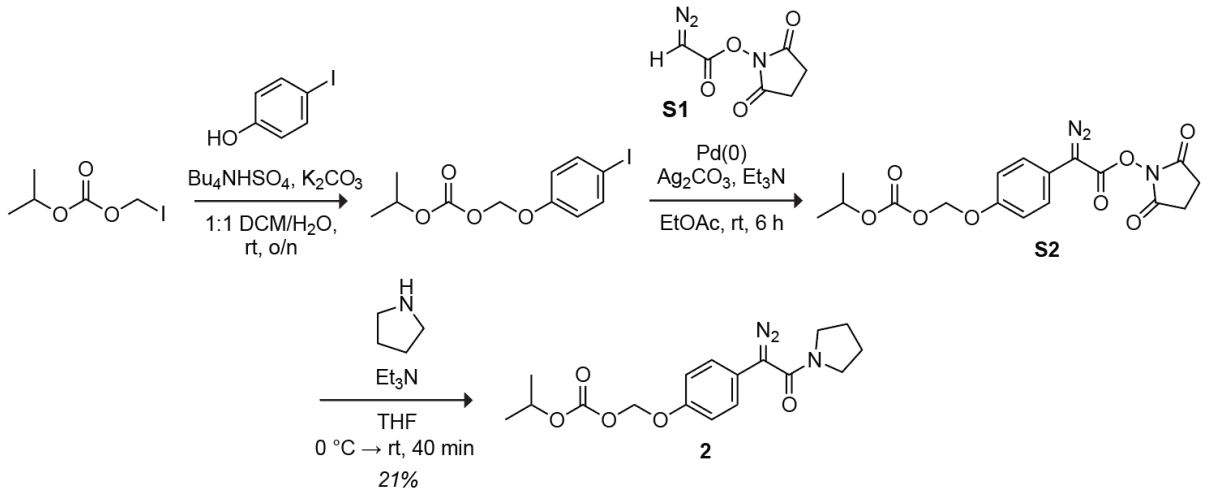

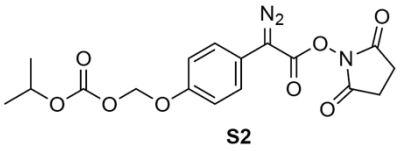

2,5-Dioxopyrrolidin-1-yl 2-diazo-2-(4-(((isopropoxycarbonyl)oxy)methoxy)phenyl)acetate (**S2**). Compound **S2** was synthesized by following a reported synthetic route[13] except iodomethyl isopropyl carbonate was purchased from AmBeed instead of being synthesized in-house. **^{1}H NMR** (400 MHz, CD_3CN, δ): 7.45 (d, J = 8.9 Hz, 2H), 7.13 (d, J = 8.9 Hz, 2H), 5.75 (s, 2H), 4.86 (sept, J = 6.3 Hz, 1 H), 2.81 (s, 4H), 1.25 (d, J = 6.3 Hz, 6H). The ^{1}H NMR spectrum of compound **S2** matched with that reported in the literature.[13]

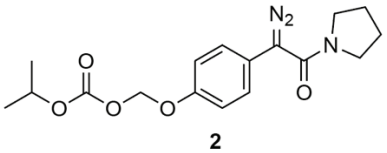

(4-(1-Diazo-2-oxo-2-(pyrrolidin-1-yl)ethyl)phenoxy)methyl isopropyl carbonate (**2**). The synthesis of diazo compound **2** was adapted from previously reported conditions.[3] Compound **S2** (105 mg, 0.268 mmol, 1.0 equiv) was added to a 20-mL vial charged with a magnetic stir bar and dissolved in 3.9 mL of THF. A solution of Et_3N (112 µL, 0.805 mmol, 3.0 equiv) in THF (388 µL) was added to the reaction and cooled to 0 °C in an ice bath. A solution containing pyrrolidine (67.2 µL, 0.805 mmol, 3.0 equiv) and Et_3N (112 µL, 0.805 mmol, 3.0 equiv) in THF (820 µL) was then added dropwise to the vial with compound **S2** on ice. The reaction mixture was stirred at 0 °C for 30 min and then allowed to warm to rt for another 10 min. The progress of the reaction was

monitored by TLC, and product formation was indicated by the color of solution changing from yellow to darker orange. The reaction mixture was filtered through a 0.2-µm PTFE filter to remove precipitated NHS-OH, concentrated under reduced pressure, and purified by silica gel chromatography (33% v/v EtOAc in hexanes) by hand to afford diazo compound **2** (19.9 mg, 21% yield) as an orange solid. **^{1}H NMR** (500 MHz, CD_3CN, δ): 7.30 (d, J = 8.9 Hz, 2H), 7.08 (d, J = 8.9 Hz, 2 H), 5.73 (s, 2H), 4.86 (sept, J = 6.3 Hz, 1H), 3.37–3.34 (m, 4H), 1.87–1.84 (m, 4H), 1.26 (d, J = 6.3 Hz, 6 H). **^{13}C NMR** (500 MHz, CD_3CN, δ): 164.0, 155.6, 154.4, 127.6, 123.0, 117.8, 89.1, 73.5, 62.5 (diazo carbon), 48.4, 25.9, 21.8. **HRMS** (ESI–TOF): Calc'd for $C_{17}H_{21}N_3O_5Na$ $[M + Na]^+$, 370.1379; found, 370.1382. For hydrogen and carbon assignments (including the ppm shift of diazo carbon), see heteronuclear multiple bond correlation (HMBC) and heteronuclear single quantum coherence (HSQC) NMR in "NMR Spectra".

IV-4. Synthesis of Diazo Compound 3

Scheme S4. Synthetic Route to Compound 3

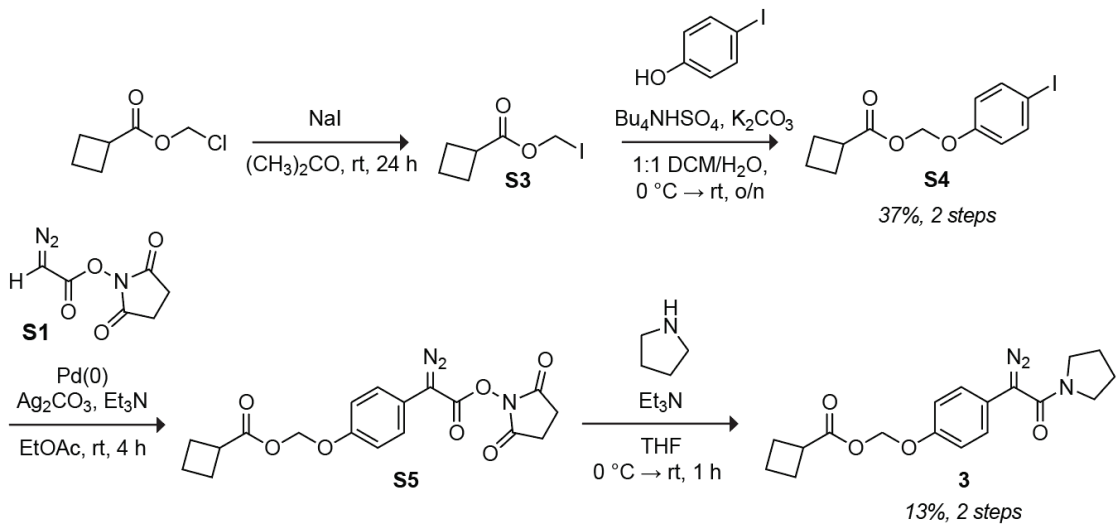

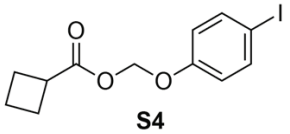

S4

(4-Iodophenoxy)methyl cyclobutanecarboxylate (**S4**). Chloromethyl cyclobutanecarboxylate (250 mg, 1.68 mmol, 1.0 equiv) was added to a 20-mL vial charged with a magnetic stir bar and dissolved in 2 mL of $(CH_3)_2CO$. In the dark, solid NaI (252 mg, 1.68 mmol, 1.0 equiv) was then added. The vial was Teflon-taped to prevent acetone evaporation and covered with aluminum foil to protect the reaction from light. The reaction mixture was stirred for 24 h at rt and then filtered through a 0.2-µm PTFE filter to remove precipitated NaCl. The resultant solution was concentrated

under reduced pressure to a brown oil (**S3**) and used in the next step, adapted from previously reported conditions,[13] without further purification in an assumed 100% yield. Compound **S3** (1.68 mmol, 1.0 equiv) was dissolved in 3.25 mL of DCM. In a separate flask charged with a stir bar was added 4-iodophenol (370 mg, 1.68 mmol, 1.0 equiv) and K_2CO_3 (696 mg, 5.05 mmol, 3.0 equiv) followed by H_2O (6.5 mL). To this mixture was added Bu_4NHSO_4 (571 mg, 1.68 mmol, 1.0 equiv) in DCM (3.25 mL) and the reagents were stirred for ~10 min until the solution was homogeneous. The mixture was than cooled on ice and the solution of **S3** was added dropwise. After 25 min of stirring on ice, the reaction was brought to rt and left overnight. The reaction was extracted with DCM (×3), the organic layer was dried with Na_2SO_4(s), and the solution was concentrated under reduced pressure. The resultant oil was triturated with Et_2O (50 mL, ×3) to crash out Bu_4NI and filtered. The filtrate was concentrated under reduced pressure and purified by silica gel chromatography (0.5% v/v acetone in hexanes) by hand to afford compound **S4** (207 mg, 37% yield over two steps) as a clear oil that spontaneously turned into a white solid upon prolonged drying under vacuum. **^{1}H NMR** (400 MHz, $CDCl_3$, δ): 7.58 (d, J = 8.9 Hz, 2H), 6.80 (d, J = 8.8 Hz, 2H), 5.73 (s, 2H), 3.17 (p, J = 8.5 Hz, 1H), 2.33–2.16 (m, 4 H), 2.04–1.85 (m, 2H). **^{13}C NMR** (500 MHz, $CDCl_3$, δ): 174.3, 156.9, 138.6, 118.5, 85.5, 85.4, 38.0, 25.2, 18.5. **HRMS** (**ESI–TOF**): Calc'd for $C_{12}H_{13}IO_3Na$ $[M + Na]^+$, 354.9807; found, 354.9794. For hydrogen and carbon assignments, see HMBC and HSQC NMR spectra in "NMR Spectra".

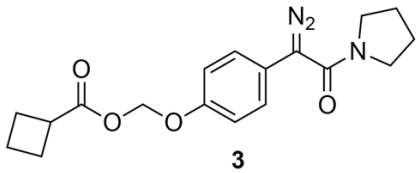

3

(4-(1-Diazo-2-oxo-2-(pyrrolidin-1-yl)ethyl)phenoxy)methyl cyclobutanecarboxylate (**3**). Compound **3** was synthesized by adapting a reported synthetic route.[13] Compound **S1** (70 mg, 0.382 mmol, 1.0 equiv), tri(furan-2-yl)phosphine (17.8 mg, 0.076 mmol, 20 mol %), and Ag_2CO_3 (53 mg, 0.191 mmol, 0.50 equiv) were added to a 20-mL vial charged with a magnetic stir bar. The vial was evacuated and backfilled with N_2(g) (×3). The following solutions were then added to the vial in rapid secession: (1) solution of **S4** (185 mg, 0.558 mmol, 1.46 equiv) in EtOAc (5.8 mL), (2) solution of Et_3N (73 µL, 0.573 mmol, 1.5 equiv) in EtOAc (0.43 mL), and (3) solution of $Pd(OAc)_2$ (8.6 mg, 0.038 mmol, 10 mol %) in EtOAc (1.4 mL). All three solutions were also evacuated and backfilled with N_2(g) (×3) prior to addition. The reaction mixture was stirred at rt for 4 h under N_2(g). The progress of the reaction was monitored by TLC. The reaction mixture was filtered through a Celite pad using a fitted syringe and washed with EtOAc. The filtrate was concentrated under reduced pressure and purified by silica gel chromatography (22% v/v EtOAc in hexanes) by hand to yield compound **S5** (76 mg, 51% yield over one step) as a yellow solid. **HRMS** (**ESI–TOF**): Calc'd for $C_{18}H_{17}N_3O_7Na$ $[M + Na]^+$, 410.0964; found, 410.0948. TLC analysis of purified compound **S5** indicated that it was relatively pure. **S5** (76 mg, 0.195 mmol, 1.0 equiv) was added to a 20-mL vial charged with a magnetic stir bar and dissolved in 2.9 mL of THF. Et_3N (82 µL, 0.586 mmol, 3.0 equiv) was added to the reaction and cooled to 0 °C in an ice

bath. A solution containing pyrrolidine (49 µL, 0.586 mmol, 3.0 equiv) and Et_3N (82 µL, 0.586 mmol, 3.0 equiv) in THF (450 µL) was then added dropwise to the vial with **S2** on ice. The reaction mixture was stirred at 0 °C for 30 min and then allowed to warm to rt for another 30 min. The progress of the reaction was monitored by TLC, and product formation was indicated by the color of solution changing from yellow to darker orange. The reaction mixture was filtered through a 0.2-µm PTFE filter to remove precipitated NHS-OH, concentrated under reduced pressure, and purified by silica gel chromatography (33% v/v EtOAc in hexanes) by hand to afford diazo compound **3** (17.6 mg, 26% yield over one step) as an orange solid. The yield of **3** over two steps was 13%. **^{1}H NMR** (500 MHz, CD_3CN, δ): 7.29 (d, J = 8.9 Hz, 2H), 7.07 (d, J = 8.9 Hz, 2H), 5.74 (s, 2H), 3.37–3.34 (m, 4H), 3.19 (p, J = 9.1 Hz, 1H), 2.24–2.16 (m, 4H), 2.01–1.95 (m, 1H), 1.88–1.82 (m, 5H). **^{13}C NMR** (500 MHz, CD_3CN, δ): 175.0, 164.0, 155.8, 127.6, 122.7, 117.8, 86.4, 62.5 (diazo carbon), 48.4, 38.6, 25.9, 25.7, 18.9. **HRMS** (**ESI–TOF**): Calc'd for $C_{18}H_{21}N_3O_4Na$ $[M + Na]^+$, 366.1430; found, 366.1423. For hydrogen and carbon assignments (including the ppm shift of diazo carbon), see HMBC and HSQC NMR spectra in "NMR Spectra".

V. Chemical Synthesis of Peptides

V-1. Synthesis of Optimal Glu-C Substrate (Opt)

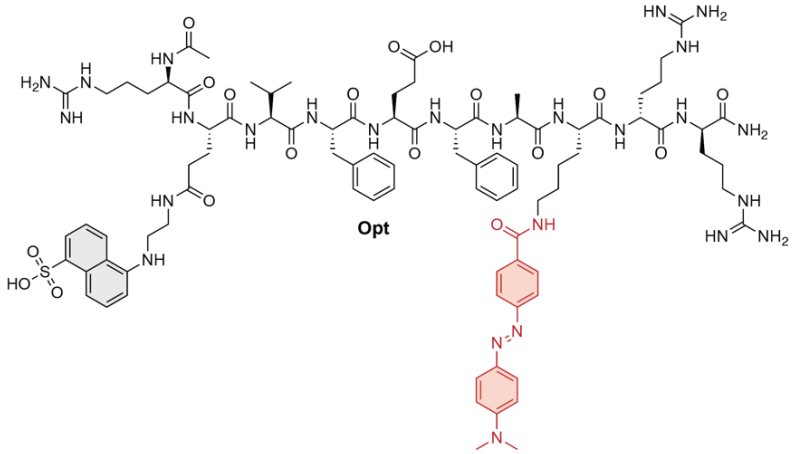

A linear peptide of the sequence H_2N-D-Arg(Pbf)-L-Glu(Edans)-L-Val-L-Phe-L-Glu(O*t*Bu)-L-Phe-L-Ala-L-Lys(Dabcyl)-D-Arg(Pbf)-D-Arg(Pbf) was extended from Rink Amide ProTide Resin (LL) (0.1 mmol, 0.2 mmol/g, 1.0 equiv) with a CEM Liberty Blue™ Automated Microwave Peptide Synthesizer. Solutions of Oxyma (1 M in DMF), DIC (0.5 M in DMF), and Fmoc-protected amino acids (0.2 M in DMF) were employed in the coupling cycles, and a solution of 4-methylpiperidine (20% v/v in DMF) was employed in the deprotection cycles. All amino acids were double coupled except for Fmoc-L-Glu(Edans)-OH, which was single coupled. Fmoc-D-Arg(Pbf)-OH was coupled at 75 °C, Fmoc-L-Glu(Edans)-OH and Fmoc-L-Lys(Dabcyl)-OH were coupled at 50 °C for 10 min, and the rest of the amino acids were coupled at 90 °C under microwave irradiation. Standard CEM methods were followed in all the coupling, wash, and deprotection cycles. After the automated solid-phase peptide synthesis (SPPS), the derivatized resin was transferred to a 12-mL polypropylene syringe equipped with a filter frit. Peptide acetylation, deprotection, and cleavage from resin were performed by hand. To a separate glass vial was sequentially added DMF (2 mL), HATU (4.75 equiv, 0.475 mmol, 181 mg, 0.19 M), glacial acetic acid (5 equiv, 0.5 mmol, 29 µL, 0.2 M), and DIPEA (10 equiv, 1.0 mmol, 174 µL). This solution was pre-incubated at rt for 5 min and then added into the syringe containing the resin. The mixture was agitated for 1 h 20 min at rt. Note that we did not use the other common peptide acetylation conditions—10% acetic anhydride in DMF—in our final synthetic route because we found that these conditions yield a doubly-acetylated peptide (one acetyl group on the N terminus and one likely on the secondary amine of Edans). After the indicated time, the resin was drained, extensively washed with DMF (×3), DCM (×3), DMF (×3), and DCM (×3), and drained again. The peptide with optimal sequence (**Opt**) was deprotected and cleaved from resin for 140 min at rt in 5 mL of cleavage cocktail (90:5:3:2 TFA/thioanisole/DODT/anisole). The resin was drained, washed with additional 5 mL of the cleavage cocktail to collect any remaining peptide, and drained again. The flowthroughs were combined and evaporated under a stream of N_2(g). **Opt** was precipitated in 45 mL of cold diethyl ether. The resultant solid was dissolved in a 1:1 MeCN/water and lyophilized to remove volatile

impurities. **Opt** was purified using reversed-phase HPLC (25–35% v/v solvent B in solvent A for 21 min) to afford an orange-red solid in the form of a TFA salt (42.2 mg based on weighing, 19% yield assuming MW of [M + 3TFA] = 2220.3 Da). Note that **Opt** was protected from light to avoid photobleaching of its Edans moiety. **HRMS** (**ESI**–**TOF**): Calc'd for $C_{89}H_{128}N_{26}O_{18}$ $[M + 4H]^{4+}$, 470.2400; found, 470.2412. For purity analysis of **Opt**, see Figure S1. **Purity analysis:** The peak containing product mass in the HPLC-UV trace in Figure S1 was quantified as 96% pure via integration.

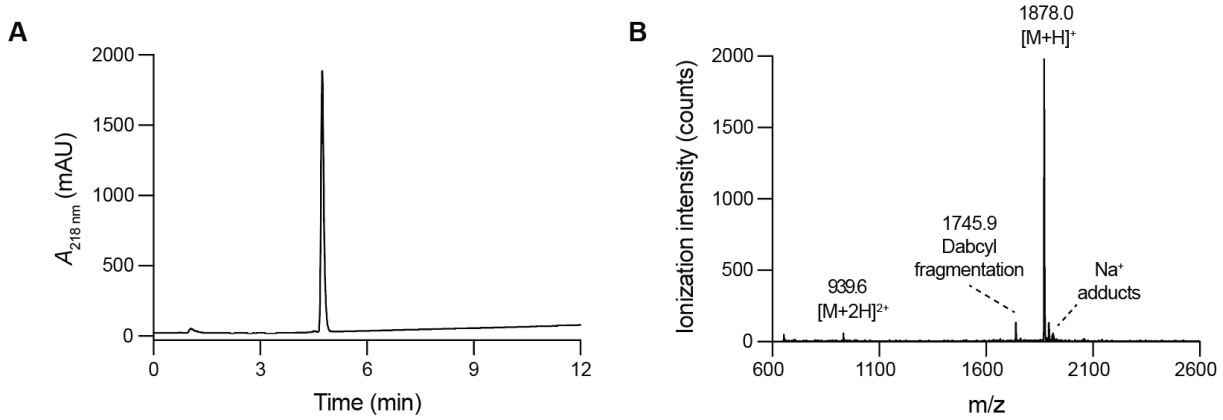

Figure S1. (A) HPLC-UV trace of **Opt**. A gradient of 25% v/v solvent B in solvent A for 2 min, and 25−95% v/v solvent B in solvent A for 2–12 min was used. (B) MALDI-TOF mass spectrum of **Opt**. Calc'd for $C_{89}H_{125}N_{26}O_{18}$ $[M + H]^+$, 1877.9; found, 1878.0. Calc'd for $C_{89}H_{126}N_{26}O_{18}$ $[M + 2H]^{2+}$, 939.5; found, 939.6. Peaks of higher mass than $[M + H]^+$ correspond to Na^+ adducts. Peak with a mass of 1745.9 Da (Δ = −132.1 Da from the observed mass of $[M + H]^+$) corresponds to artifactual, ionization-induced fragmentation at Dabcyl that was documented previously.[14]

V-2. Synthesis of Fluorescent Standard (Std)

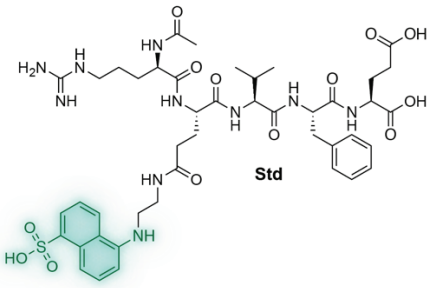

A linear peptide of the sequence H_2N-D-Arg(Pbf)-L-Glu(Edans)-L-Val-L-Phe-L-Glu(O*t*Bu)-OH was extended from Cl-TCP(Cl) ProTide Resin (LL) (0.05 mmol, 0.45 mmol/g, 1.0 equiv) with a CEM Liberty Blue™ Automated Microwave Peptide Synthesizer. The resin was automatically pre-loaded with Fmoc-Glu(O*t*Bu)-OH using the standard chloride loading CEM cycle. The loading was mediated by a solution of KI (120 mM) in DMF containing DIPEA (15.6% v/v). Solutions of Oxyma (1 M in DMF), DIC (0.5 M in DMF), and Fmoc-protected amino acids (0.2 M in DMF) were employed in the coupling cycles and a solution of 4-methylpiperidine (20% v/v in DMF) was employed in the deprotection cycles. All amino acids were double coupled except for Fmoc-L-

Glu(Edans)-OH and Fmoc-L-Glu(O*t*Bu)-OH, which were single coupled. Fmoc-D-Arg(Pbf)-OH was coupled at 75 °C, Fmoc-L-Glu(Edans)-OH was coupled at 50 °C for 10 min, and the rest of the amino acids were coupled at 90 °C under microwave irradiation. Standard CEM methods were followed in all the coupling, wash, and deprotection cycles. After the automated SPPS, the derivatized resin was transferred to a 12-mL polypropylene syringe equipped with a filter frit. Peptide acetylation, deprotection, and cleavage from resin were performed by hand. Note that, in general, for reproducible selective acetylation of Glu(Edans)-containing peptides at the N terminus, we recommend using glacial acetic acid and HATU as described in the section on **Opt** synthesis (we found that fresh acetic anhydride can acetylate the secondary amine in Edans). However, in the synthesis of the fluorescent standard (**Std**), we employed 10% acetic anhydride in DMF (10 min incubation at rt) and observed only one acetylation event by MALDI-TOF mass spectrometry. The reaction was likely selective because the acetic anhydride we employed was old and thus we likely overestimated the actual concentration of acetic anhydride in our solution. After 10-min acetylation, the resin was drained, extensively washed with DMF (×3), DCM (×3), DMF (×3), and DCM (×3), and drained again. The **Std** peptide was deprotected and cleaved from resin for 140 min at rt in 5 mL of cleavage cocktail (90:5:3:2 TFA/thioanisole/DODT/anisole). The resin was drained, washed with additional 5 mL of the cleavage cocktail to collect any remaining peptide, and drained again. The flowthroughs were combined and evaporated under a stream of N_2(g). **Std** was precipitated in 45 mL of cold diethyl ether. The resultant solid was dissolved in 1:1 MeCN/water and lyophilized to remove volatile impurities. **Std** was purified using reversed-phase HPLC (13–30% v/v solvent B in solvent A for 40 min) to afford an orange-red solid in the form of a TFA salt (5.1 mg based on weighing, 9.4% yield assuming MW of [M + 3TFA] = 1083.1 Da). Note that **Std** was protected from light to avoid photobleaching of its Edans moiety. **HRMS** (**ESI–TOF**): Calc'd for $C_{44}H_{60}N_{10}O_{13}SNa$ $[M + Na]^+$, 991.3960; found, 991.3966. For purity analysis of **Std**, see Figure S2. **Purity analysis:** The peak containing product mass in the HPLC-UV trace in Figure S2 was quantified as 99% pure via integration.

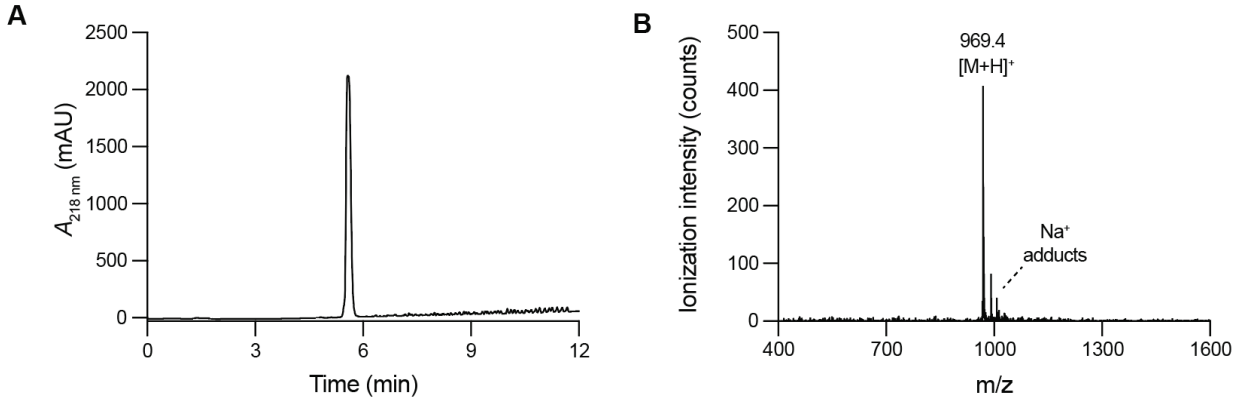

Figure S2. (A) HPLC-UV trace of **Std**. A gradient of 10% v/v solvent B in solvent A for 2 min, and 10−95% v/v solvent B in solvent A for 2–12 min was used. (B) MALDI-TOF mass spectrum of **Std**. Calc'd for $C_{44}H_{61}N_{10}O_{13}S$ $[M + H]^+$, 970.1; found, 969.4. Peaks of higher mass than $[M + H]^+$ correspond to Na adducts.

V-3. Synthesis of Optimal Glu-C Substrate Containing an Ethyl Ester (Opt-Et)

Scheme S5. Synthetic Route to Opt-Et

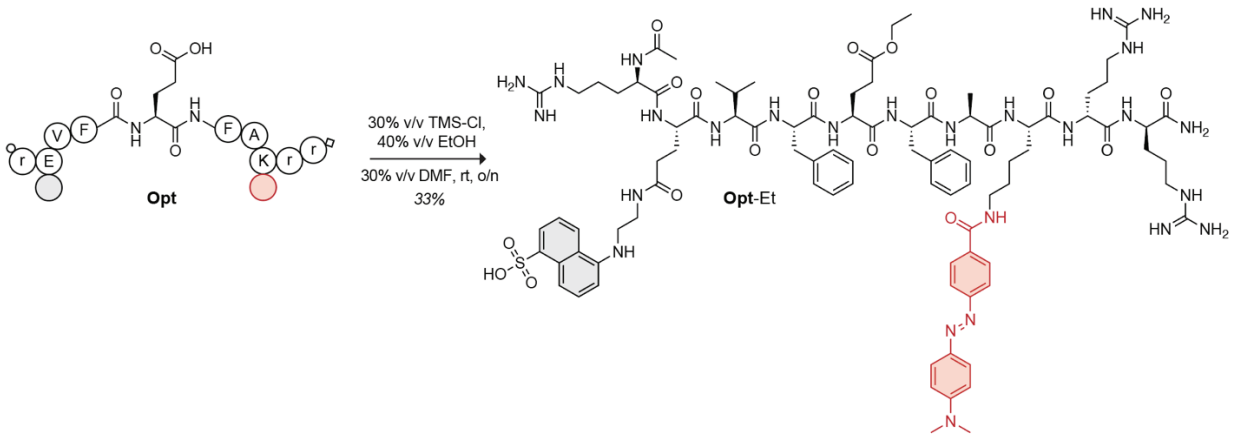

Opt was synthesized using an esterification procedure adapted from procedures reported by Sha and Li,[15] Vite and coworkers,[16] and Fukase and coworkers.[17] **Opt** (3 mg, 0.0016 mmol, 1.0 equiv) was placed into a plastic Eppendorf tube. DMF (30% v/v, 240 µL) was added to the solid. The solution was vortexed and sonicated until **Opt** was fully solubilized. Then, to the solution was added EtOH (40% v/v, 320 µL) followed by trimethylsilyl chloride (30% v/v, 240 µL). The reaction was incubated overnight at rt on a shaker (300 rpm). The progress of the esterification reaction was monitored by LC-MS. After the overnight incubation, the reaction was concentrated under reduced pressure, dissolved in 20 mL of 1:1 solution of MeCN/water, and lyophilized to remove residual volatile impurities and DMF. **Opt**-Et was purified using reversed-phase HPLC (20–90% v/v solvent B in solvent A for 25 min) to afford an orange-red solid in the form of a TFA salt (1.0 mg based on concentration measurements using the method described in "Preparation of Stock Solutions of Glu-C and Peptides", 33% yield assuming MW of [M + 3TFA] = 2248.3 Da). Note that **Opt**-Et was protected from light to avoid photobleaching of the Edans moiety. **HRMS** (**ESI**–**TOF**): Calc'd for $C_{91}H_{132}N_{26}O_{18}S$ $[M + 4H]^{4+}$, 477.2478; found, 477.2492. For purity analysis of **Opt**-Et, see Figure S3. For evidence of the carboxyl group (as opposed to sulfonic acid) being predominantly esterified in purified **Opt**-Et, see "MS Assessment of the Stability of Esterified Peptides in the Presence of Glu-C". **Purity analysis:** The peak containing product mass in the HPLC-UV trace in Figure S3 was quantified as 96% pure via integration.

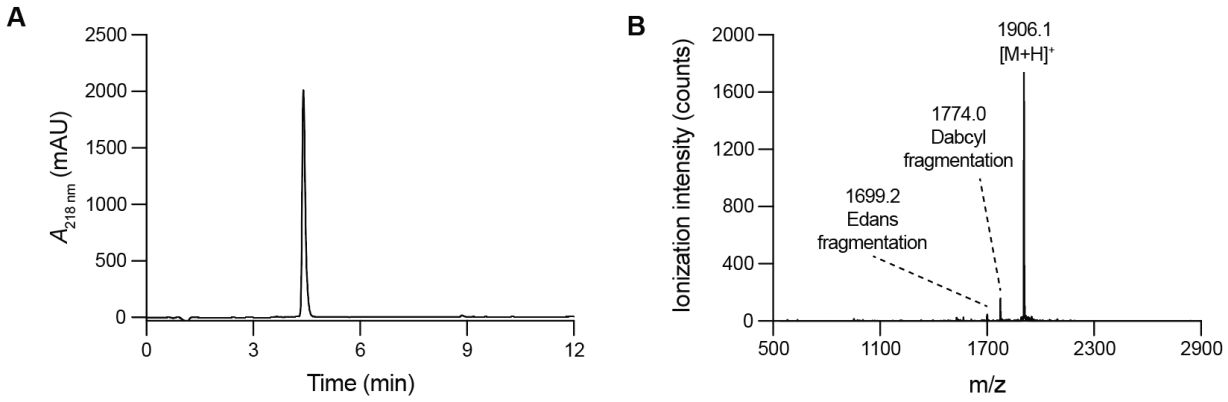

Figure S3. (A) HPLC-UV trace of **Opt**-Et. A gradient of 25% v/v solvent B in solvent A for 2 min, and 25–95% v/v solvent B in solvent A for 2–12 min was used. (B) MALDI-TOF mass spectrum of **Opt**-Et. Calc'd for $C_{91}H_{129}N_{26}O_{18}S$ $[M + H]^+$, 1906.0; found, 1906.1. Peak with a mass of 1774.0 Da ($\Delta = -132.1$ Da from the observed mass of $[M + H]^+$) corresponds to artifactual, ionization-induced Dabcyl. Peak with a mass of 1699.2 Da ($\Delta = -206.9$ Da from the observed mass of $[M + H]^+$) corresponds to fragmentation of Edans. Both instances were previously documented.[14]

V-4. Synthesis of Optimal Glu-C Substrate Esterified with Diazo Compound 1 (Opt–1)

Scheme S6. Synthetic route to Opt–1

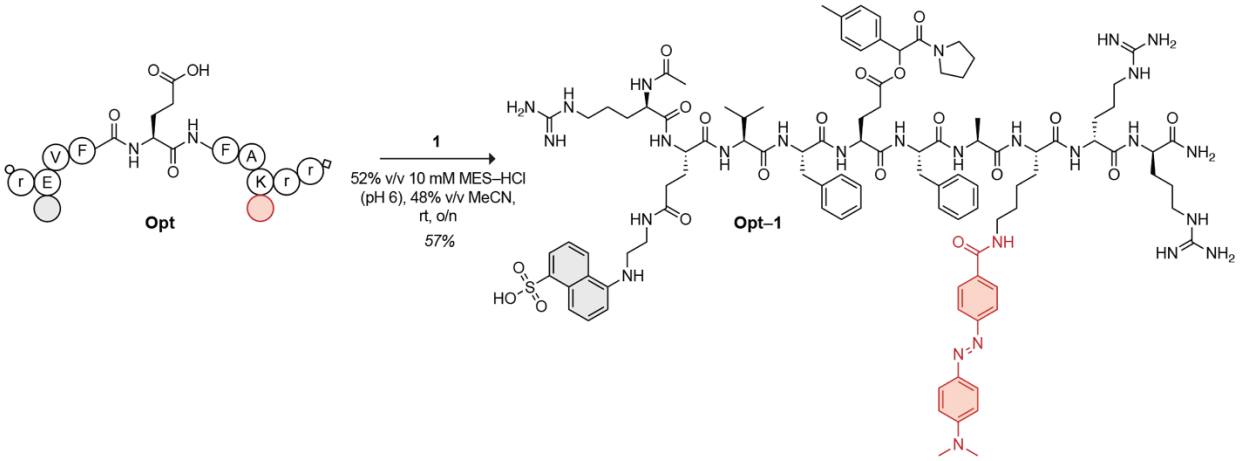

Opt (1.7 mg, 0.000905 mmol, 1.0 equiv) was placed into a plastic Eppendorf tube. MeCN (50 µL) was added to the peptide, followed by 10 mM MES–HCl buffer, pH 6.0 (100 µL). The solution was vortexed and sonicated until **Opt** was fully solubilized. In a separate glass vial, diazo compound **1** (15 mg) was dissolved in 833 µL of MeCN. A 50 µL solution of diazo compound **1** (0.9 mg, 0.00393 mmol, 4.34 equiv) was added to the solution of **Opt**. The reaction was incubated overnight at rt on a shaker (300 rpm). The progress of the esterification reaction was monitored by LC-MS. After the overnight incubation, the reaction was deemed incomplete and another 10 µL of the solution of diazo compound **1** (0.18 mg, 0.00079 mmol, 0.86 equiv) was added to the Eppendorf tube. The reaction was incubated at rt on a shaker (300 rpm) for 1 h. Note that, in addition to detecting the mass of the major expected product, **Opt**–**1**, we detected the mass of a less abundant byproduct that corresponded to doubly esterified **Opt**. This byproduct most likely

corresponded to diazo esterification at both the carboxyl group in the Glu residue and the sulfonic acid in Edans. It has been previously suggested that some diazo compounds, including α-aryl-α-diazoacetamides, preferentially label acids of higher pK_a in aqueous buffers where pH is close to or larger than the pK_a of the target acid.[18,19] Thus, we expected that, under our reaction conditions, diazo compound **1** would label the Glu residue (pK_a 4) faster than the sulfonic acid (the experimentally-determined pK_a of *p*-toluenesulfonic acid in water is −2.8),[20] yielding **Opt**–**1** esterified at the carboxyl group as the major product. **Opt**–**1** was purified using reversed-phase HPLC (20–60% v/v solvent B in solvent A for 35 min) to afford an orange-red solid in the form of a TFA salt (1.1 mg based on concentration measurements using the method described in "Preparation of Stock Solutions of Glu-C and Peptides", 57% yield assuming MW of [M + 3TFA] = 2423.5 Da). Note that **Opt**–**1** was protected from light to avoid photobleaching of its Edans moiety. **HRMS** (**ESI**–**TOF**): Calc'd for $C_{102}H_{143}N_{27}O_{19}S$ $[M + 4H]^{4+}$, 520.7697; found, 520.7707. For purity analysis of **Opt**–**1**, see Figure S4. For evidence of the carboxyl group (as opposed to sulfonic acid) being predominantly esterified in purified **Opt**–**1**, see "MS Assessment of the Stability of Esterified Peptides in the Presence of Glu-C". **Purity analysis:** The peak containing product mass in the HPLC-UV trace in Figure S4 was quantified as 99% pure via integration.

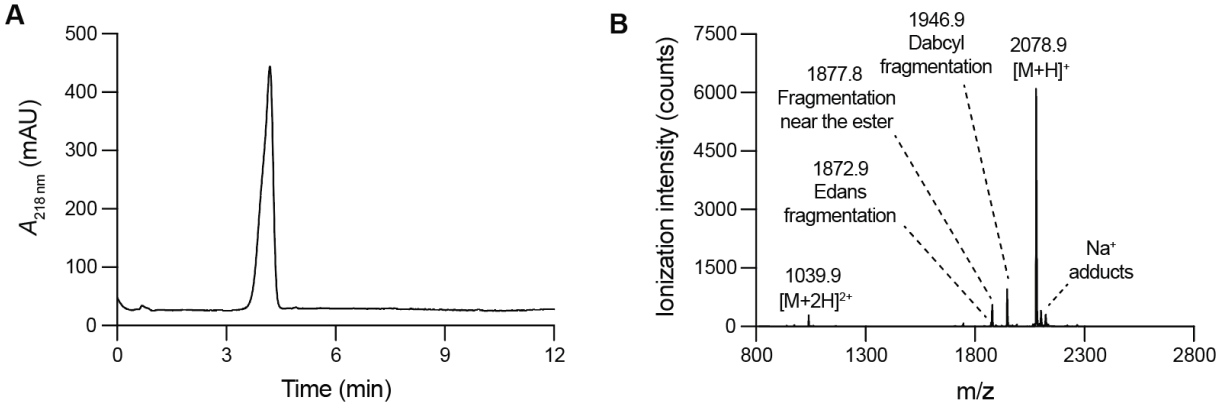

Figure S4. (A) HPLC-UV trace of **Opt**–**1**. A gradient of 25% v/v solvent B in solvent A for 2 min, and 25–95% v/v solvent B in solvent A for 2–12 min was used. (B) MALDI-TOF mass spectrum of **Opt**–**1**. Calc'd for $C_{102}H_{140}N_{27}O_{19}S$ $[M + H]^+$, 2079.1; found, 2078.9. Calc'd for $C_{102}H_{141}N_{27}O_{19}S$ $[M + 2H]^{2+}$, 1040.5; found, 1039.9. Peaks of higher mass than $[M + H]^+$ correspond to Na adducts. Peak with a mass of 1946.9 Da (Δ = −132.0 Da from the observed mass of $[M + H]^+$) corresponds to artifactual, ionization-induced fragmentation of Dabcyl. Peak with a mass of 1872.9 Da (Δ = −206.0 Da from the observed mass of $[M + H]^+$) corresponds to Edans fragmentation. Both instances were previously documented.[14] Peak with a mass of 1877.8 Da (Δ = −201.1 Da from the observed mass of $[M + H]^+$) most likely corresponds to fragmentation (the observed mass of 1877.8 Da is close to the expected mass of **Opt**, which is 1877.9) near the ester bond.

V-5. Synthesis of Optimal Glu-C Substrate Esterified with Diazo Compound 2 (Opt–2)

Scheme S7. Synthetic Route to Opt–2

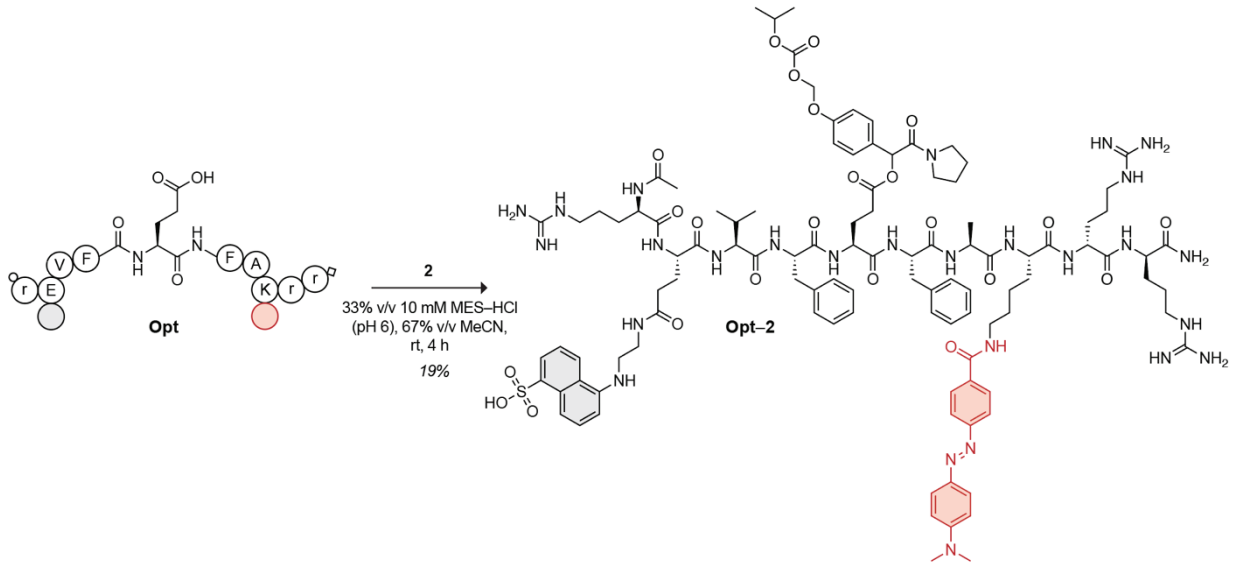

Opt (4.7 mg, 0.0025 mmol, 1.0 equiv) was placed into a plastic Eppendorf tube. MeCN (90 µL) was added to the peptide, followed by 10 mM MES–HCl buffer, pH 6.0 (120 µL). The solution was vortexed and sonicated until **Opt** was fully solubilized. In a separate glass vial, diazo compound **2** (18 mg) was dissolved in 354 µL of MeCN. A solution (36 µL) of diazo compound **2** (1.83 mg, 0.00527 mmol, 2.11 equiv) was added to the solution of **Opt**. The reaction was incubated for 1 h at rt on a shaker (300 rpm). The progress of the esterification reaction was monitored by LC-MS. After all the diazo compound was consumed, another solution (36 µL) of diazo compound **2** (1.83 mg, 0.00527 mmol, 2.11 equiv) was added to the Eppendorf tube. The addition of the solution (36 µL) was repeated two more times. After a total of 8.44 equiv of **2** was added to **Opt**, another solution (15 µL) of diazo compound **2** (0.763 mg, 0.0022 mmol, 0.88 equiv) was spiked into the Eppendorf tube and the reaction was incubated for 30 min at rt. Note that, in addition to detecting the mass of the expected product **Opt**–**2**, we detected the mass of a byproduct that corresponded to double esterification of **Opt**. The identity of this byproduct most likely corresponds to diazo esterification at both the carboxyl group in the Glu residue and the sulfonic acid functional group in Edans. See "Synthesis of Optimal Glu-C Substrate Esterified with **1** (**Opt**–**1**)" for discussion of the implications of this observation. After a total of 4 h of the esterification reaction, **Opt**–**2** was purified using reversed-phase HPLC (28–40% v/v solvent B in solvent A for 40 min) to afford an orange-red solid in the form of a TFA salt (1.2 mg based on concentration measurements described in the "Preparation of Stock Solutions of Glu-C and Peptides", 19% yield assuming MW of [M + 3TFA] = 2539.6 Da). **Opt**–**2** was protected from light to avoid photobleaching of its Edans moiety. **HRMS** (**ESI**–**TOF**): Calc'd for $C_{106}H_{149}N_{27}O_{23}S$ $[M + 4H]^{4+}$, 550.2763; found, 550.2772. For purity analysis of **Opt**–**2**, see Figure S5. For evidence of the carboxyl group (as opposed to sulfonic acid) being predominantly esterified in purified **Opt**–**2**, see "MS Assessment of the Stability of Esterified Peptides in the Presence of Glu-C". **Purity analysis:**

The peak containing product mass in the HPLC-UV trace in Figure S5 was quantified as 91% pure via integration.

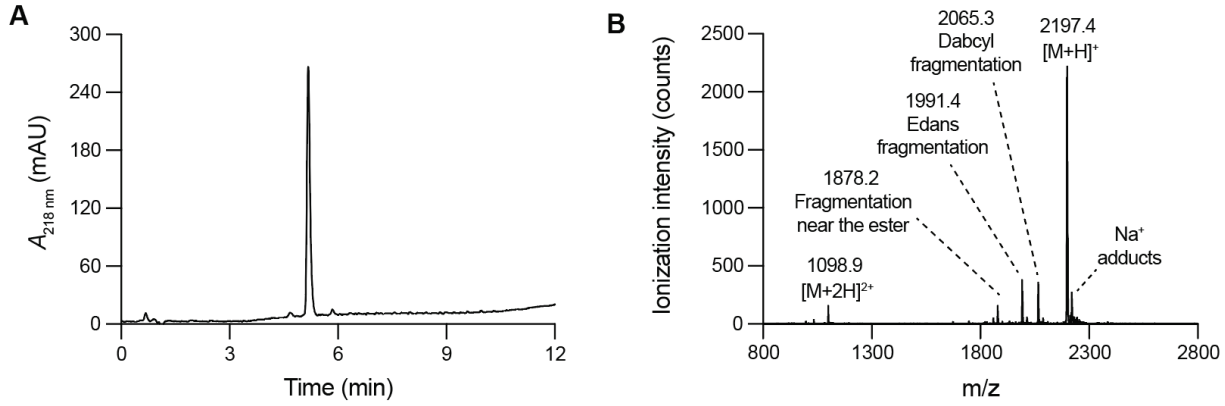

Figure S5. (A) HPLC-UV trace of **Opt**–**2**. A gradient of 25% v/v solvent B in solvent A for 2 min, and 25–95% v/v solvent B in solvent A for 2–12 min was used. (B) MALDI-TOF mass spectrum of **Opt**–**2**. Calc'd for $C_{106}H_{146}N_{27}O_{23}S$ $[M + H]^+$, 2197.1; found, 2197.4. Calc'd for $C_{106}H_{147}N_{27}O_{23}S$ $[M + 2H]^{2+}$, 1099.5; found, 1098.9. Peaks of higher mass than $[M + H]^+$ correspond to Na adducts. Peak with a mass of 2065.3 Da (Δ = −132.1 Da from the observed mass of $[M + H]^+$) corresponds to artifactual, ionization-induced fragmentation at Dabcyl. Peak with a mass of 1991.4 Da (Δ = −206.0 Da from the observed mass of $[M + H]^+$) corresponds to Edans fragmentation. Both instances have been previously documented.[14] Peak with a mass of 1878.2 Da (Δ = −319.2 Da from the observed mass of $[M + H]^+$) most likely corresponds to fragmentation (the observed mass of 1878.2 Da is close to the expected mass of **Opt**, which is 1877.9) near the ester bond.

V-6. Synthesis of Optimal Glu-C Substrate Esterified with Diazo Compound 3 (Opt–3)

Scheme S8. Synthetic Route to Opt–3

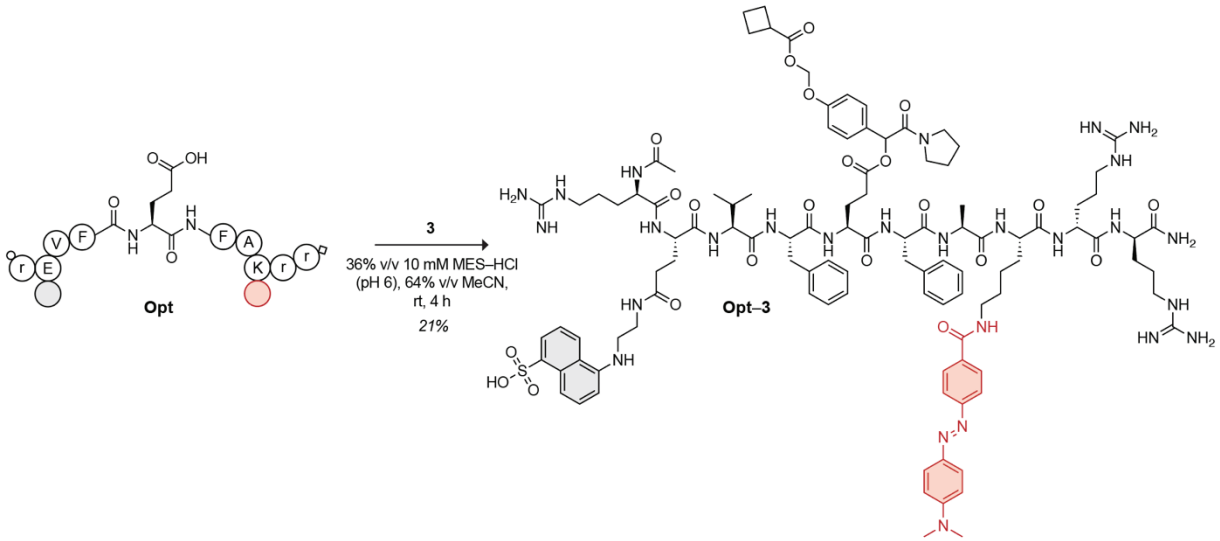

Opt (3.9 mg, 0.00208 mmol, 1.0 equiv) was placed into a plastic Eppendorf tube. MeCN (75 µL) was added to the peptide, followed by 10 mM MES–HCl buffer, pH 6.0 (100 µL). The resulting

solution was vortexed and sonicated until **Opt** was fully solubilized. In a separate glass vial, diazo compound **3** (5 mg) was dissolved in 100 µL of MeCN. A solution (30 µL) of diazo compound **3** (1.5 mg, 0.00437 mmol, 2.1 equiv) was added to the solution of **Opt**. The reaction was incubated for 1 h at rt on a shaker (300 rpm). The progress of the esterification reaction was monitored by LC-MS. After all the diazo compound was consumed, another solution (30 µL) of diazo compound **3** (1.5 mg, 0.00437 mmol, 2.1 equiv) was added to the Eppendorf tube. The addition of the solution (30 µL) was repeated one more time. After a total of 6.3 equiv of diazo compound **3** was added to **Opt**, another solution (10 µL) of **3** (0.5 mg, 0.00146 mmol, 0.702 equiv) was spiked into the Eppendorf tube and the reaction was incubated for 30 min at rt. Note that, in addition to detecting the mass of the expected product **Opt**–**3**, we detected the mass of a byproduct that corresponded to double esterification of **Opt**. The identity of this byproduct most likely corresponds to diazo esterification at both the carboxyl group in the Glu residue and the sulfonic acid functional group in Edans. See "Synthesis of Optimal Glu-C Substrate Esterified with Diazo Compound **1** (**Opt**–**1**)" discussion of the implications of this observation. After a total of 4 h of the esterification reaction, **Opt**–**3** was purified using reversed-phase HPLC (30–50% v/v solvent B in solvent A for 40 min) to afford an orange-red solid in the form of a TFA salt (0.87 mg based on concentration measurements described in "Preparation of Stock Solutions of Glu-C and Peptides", 21% yield assuming MW of [M + 3TFA] = 2539.6 Da). **Opt**–**3** was protected from light to avoid photobleaching of its Edans moiety. **HRMS** (**ESI**–**TOF**): Calc'd for $C_{107}H_{148}N_{27}O_{22}S$ $[M + 3H]^{3+}$, 732.0343; found, 732.0359. For purity analysis of **Opt**–**3**, see Figure S6. For evidence of the carboxyl group (as opposed to sulfonic acid) being predominantly esterified in purified **Opt**–**3**, see "MS Assessment of the Stability of Esterified Peptides in the Presence of Glu-C". **Purity analysis:** The peak containing product mass in the HPLC-UV trace in Figure S6 was quantified as 94% pure via integration.

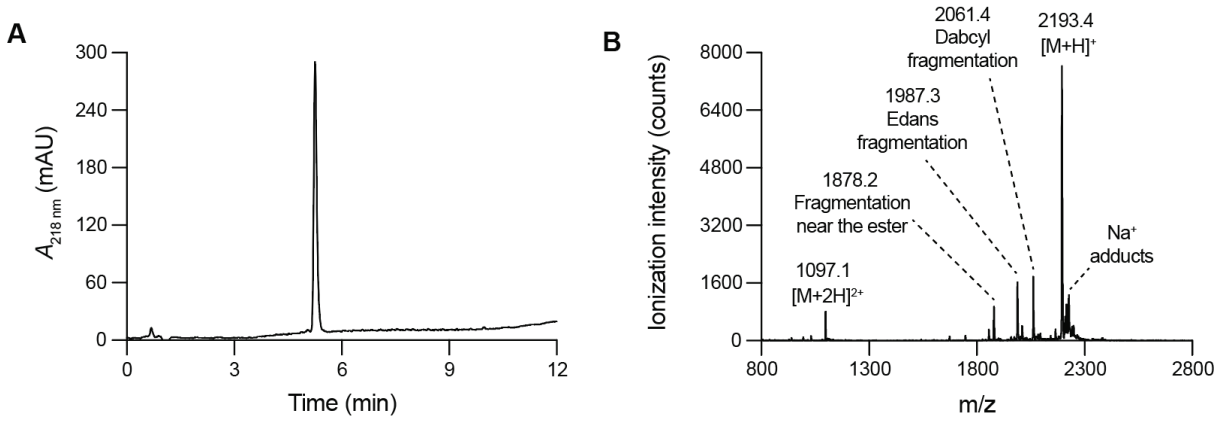

Figure S6. (A) HPLC-UV trace of **Opt**–**3**. A gradient of 25% v/v solvent B in solvent A for 2 min, and 25–95% v/v solvent B in solvent A for 2–12 min was used. (B) MALDI-TOF mass spectrum of **Opt**–**3**. Calc'd for $C_{107}H_{146}N_{27}O_{22}S$ $[M + H]^+$, 2193.1; found, 2193.4. Calc'd for $C_{107}H_{147}N_{27}O_{22}S$ $[M + 2H]^{2+}$, 1097.5; found, 1097.1. Some peaks of higher mass than $[M + H]^+$ correspond to Na adducts. Peak with a mass of 2061.4 Da ($\Delta = -132.0$ Da from the observed mass of $[M + H]^+$) corresponds to artifactual, ionization-induced fragmentation at Dabcyl. Peak with a mass of 1987.3 Da ($\Delta = -206.1$ Da from the observed mass of $[M + H]^+$) corresponds to Edans fragmentation. Both instances have been previously documented.[14] Peak with a mass of 1878.2 Da ($\Delta = -315.2$ Da from the observed mass of $[M + H]^+$) most likely corresponds to fragmentation (the observed mass of 1878.2 Da is close to the expected mass of **Opt**, which is 1877.9) near the ester bond.

VI. Optimization of Glu-C-Based FRET Assay for Carboxylase Activity

VI-1. Preparation of Stock Solutions of Glu-C and Peptides

Glu-C Stock Solution

Lyophilized bacteria-derived V8 protease (endoprotease Glu-C) (1 mg) from Innovative Research was placed on ice and dissolved in 463 µL of ice-cold water, yielding an ~80 µM solution based on the reported molecular weight[21] of 27 kDa. The solution was split into small aliquots, flash frozen with N_2(l), and stored at –80 °C. Before use in assays, the enzyme was rapidly thawed at 37 °C and placed on ice until further handling. The ~80 µM solution of Glu-C was diluted further with water or buffer post-thawing, if required.

Peptide Stock Solution

Stock solutions of **Std**, **Opt**, **Opt**-Et, **Opt**–**1**, **Opt**–**2**, and **Opt**–**3** were prepared in dry DMF using absorbance measurements. First, a 1.5-mM solution of each peptide was prepared in DMF based on weight measurements (for **Std** and **Opt**) or a weight that would be expected from 20% yield (for **Opt**-Et, **Opt**–**1**, **Opt**–**2**, and **Opt**–**3**). Then, 5 µL of the respective stock was added to 146 µL of 10 mM MES–HCl buffer, pH 6.0, containing 0.8% w/v Triton X-100 (n = 2 replicates) in low-binding Eppendorf tubes (3% v/v final DMF concentration). The absorbance of the solutions was recorded using DS-11 UV–vis spectrophotometer (n = 6 measurements per replicate) at 336 or 472 nm. As a blank, 10 mM MES–HCl buffer, pH 6.0, containing DMF (3% v/v) and Triton X-100 (0.8% w/v) was used. In the case of **Std**, the reported extinction coefficient of Edans ($\varepsilon_{336\text{nm}}$ = 5438 M^{-1} cm^{-1})[4] was used to calculate concentrations; in the case of **Opt**, **Opt**-Et, **Opt**–**1**, **Opt**–**2**, and **Opt**–**3**, the reported extinction coefficient of Dabcyl ($\varepsilon_{472\text{ nm}}$ = 15,100 M^{-1} cm^{-1})[4] was employed (because Dabcyl also absorbs at 336 nm, we could not use the extinction coefficient of Edans for determining the concentrations of quenched peptides; Edans, on the other hand, does not absorb at 472 nm; see Figure S8 for experimental confirmation of these points). The obtained concentrations of peptide solutions in the buffer were averaged and used to back-calculate the concentration of peptide stocks in DMF. Note that we found that both 3% v/v DMF and 0.8% w/v Triton X-100 were important to include and keep constant during absorbance measurements to prevent underestimating peptide concentrations. In the absence of detergent and organic solvent, peptides tended to stick to plastic surfaces of Eppendorf tubes.

Note on Discrepancy Between Std Fluorescence and Cleaved Opt Fluorescence

During plate reader assays, we noticed that 10 µM **Std** fluoresces more intensely (~52,700 RFUs) than does 10 µM **Opt** fully cleaved by 250 nM Glu-C (~29,500 RFUs) when both peptides are in 10 mM HEPES-NaOH, pH 7.4, containing 1.5% v/v DMF and 0.8% w/v Triton X-100 (the two listed fluorescence intensities were both blank subtracted). See "Fluorescence Measurements with Microplate Reader" for plate-reader setup. Although some of this discrepancy in fluorescence can be explained by the inner filter effect (~14%) of fully cleaved **Opt** at 10 µM (see "Inner Filter Effect Characterization and Limit of Detection (LOD)" for more discussion), the remaining

discrepancy in fluorescence most likely comes from both (1) fluorescence suppression of **Opt** in the presence of Glu-C, and (2) the fact that the concentrations of **Std** and **Opt** were slightly offset because we used different extinction coefficients (see section above) to access the concentrations of their stocks in DMF. The reported[4] extinction coefficients of Edans and Dabcyl that we used for concentration calculations were obtained in the following buffer: 0.10 M sodium acetate, pH 4.7, containing NaCl (1.0 M), EDTA (1.0 mM), dithiothreitol (1.0 mM), dimethylsulfoxide (10% v/v), and bovine serum albumin (1 mg/mL). On the other hand, we used 10 mM MES–HCl buffer, pH 6.0, containing DMF (3% v/v) and Triton X-100 (0.8% w/v) for absorbance measurements. We chose pH 6 because, at lower pH, additional carboxylate groups in **Opt** could become protonated, decreasing the solubility of the peptide. It is possible that whereas the extinction coefficient of Edans in both buffer systems is about the same (the experimentally determined pK_a of *p*-toluenesulfonic acid in water is −2.8[20]), the extinction coefficient of Dabcyl slightly changed at higher pH (the experimentally determined pK_a of the conjugate acid of dimethylaniline in water is 5.07[22]) in our buffer system (pH 6.0) relatively to the one previously reported (pH 4.7). Hence, our reported concentrations of **Opt** and esterified **Opt** peptides (all determined using the same extinction coefficient) might be slightly perturbed from absolute values.

VI-2. Screen of Glu-C Concentrations for Complete Cleavage of Opt

2× solutions (20 μM and 2 μM) of **Opt** were prepared in 10 mM HEPES–NaOH buffer, pH 7.4, containing 3% v/v DMF and 0.8% w/v Triton X-100 by diluting the stock solution in DMF. 2× solutions of Glu-C (2 μM, 0.4 μM, and 0.2 μM) were prepared in 10 mM HEPES–NaOH buffer, pH 7.4, containing 0.8% w/v Triton X-100 from the stock solution in water and placed on ice. See "Preparation of Stock Solutions of Glu-C and Peptides" for more details. To wells of a 96-well plate were added 50 μL of the 2× solution of **Opt**. The 2× solutions of Glu-C were pipetted into PCR tubes (60 μL) that served as chambers for a multichannel pipette. The PCR tubes and pipette tips were placed into a heated (37 °C) incubator for 10 min. The plate was pre-equilibrated inside a heated (37 °C) plate reader for 10 min. The assay components were pre-equilibrated in this manner to ensure that they are close to 37 °C at the start of fluorescence measurements. After 10 min, with a multichannel pipette, 50 μL of 2× solutions of Glu-C were added to wells containing **Opt**. The plate was rapidly returned to the plate reader and shaken for 15 s at 37 °C to allow for proper mixing and temperature equilibration. The measurements were taken every 20 s for 280 s post-shaking as described in the plate-reader setup (see "Instrumentation" for details). The fluorescence values were averaged and plotted along with the SD (see "Statistical Analysis: Computing Errors" for details) in Figures 4A and S7. In the presence of 1 μM Glu-C, both 10 μM **Opt** (1:10 enzyme/peptide) and 1 μM **Opt** (1:1 enzyme/peptide) were cleaved nearly instantaneously, which motivated us to choose 1 μM Glu-C as the optimal concentration for the assay (to be able to disregard the kinetics of the Glu-C cleavage step).

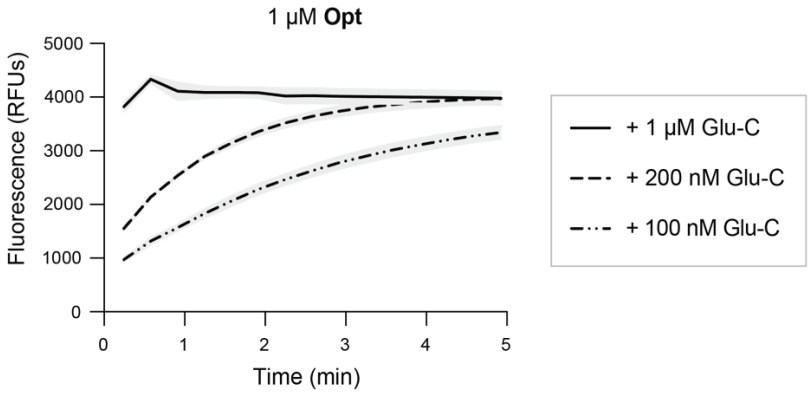

Figure S7. Fluorescence progress curves of 1 µM **Opt** upon addition of respective amounts of Glu-C. Assays were performed in 10 mM HEPES–NaOH buffer, pH 7.4, containing DMF (1.5% v/v) and Triton X-100 (0.8% w/v). Gray areas represent the SD. Progress curves were fitted from data points spaced apart by 20 s. $n = 2$ independent replicates, $n = 3$ technical replicates.

VI-3. Mass Spectrometry Validation of Opt Cleavage by Glu-C at Glu↓Phe

A solution (64 µM) of **Opt** was prepared in 10 mM HEPES–NaOH buffer, pH 7.4, containing DMF (5% v/v) by diluting the stock solution in DMF. See "Preparation of Stock Solutions of Glu-C and Peptides" for details. Note that Triton X-100 was not used during LC-MS analysis to avoid damaging the mass spectrometer (detergents are typically incompatible with mass spectrometry because they can cause ion suppression). To 20 µL of the 64 µM **Opt** solution were added 16 µL of MeCN and 44 µL of solvent C (20% MeCN v/v). The diluted solution was then filtered and analyzed by Q-TOF LC-MS. See "LC-MS Analysis (336 nm and 472 nm) of Peptide Transformations" for details on the Q-TOF method and filtration. The starting material spectra are show in Figures 4B and S8B. To 30 µL of the 64 µM **Opt** solution were added 2 µL of 30-µM solution of Glu-C (1:32 enzyme/peptide by molar equivalents) in 10 mM HEPES–NaOH buffer, pH 7.4 (prepared from stock solution in water), and incubated for 5 min at 37 °C on a shaker (300 rpm). The solution containing Glu-C and **Opt** was diluted, filtered as described above, and analyzed by Q-TOF LC-MS. Figures 4B and S8 demonstrate that Glu-C completely and rapidly cleaves **Opt** at Glu↓Phe without generating byproducts. It was also observed that, whereas Dabcyl absorbs at 336 nm in addition to 472 nm, Edans only absorbs at 336 nm (compare Figure S8C,D).

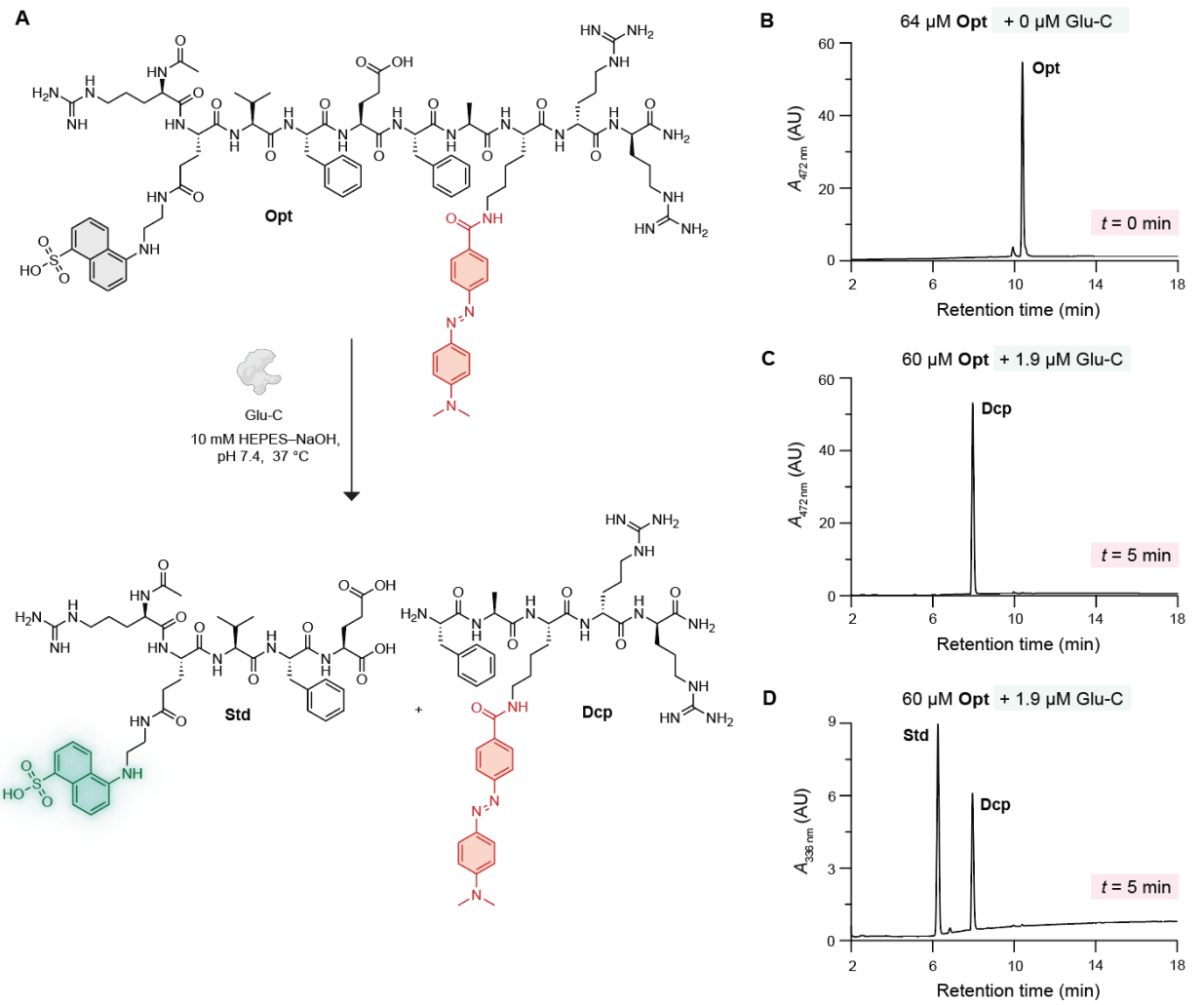

Figure S8. (A) Expected products generated upon **Opt** cleavage by Glu-C at Glu↓Phe: **Std** and **Dcp**. Representative LC-MS absorbance traces of 4× dilutions of (B) 64 μM **Opt** recorded at $\lambda_{472\ nm}$, (C) 60 μM **Opt** incubated in the presence of 1.9 μM Glu-C for 5 min at 37 °C recorded at $\lambda_{472\ nm}$, and (D) 60 μM **Opt** incubated in the presence of 1.9 μM Glu-C for 5 min at 37 °C recorded at $\lambda_{336\ nm}$. The cleavage reaction was performed in 10 mM HEPES–NaOH buffer, pH 7.4, containing DMF (5% v/v). Calc'd for **Opt**, $C_{89}H_{127}N_{26}O_{18}S$ $[M + 3H]^{3+}$, 626.6509; found, 626.9903. Calc'd for **Std**, $C_{44}H_{61}N_{10}O_{13}S$ $[M + H]^{+}$, 969.4135; found, 969.4174. Calc'd for **Dcp**, $C_{45}H_{69}N_{16}O_6$ $[M + 3H]^{3+}$, 309.8523; found, 309.8554. A part of this figure is presented in Figure 4B.

VI-4. MS Assessment of the Stability of Esterified Peptides in the Presence of Glu-C

To provide evidence that **Opt**-Et, **Opt**–**1**, **Opt**–**2**, and **Opt**–**3** are (1) predominantly esterified at the carboxyl group of the Glu residue as opposed to the sulfonic acid of Edans, and (2) are stable to incubation with Glu-C, the esterified peptides were incubated with Glu-C for 5 min (using amounts sufficient to completely cleave 10 μM **Opt** within the same time period, or >1:50 ratio of Glu-C/peptide, see Figure 4A) and the resultant solutions were analyzed for the presence of cleavage product **Dcp** by Q-TOF LC-MS. See "LC-MS Analysis (336 nm and 472 nm) of Peptide Transformations" for details on the Q-TOF method and filtration. Solutions of **Opt**-Et (87 μM), **Opt**–**1** (72 μM), **Opt**–**2** (97 μM), and **Opt**–**3** (58 μM) were prepared in 10 mM HEPES–NaOH buffer, pH 7.4, containing DMF (5% v/v) by diluting the stock solution in DMF. Note that Triton X-100 was not used during LC-MS analysis. Due to the tendency of esterified peptides to stick to Eppendorf tubes, the reaction buffer containing DMF had to be pre-warmed to 37 °C before esterified peptides were added as this approach minimized analyte loss. All further manipulations were also performed at 37 °C for the same reason. To 20 μL of the prepared solutions of esterified peptides were added 16 μL MeCN and 44 μL of solvent C (20% MeCN v/v). The diluted solutions were then filtered as described previously and analyzed by LC-MS (Figures 4C and S9A,C,E,G). Next, to 30 μL of the prepared solutions of esterified peptides were added 2 μL of 30-uM solution of Glu-C (peptide to Glu-C ratio of 1:44 for **Opt**-Et, 1:36 for **Opt**–**1**, 1:49 for **Opt**–**2**, and 1:29 for **Opt**–**3**) in 10 mM HEPES–NaOH buffer, pH 7.4 (prepared from stock solution in water), and incubated for 5 min at 37 °C on a shaker (300 rpm). See "Preparation of Stock Solutions of Glu-C and Peptides" for more details. The enzyme-containing solutions were then diluted by the addition of 25.6 μL of MeCN and 70.4 μL of solvent C (final MeCN concentration of 20% v/v), filtered, analyzed by LC-MS (Figures 4C and S9B,D,F,H). In all cases, less than 10% of the starting material was converted to **Dcp**, as indicated by analysis at 472 nm. The percentage was calculated by dividing the area of the **Dcp** peak by the sum of the areas of the **Dcp** peak and the starting material peak in spectra obtained at t = 5 min. These findings suggest that the carboxyl group (rather than the sulfonic acid) was predominantly esterified in **Opt**-Et, **Opt**–**1**, **Opt**–**2**, and **Opt**–**3** (*i.e.,* 100% of ester groups are on the Glu residue in **Opt**-Et and **Opt**–**1**, and at least 97% and 92% of the ester groups are on the Glu residue in **Opt**–**2** and **Opt**–**3**, respectively; see Figure S9). Note that we cannot rule out that Glu-C could be simply erring occasionally, de-esterifying background amounts of **Opt**–**2** and **Opt**–**3** (the observed cleavage might have nothing to do with the ester being on Edans). In any case, the esterified peptides were much more stable to Glu-C relative to **Opt**, which was completely cleaved under comparable conditions (see Figures 4B and S8). Note that the listed percentages are rough estimates as our LC-MS analysis cannot be used to measure the exact ratio between formed products and starting materials due to the omission of Triton X-100 (we noticed that the more hydrophobic peptides stuck more to plastic surfaces, leading to an artificial enlargement of peak areas of more hydrophilic peptides relative to less hydrophilic ones). For additional data on **Opt**–**3** stability in the presence of Glu-C at longer time points (40 min), see Figure S13H.

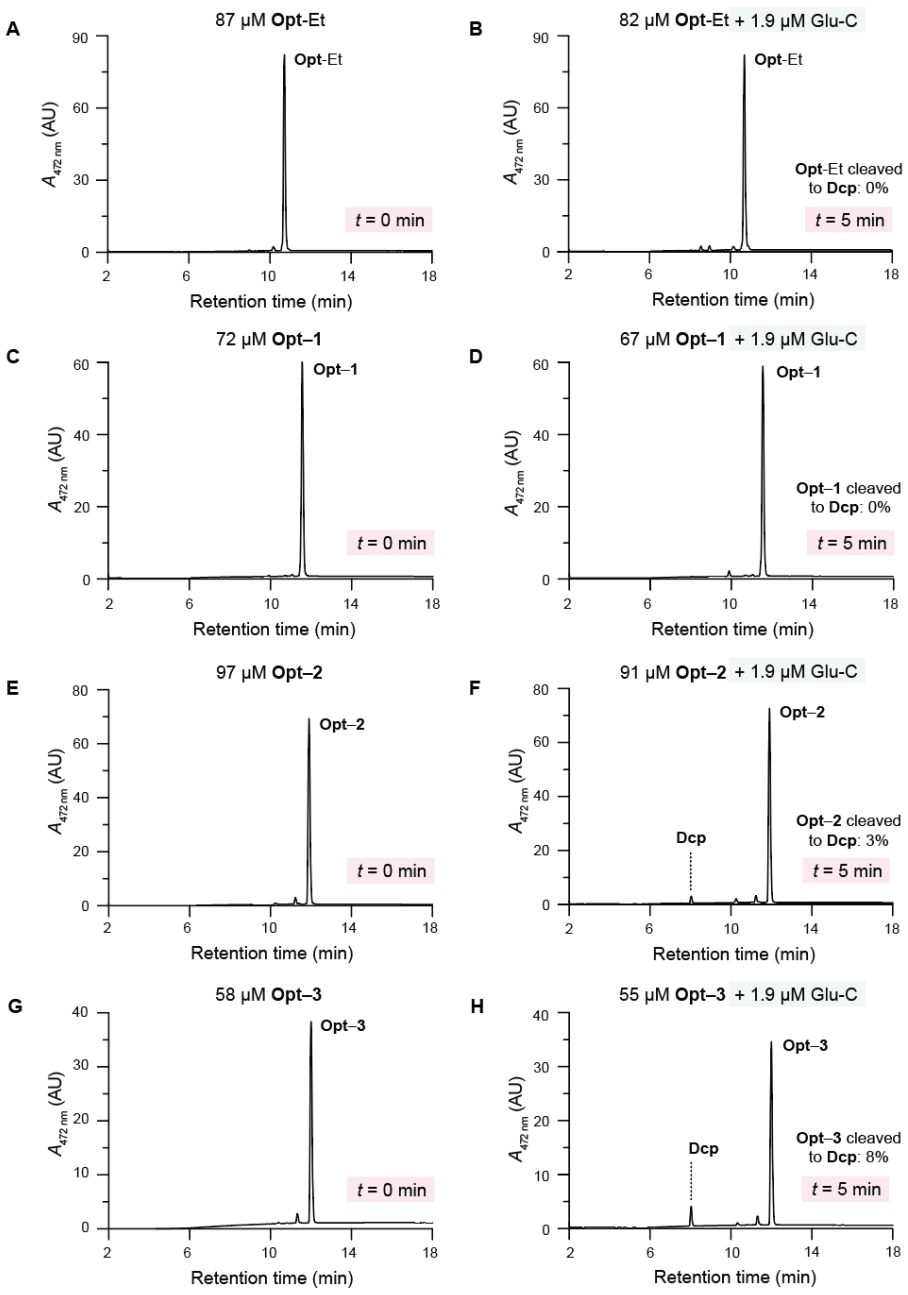

Figure S9. Representative LC-MS absorbance traces recorded at $\lambda_{472\ nm}$ of 4× dilutions of (A) **Opt**-Et before (87 µM) and (B) after (82 µM) incubation with Glu-C; (C) **Opt**–**1** before (72 µM) and (D) after (67 µM) incubation with Glu-C; (E) **Opt**–**2** before (97 µM) and (F) after (91 µM) incubation with Glu-C; and (G) **Opt**–**3** before (58 µM) and (H) after (55 µM) incubation with Glu-C. The reactions were performed in 10 mM HEPES–NaOH buffer, pH 7.4, containing DMF (5% v/v) and the final concentration of Glu-C was 1.9 µM. Calc'd for **Opt**-Et, $C_{91}H_{131}N_{26}O_{18}S$ $[M + 3H]^{3+}$, 635.9946; found, 636.3357. Calc'd for **Opt**–**1**, $C_{102}H_{142}N_{27}O_{19}S$ $[M + 3H]^{3+}$, 694.0238; found, 694.0300. Calc'd for **Opt**–**2**, $C_{106}H_{148}N_{27}O_{23}S$ $[M + 3H]^{3+}$, 733.3660; found, 733.3725. Calc'd for **Opt**–**3**, $C_{107}H_{148}N_{27}O_{22}S$ $[M + 3H]^{3+}$, 732.0343; found, 732.0400. Calc'd for **Dcp**, $C_{45}H_{69}N_{16}O_6$ $[M + 3H]^{3+}$, 309.8523; found, 309.8556. A part of this figure is presented in Figure 4C.

VI-5. Inner Filter Effect Characterization and Limit of Detection (LOD)

The inner filter effect is a fluorescence suppression phenomenon that arises from fluorescent light absorption by quenching groups (*i.e.,* Dabcyl in our system) that results in lower amount of fluorescence reaching the detector.[23] The magnitude of the inner filter effect is positively correlated with the concentration of quenching groups. In some FRET assays, an inner filter effect correction[14,23,24] is required to determine the concentration of cleaved substrate. To characterize the inner filter effect at different substrate concentrations in our assay, we evaluated the change in fluorescence of **Std** in the presence of varying concentrations of **Opt** in 10 mM HEPES–NaOH buffer, pH 7.4, containing 1.5% v/v DMF and 0.8% w/v Triton X-100, following previously reported methods.[14,23] See "Preparation of Stock Solutions of Glu-C and Peptides" as well as "Instrumentation" for additional details on preparation of stock solutions and plate-reader setup. Endpoint values from blank (buffer with 1.5% v/v DMF and 0.8% w/v Triton X-100) fluorescence, **Std** (2.5 μM) fluorescence, **Opt** (0–10 μM) fluorescence, and combined fluorescence from **Std** (2.5 μM) and **Opt** (0–10 μM) were averaged and summarized in Table S1. The fluorescence of **Std** in the presence of **Opt**, f(**Std**), was derived by subtracting the fluorescence of **Opt**, f(**Opt**), from the combined fluorescence of **Std** and **Opt**, f(**Std** + **Opt**).

Table S1. Fluorescence values used to derive f(**Std**) in the presence of various concentrations of **Opt** in 10 mM HEPES–NaOH buffer, pH 7.4, containing 1.5% v/v DMF and 0.8% w/v Triton X-100. n = 2 independent replicates, n = 3 technical replicates.

[**Opt**], μM	f(**Opt**), RFUs	f(**Std** + **Opt**), RFUs	f(**Std**), RFUs	Attenuation of f(**Std**), %
0.0	151	12826	12675	0
0.5	251	13056	12805	0
1.0	318	12976	12658	0
2.0	458	12472	12014	5
3.0	654	13017	12363	3
4.0	809	13123	12314	3
5.0	944	12121	11177	13
6.0	1108	12600	11493	10
7.0	1295	12699	11404	11
8.0	1442	13390	11948	6
9.0	1554	13078	11524	10
10.0	1736	12840	11105	14

The fluorescence of f(**Std**) was plotted as a function of **Opt** concentration in Figure S10A. See "Statistical Analysis: Computing Errors" for more details on data analysis. Because the inner filter

effect was relatively minor (<15%) within the tested **Opt** concentration range, we decided not to apply the inner filter effect correction[23] and limited the working range of our assay to 0–10 µM of substrate.

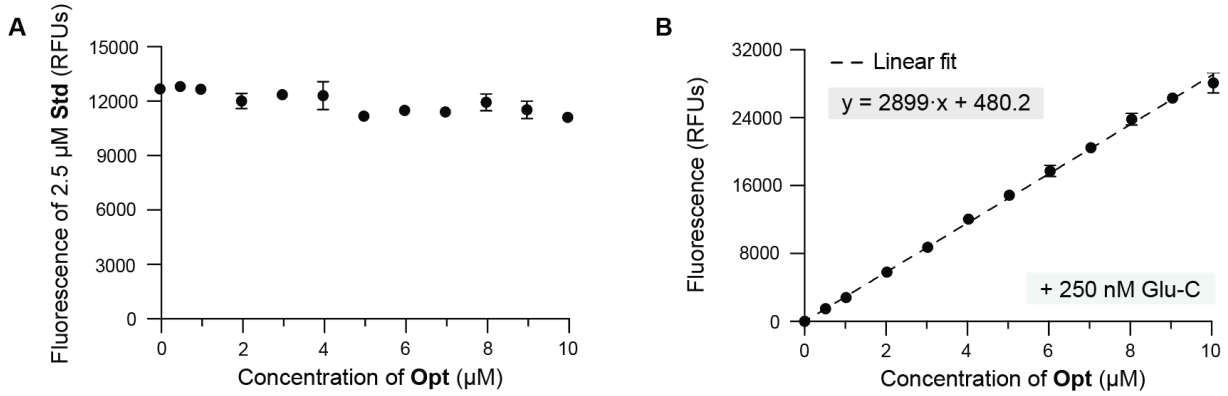

Figure S10. (A) Fluorescence of **Std** (2.5 µM) (see Table S1 for more details) plotted as a function of various concentrations of **Opt**. (B) Linearity of fluorescence of **Opt** fully cleaved by Glu-C (250 nM). Assays were performed in 10 mM HEPES–NaOH buffer, pH 7.4, containing DMF (1.5% v/v) and Triton X-100 (0.8% w/v). Error bars represent the SD. n = 2 independent replicates, n = 3 technical replicates.

To complement the analysis in Figure S10A, we also accessed the inner filter effect by measuring the fluorescence of varying concentrations of **Opt** (0–10 µM) fully cleaved by Glu-C (generating **Std** and **Dcp**, in 1:1 ratio) in 10 mM HEPES–NaOH buffer, pH 7.4, containing 1.5% v/v DMF and 0.8% w/v Triton X-100. **Opt** was incubated in the presence of 250-nM Glu-C for 10 min at 37 °C before fluorescence measurements. Full cleavage of **Opt** was verified by ensuring that fluorescence of the wells does not increase over time. The fluorescence values from cleaved **Opt** were averaged and blank (buffer containing 1.5% v/v DMF and 0.8% w/v Triton X-100) subtracted. Figure S10B demonstrates that, in the 0–10 µM concentration range, the inner filter effect from increasing concentrations of **Dcp** does not strongly affect the linearity of fluorescence emitted by **Std**. To estimate the LOD of the assay, a linear regression analysis was performed in Prism using the data in Figure S10B. We calculated the LOD using the formula[25]

$$\mathrm{LOD} \geq \frac{3.3 \cdot \mathrm{SE}_{y-\mathrm{int}}}{m} \geq \frac{3.3 \cdot 213.8}{2898.5} \geq 240\ \mathrm{nM} \tag{S1}$$

where $\mathrm{SE}_{y\text{-int}}$ is the standard error of the y-intercept and m is the slope of the regression line.

VI-6. Fold Increase in Fluorescence Intensity Upon Opt Cleavage by Glu-C

A solution (10 µL) of **Opt** in 10 mM HEPES–NaOH buffer, pH 7.4, containing DMF (1.5% v/v) and Triton X-100 (0.8% w/v) was incubated in the absence or presence of 250 nM Glu-C for 10 min at 37 °C. See "Preparation of Stock Solutions of Glu-C and Peptides" and "Instrumentation" for details. Endpoint fluorescence values from **Opt** and cleaved **Opt** were averaged and blank (buffer containing 1.5% v/v DMF and 0.8% w/v Triton X-100) subtracted. See "Statistical Analysis: Computing Errors" for details. Figure S11 shows the increase in fluorescence intensity upon **Opt** cleavage by Glu-C. The "turn-on" was calculated using the formula[6]

$$\frac{I_\mathrm{f}}{I_\mathrm{o}} = \frac{28468}{1607} \approx 18 \tag{S2}$$

where I_f is the fluorescence of **Opt** cleaved by Glu-C and I_o is the fluorescence of **Opt**.

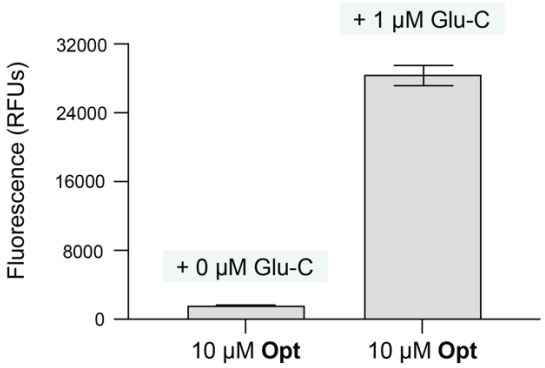

Figure S11. Fluorescence of **Opt** (10 µM) and **Opt** (10 µM) cleaved by Glu-C (1 µM) in 10 mM HEPES–NaOH buffer, pH 7.4, containing Triton X-100 (0.8% w/v). Error bars represent the SD. n = 2 independent replicates, n = 3 technical replicates.

VII. Evaluating Kinetic Parameters: Examples with Pig Liver Esterase (PLE)

VII-1. Assaying Esterified Peptides for Cleavage by PLE

Solutions (2× 20 μM) of **Opt**, **Opt**-Et, **Opt**–**1**, **Opt**–**2**, and **Opt**–**3** were prepared in 10 mM HEPES–NaOH buffer, pH 7.4, containing 3% v/v DMF and 0.8% w/v Triton X-100 by diluting the stock solution in DMF. 4× solutions of PLE (8 μM) and Glu-C (4 μM) were prepared in 10 mM HEPES–NaOH buffer, pH 7.4, containing Triton X-100 (0.8% w/v). See "Absorbance-Based Concentration Measurements" for preparation of the PLE stock (lot activity: 62.6 U/mg) and "Preparation of Stock Solutions of Glu-C and Peptides" for additional details. Aliquots (50 μL) of the 20 μM peptide solutions were added to the wells of a 96-well plate. The plate was placed into a pre-warmed plate reader for 10 min to pre-equilibrate it to 37 °C. The following 6 strips of 12 PCR tubes each were prepared: (1) strips containing 45 μL of 4× Glu-C solution, (2) strips containing 35 μL of 4× PLE solution, (3) strips containing 45 μL of reaction buffer without DMF, (4) strips containing 35 μL of 4× Glu-C solution, (5) strips containing 45 μL of reaction buffer without DMF, and (6) strips containing 35 μL of 4× PLE solution. The 6 strips of PCR tubes together with a set of pipet tips were placed into an incubator to equilibrate them to 37 °C for 10 min. After 10 min, using a multichannel pipet, 35 μL of PCR strip 1 was added to PCR strip 2 (resulting in a solution containing 4 μM PLE and 2 μM Glu-C), 35 μL of PCR strip 3 was added to PCR strip 4 (resulting in a solution containing 2 μM Glu-C), and 35 μL of PCR strip 5 was added to PCR strip 6 (resulting in a solution containing 4 μM PLE). Then, 50 μL solutions of either 4 μM PLE and 2 μM Glu-C, 2 μM Glu-C, or 4 μM PLE were rapidly added to the 50 μL peptide solutions in the 96-well plate using a multichannel pipette. The plate was rapidly returned into the plate reader and shaken for 15 s at 37 °C to allow for proper mixing and temperature equilibration. The measurements were taken every 20 s for 40 min post-shaking as described in the plate reader assay set (see "Instrumentation" for more details). The final concentrations were: 10 μM of **Opt** or esterified peptides, 2 μM of PLE, and 1 μM of Glu-C. Note that PLE and Glu-C were premixed and added to the plate after rather than before 10-min equilibration to 37 °C. This precaution was carried out to minimize undesired PLE cleavage by Glu-C. Fluorescence values were averaged and blank (fluorescence of 10 mM HEPES–NaOH buffer, pH 7.4, containing 1.5% v/v DMF and 0.8% w/v Triton X-100) subtracted. See "Statistical Analysis: Computing Errors" for data analysis. Progress curves of **Opt**-Et, **Opt**–**1**, **Opt**–**2**, and **Opt**–**3** cleavage by PLE (read out by Glu-C fluorescence) are shown in Figure 5A with all controls. Overall, under the employed experimental conditions, no PLE-mediated cleavage of **Opt**-Et and **Opt**–**1** was observed. In contrast, both **Opt**–**2** and **Opt**–**3** were completely cleaved by PLE, with **Opt**–**3** being cleaved slightly faster.

VII-2. MS Analysis of Products Formed Within the PLE Assay

VII-2a. Opt–3 and Opt–2 Cleavage by PLE: Phenolic Intermediate

Using Q-TOF LC-MS, we first investigated the products generated upon **Opt**–**3** incubation with PLE, PLE in the presence of Glu-C, and Glu-C at various time points. This experiment served (1) to study the mechanism of esterase cleavage of substrates that can undergo 1,6-quinone methide elimination, and (2) to obtain a more complete picture of enzymatic and chemical reactions that take place "behind" each progress curve in the Glu-C assay. To begin, we prepared a solution of **Opt**–**3** (40 μM) in 10 mM HEPES–NaOH buffer, pH 7.4, containing DMF (6% v/v) by diluting the stock solution in DMF. See "Preparation of Stock Solutions of Glu-C and Peptides" for more details. Due to the tendency of esterified peptides to stick to Eppendorf tubes, the reaction buffer containing DMF had to be pre-warmed to 37 °C before the esterified peptide was added as this approach minimized analyte loss. See "Absorbance-Based Concentration Measurements" for preparation of the PLE stock. All further manipulations were also performed at 37 °C for the same reason. To aliquots (30 μL) of the 40 μM solution were added (1) 30 μL of 10 mM HEPES–NaOH buffer, pH 7.4, containing 8 μM PLE and 4 μM Glu-C, (2) 30 μL of 10 mM HEPES–NaOH buffer, pH 7.4, containing 8 μM PLE, (3) 30 μL of 10 mM HEPES–NaOH buffer, pH 7.4, containing 4 μM Glu-C, or (4) 30 μL of 10 mM HEPES–NaOH buffer alone. The solutions were incubated for 0 min, 4 min, 40 min, or 130 min at 37 °C on a shaker (300 rpm). After the indicated times, 20 μL of the prepared solutions of esterified peptides were combined with 16 μL MeCN and 44 μL of solvent C (20% MeCN v/v). The diluted solutions were then filtered as described and analyzed by Q-TOF LC-MS (see "LC-MS Analysis (336 nm and 472 nm) of Peptide Transformations" for more details). Our findings are summarized in Figure S12. First, we found that the phenolic intermediate generated upon **Opt**–**2** and **Opt**–**3** cleavage by PLE is stable enough to be detected by LC-MS. Furthermore, at the high PLE concentrations employed, **Opt**–**3** was converted into the phenolic intermediate faster than the intermediate decayed into **Opt**. At longer time points, most of the intermediate decayed. Glu-C-mediated cleavage of **Opt** into **Std** and **Dcp** was nearly instantaneous, as expected. Surprisingly, we also observed that PLE cleaves off the C-terminal Phe residue from **Dcp**, producing **Pcp** (PLE cleavage product). This process (1) seemed much slower than PLE-catalyzed hydrolysis of the esterified substrates, (2) was downstream of product and **Std** formation, and (3) did not generate any additional fluorescence (fluorescence of **Std** does not change if all **Dcp** is converted to **Pcp**). Hence, we did not take **Pcp** into account when constructing our subsequent kinetic model.

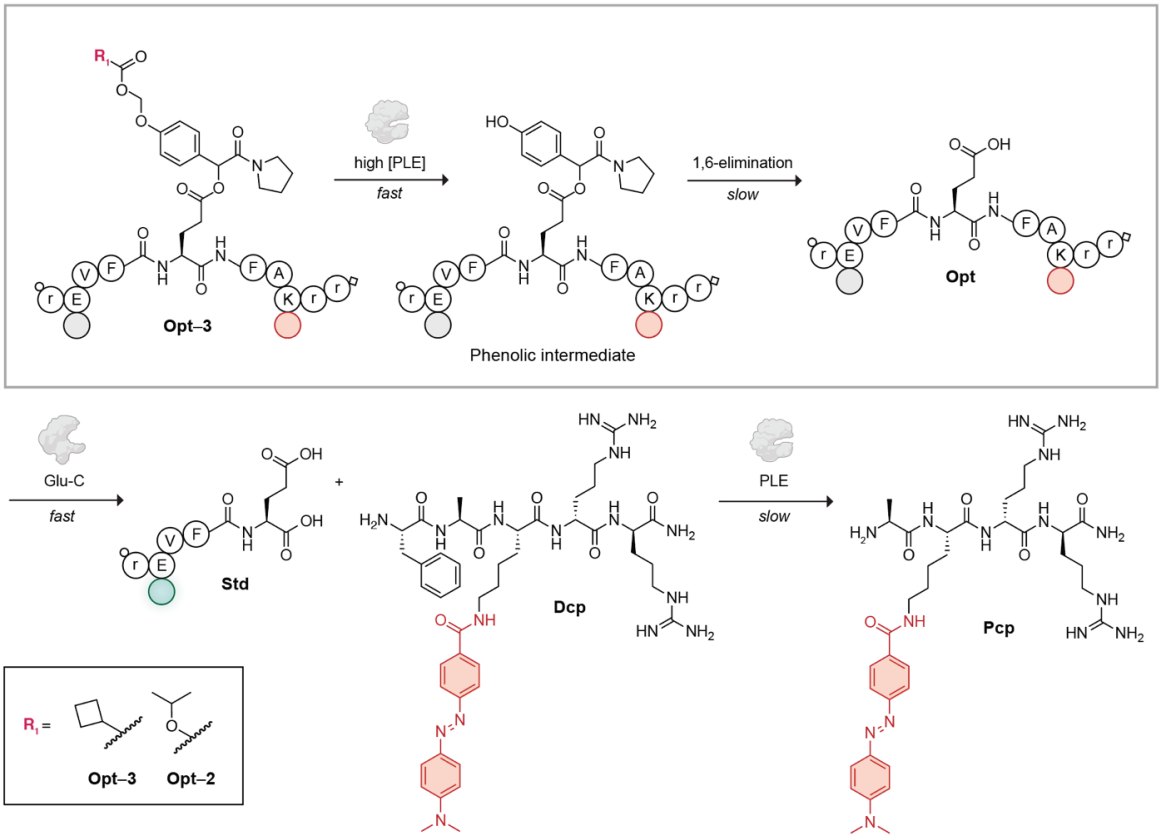

Figure S12. (Top) Phenolic intermediate formation upon **Opt–2** and **Opt–3** cleavage by PLE. (Bottom) Downstream processing of the formed **Dcp** into **Pcp** by PLE.

The LC-MS traces that served as a foundation for Figure S12 are shown in Figure S13. We point out that, whereas LC-MS data can be used to understand what products form within a given reaction, it cannot be used to accurately calculate ratios between products and starting materials due to the absence of solubilizing Triton X-100 (see more discussion in "MS Assessment of the Stability of Esterified Peptides in the Presence of Glu-C"). During LC-MS analysis, we had to use higher peptide concentrations than in the PLE assay (Figure 5A) because, at lower concentrations, we observed peptide loss due to sticking to plastic surfaces. To keep our LC-MS analysis representative of the PLE assay in Figure 5A, all enzyme concentrations were scaled proportionally to peptide concentrations. Note that the absorbance of **Opt–3** (Figure S13A) is lower in the absence of enzymes, highlighting the "sticking" effect. Enzymes, like Triton X-100, coat plastic surfaces and prevent peptide loss due to sticking. Rough estimates of percentage of **Dcp** formation in Figure S13G,H were made the same way as in Figure S9. Note also that the LC-MS analysis was performed in presence of formic acid (0.1% v/v). Acidic environment is known to slow down quinone methide elimination,[26] allowing for some degree of intermediate "trapping" before it decays. Acid can also influence the reversibility/equilibrium of quinone methide quenching by weak nucleophiles. Although quinone methide quenching by water is irreversible

and eventually inevitable, quinone methides can “jump around” weak nucleophiles in a reversible fashion before finally getting quenched.[27,28] Due to the complexity of the quinone methide elimination mechanism and the subsequent fate of the quinone methide, LC-MS data is only useful for detecting the existence of an intermediate. It cannot be used to predict decay rates at pH 7.4. Another observation is that, at 40 min, the amount of **Opt**–**3** cleaved by Glu-C (Figure 13H) was similar to the extent of background fluorescence corresponding to Glu-C incubated with **Opt**–**3** (Figure 5A). This similarity suggests that fluorescence from the off-target cleavage activity of Glu-C with esterified peptides can be partially accounted for when product (**Opt**) concentrations are measured (see eqs S3–S5 for more details).

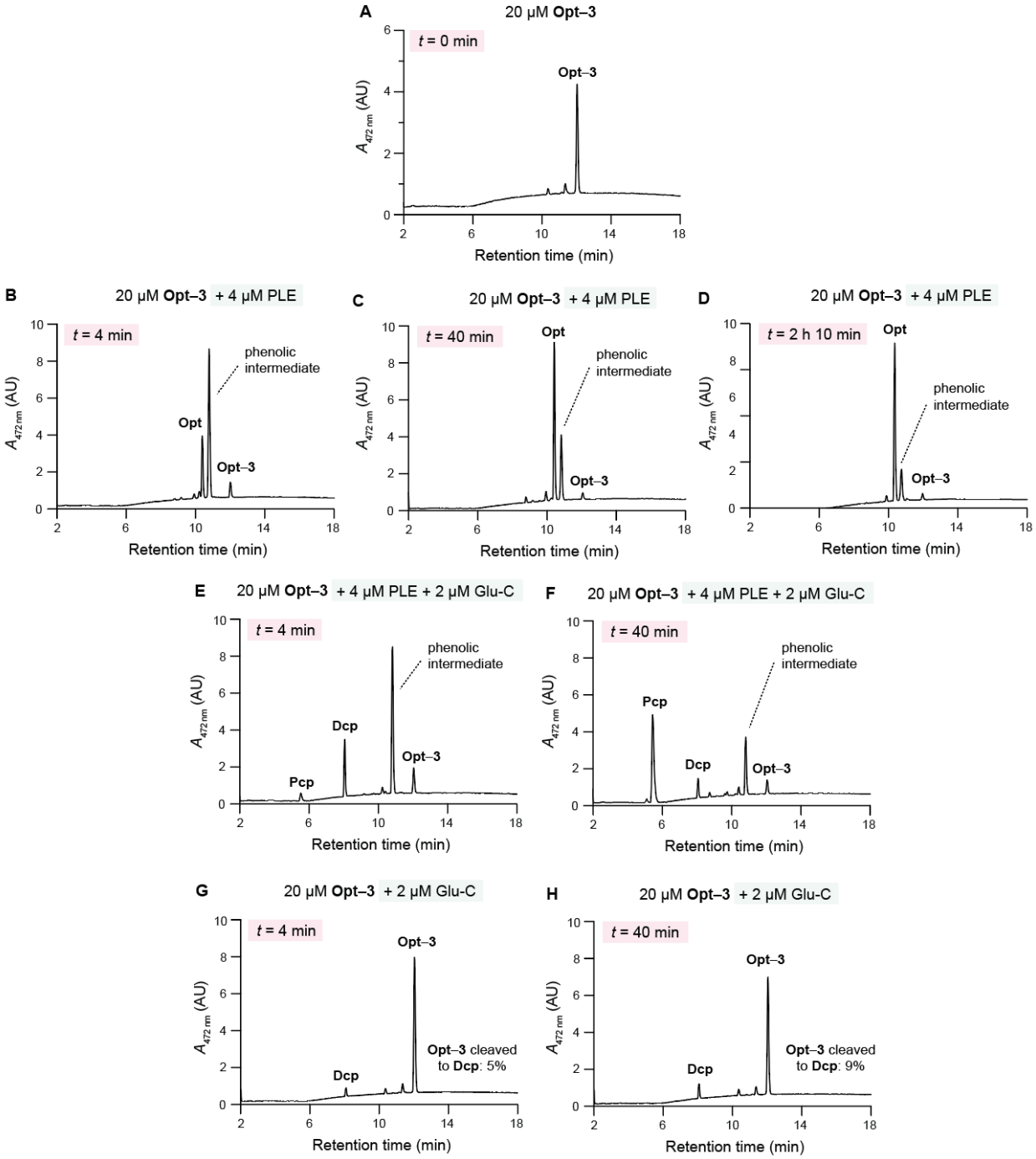

Figure S13. Representative LC-MS absorbance traces recorded at $\lambda_{472\ nm}$ of 4× dilutions of (A) **Opt**–**3** starting material (20 μM), (B) **Opt**–**3** in presence of PLE (4 μM) at 4 min, (C) **Opt**–**3** in presence of PLE (4 μM) at 40 min, (D) **Opt**–**3** in presence of PLE (4 μM) at 130 min, (E) **Opt**–**3** in presence of PLE (4 μM) and Glu-C (2 μM) at 4 min, (F) **Opt**–**3** in presence of PLE (4 μM) and Glu-C (2 μM) at 40 min, (G) **Opt**–**3** in presence of Glu-C (2 μM) at 4 min, and (H) **Opt**–**3** in presence of Glu-C (2 μM) at 40 min. Calc'd for **Opt**–**3**, $C_{107}H_{148}N_{27}O_{22}S$ $[M + 3H]^{3+}$, 732.0343; found, 732.0314. Calc'd for phenolic intermediate, $C_{101}H_{140}N_{27}O_{20}S$ $[M + 3H]^{3+}$, 694.6835; found, 694.6832. Calc'd for **Opt**, $C_{89}H_{127}N_{26}O_{18}S$ $[M + 3H]^{3+}$, 626.6509; found, 626.9850. Calc'd for **Dcp**, $C_{45}H_{69}N_{16}O_6$ $[M + 3H]^{3+}$, 309.8523; found, 309.2267. Calc'd for **Pcp**, $C_{36}H_{61}N_{15}O_5$ $[M + 3H]^{3+}$, 261.1655; found, 260.8304. Reactions were performed in 10 mM HEPES–NaOH buffer, pH 7.4, containing DMF (6% v/v).

To confirm that PLE cleavage of **Opt**–**2** results in the same phenolic intermediate (Figure S13B) as the cleavage of **Opt**–**3**, two samples consisting of (1) **Opt**–**2** starting material, and (2) **Opt**–**2** incubated with PLE for 4 min were analyzed by Q-TOF MS (samples were prepared and analyzed in the same manner as for **Opt**–**3** above). As demonstrated in Figures 5B and S14, the formation of the same phenolic intermediate was detected.

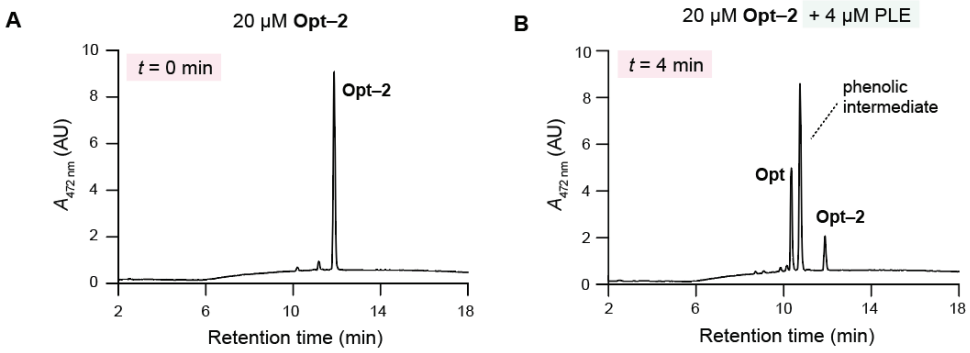

Figure S14. Representative LC-MS absorbance traces recorded at $\lambda_{472\ nm}$ of 4× dilution of (A) **Opt**–**2** starting material (20 μM), and (B) **Opt**–**2** (20 μM) incubated with PLE (4 μM) for 4 min. Calc'd for **Opt**–**2**, $C_{106}H_{148}N_{27}O_{23}S$ $[M + 3H]^{3+}$, 733.3660; found, 7323.3679. Calc'd for phenolic intermediate, $C_{101}H_{140}N_{27}O_{20}S$ $[M + 3H]^{3+}$, 694.6835; found, 694.6863. Calc'd for **Opt**, $C_{89}H_{127}N_{26}O_{18}S$ $[M + 3H]^{3+}$, 626.6509; found, 626.9839. Reactions were performed in 10 mM HEPES–NaOH buffer, pH 7.4, containing DMF (6% v/v). An adaptation of this figure is presented in Figure 5B.

VII-2b. Confirmation of Opt-Et and Opt–1 Stability to Incubation with PLE

To confirm that the Glu-C assay correctly read out the lack of PLE-mediated cleavage of **Opt**-Et and **Opt**–**1** (Figure 5A), we incubated these peptides with PLE under similar conditions as with **Opt**–**3** and **Opt**–**2** (see "**Opt**–**3** and **Opt**–**2** Cleavage by PLE: Phenolic Intermediate"). First, we prepared a solution of **Opt**–**1** (40 μM) in 10 mM HEPES–NaOH buffer, pH 7.4, containing DMF (6% v/v) by diluting the stock solution in DMF (see "Preparation of Stock Solutions of Glu-C and Peptides" for more details). Due to the tendency of esterified peptides to stick to Eppendorf tubes, the reaction buffer containing DMF had to be pre-warmed to 37 °C before the esterified peptide was added as this approach minimized analyte loss. All further manipulations were also performed at 37 °C for the same reason. To aliquots (30 μL) of the 40 μM solution were added either (1) 30 μL of 10 mM HEPES–NaOH buffer, pH 7.4, containing 8 μM PLE, or (2) 30 μL of 10 mM HEPES–NaOH buffer. The starting material solution was analyzed immediately, and the PLE-containing solution was analyzed after 4 min on a heated shaker (37 °C, 300 rpm). After the indicated times, 20 μL of the prepared solutions of esterified peptides were combined with 16 μL MeCN and 44 μL of solvent C (20% v/v MeCN). The diluted solutions were then filtered and analyzed by Q-TOF LC-MS (see "LC-MS Analysis (336 nm and 472 nm) of Peptide Transformations" for details). As seen in Figure S15, no PLE-mediated cleavage of **Opt**–**1** to **Opt** was observed, validating that **Opt**–**1** is not a substrate of PLE.

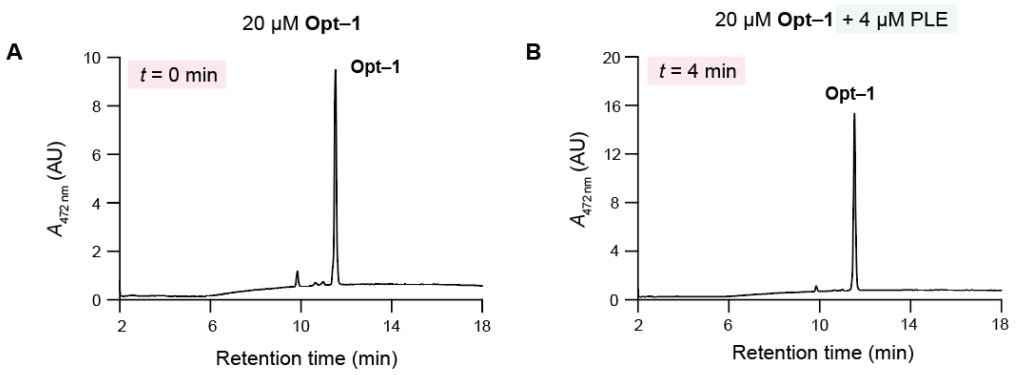

Figure S15. Representative LC-MS absorbance traces recorded at $\lambda_{472\,nm}$ of 4× dilutions of (A) **Opt**–**1** starting material (20 μM), and (B) (20 μM) incubated with PLE (4 μM) for 4 min. Calc'd for **Opt**–**1**, $C_{102}H_{142}N_{27}O_{19}S$ $[M + 3H]^{3+}$, 694.0238; found, 694.0272. Reactions were performed in 10 mM HEPES–NaOH buffer, pH 7.4, containing DMF (6% v/v).

Next, we analyzed **Opt**-Et starting material and **Opt**-Et incubated with PLE in the same way as **Opt**–**1** (see above). Substantial analyte loss was observed in the LC-MS chromatogram of starting material **Opt**-Et analyzed under these conditions (data not shown), hence we resorted to using the chromatogram previously used in Figure S9A as a reference spectrum (also see the reused chromatogram in Figure S16A). The chromatogram of **Opt**-Et incubated with PLE (Figure S16B) did not exhibit analyte loss, likely because the enzyme acted as a "coating agent" of plastic surfaces. Overall, the results of this experiment indicate that **Opt**-Et does not get cleaved by PLE, as no peak corresponding to **Opt** was observed.

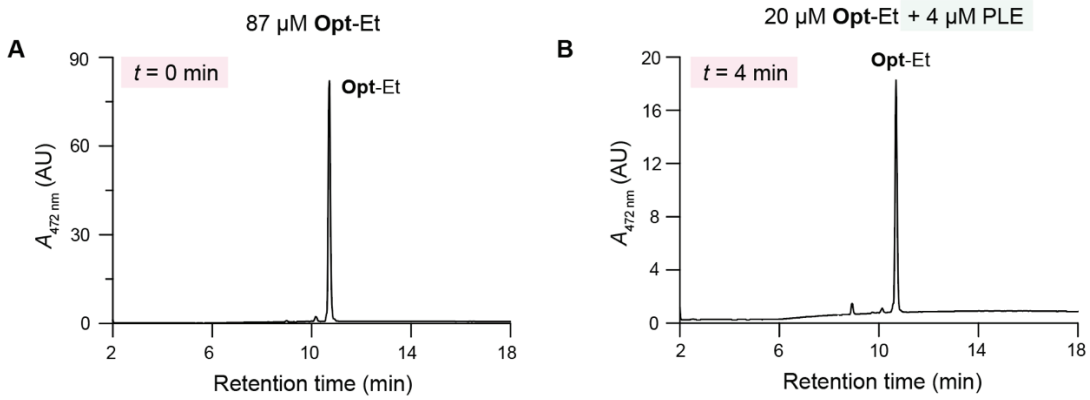

Figure S16. Representative LC-MS absorbance traces recorded at $\lambda_{472\,nm}$ of 4× dilutions of (A) **Opt**-Et starting material (87 μM), and (B) **Opt**-Et (20 μM) incubated with PLE (4 μM) for 4 min. Calc'd for **Opt**-Et, $C_{91}H_{131}N_{26}O_{18}S$ $[M + 3H]^{3+}$, 635.9946; found, 636.3320. Reactions were performed in 10 mM HEPES–NaOH buffer, pH 7.4, containing DMF (5% v/v in the case of **Opt**-Et starting material, or 6% v/v in the case of **Opt**-Et incubated with PLE).

VII-2c. Evaluation of the Stability of Esterified Peptides to Hydrolysis

We assessed the stability of esterified peptides to aqueous hydrolysis in assay buffer. Note that Triton X-100 was not used during LC-MS analysis (see "MS Assessment of the Stability of Esterified Peptides in the Presence of Glu-C" for reasoning). Solutions of **Opt**-Et (87 μM), **Opt**–**1** (72 μM), **Opt**–**2** (97 μM), and **Opt**–**3** (58 μM) were prepared in 10 mM HEPES–NaOH buffer, pH 7.4, containing DMF (5% v/v) by diluting the stock solution in DMF (see "Preparation of Stock Solutions of Glu-C and Peptides"). Due to the tendency of esterified peptides to stick to Eppendorf tubes, the reaction buffer containing DMF had to be pre-warmed to 37 °C before esterified peptides were added as this approach minimized analyte loss. All further manipulations were also performed at 37 °C for the same reason. To 20 μL of the prepared solutions of esterified peptides were added 16 μL MeCN and 44 μL of solvent C (20% v/v MeCN). The diluted solutions were then filtered and analyzed by Q-TOF LC-MS (see "LC-MS Analysis (336 nm and 472 nm) of Peptide Transformations" for details). The chromatograms of starting materials are shown in Figure S17A,C,E,G. The remaining solution of esterified peptides was incubated for 4 h at 37 °C on a shaker (300 rpm). After the indicated time, the reaction solutions were diluted and filtered as described above and analyzed by Q-TOF LC-MS (Figure S17B,D,F,H). **Opt**-Et and **Opt**–**1** were stable to hydrolysis within the 4-h time frame and did not release unmodified **Opt**. In contrast, a small amount of **Opt**–**2** and **Opt**–**3** hydrolyzed to **Opt**, as indicated by analysis at 472 nm.

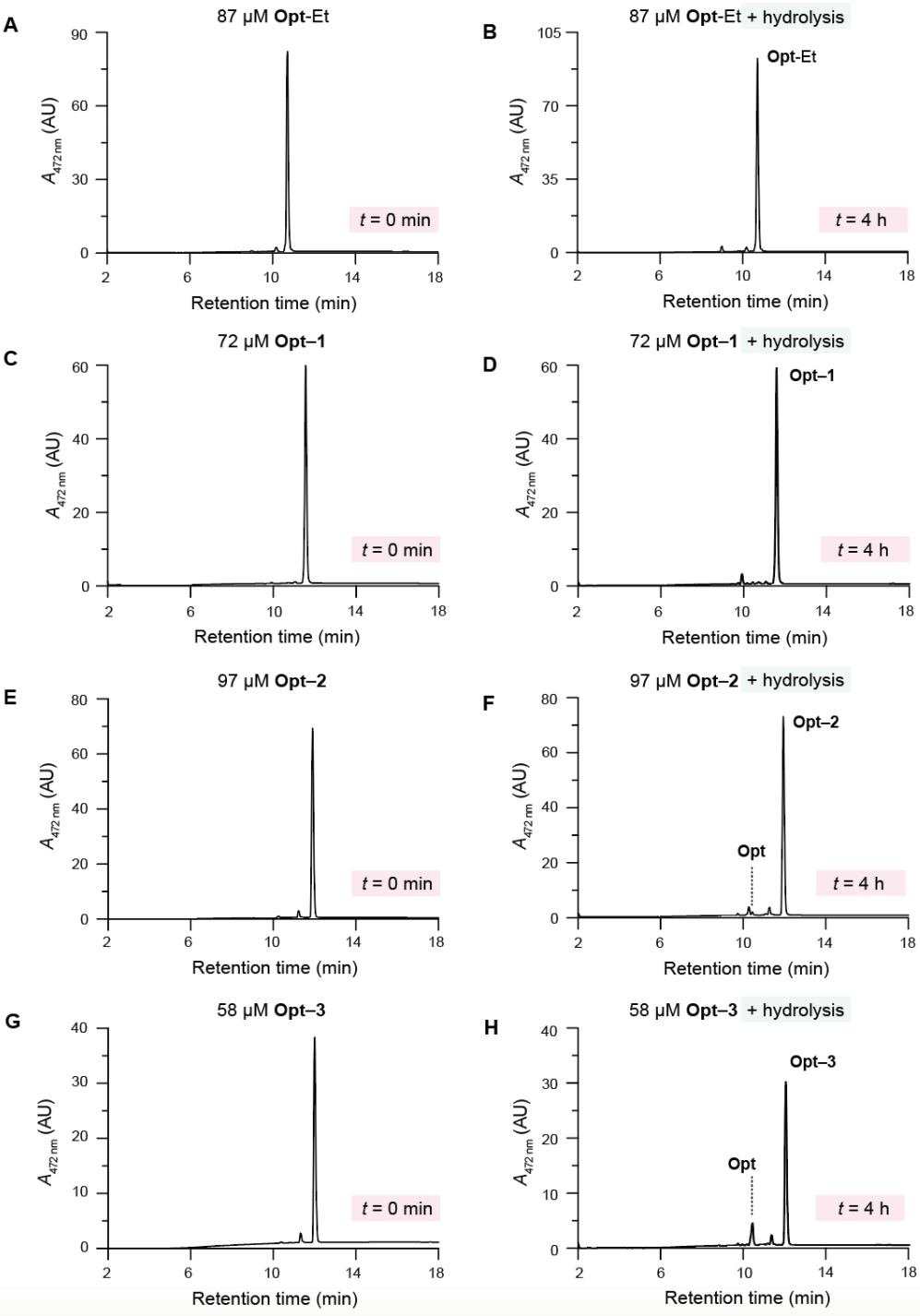

Figure S17. Representative LC-MS absorbance traces recorded at $\lambda_{472\ nm}$ of 4× dilutions of (A) **Opt**-Et (87 μM), (C) **Opt**–**1** (72 μM), (E) **Opt**–**2** (97 μM) and (G) **Opt**–**3** (58 μM) before and after hydrolysis (panels B, D, F, H, respectively). The peptides were hydrolyzed in 10 mM HEPES–NaOH buffer, pH 7.4, containing DMF (5% v/v). Calc'd for **Opt**-Et, $C_{91}H_{131}N_{26}O_{18}S$ $[M + 3H]^{3+}$, 635.9946; found, 636.3357. Calc'd for **Opt**–**1**, $C_{102}H_{142}N_{27}O_{19}S$ $[M + 3H]^{3+}$, 694.0238; found, 694.0300. Calc'd for **Opt**–**2**, $C_{106}H_{148}N_{27}O_{23}S$ $[M + 3H]^{3+}$, 733.3660; found, 733.3725. Calc'd for **Opt**–**3**, $C_{107}H_{148}N_{27}O_{22}S$ $[M + 3H]^{3+}$, 732.0343; found, 732.0400. Calc'd for **Opt**, $C_{89}H_{127}N_{26}O_{18}S$ $[M + 3H]^{3+}$, 626.6509; found, 626.9913.

VII-3. Progress Curve Analysis: Using Fluorescence(*t*) to Find Product Concentration(*t*)

To construct progress curves of the product (**Opt**) concentration, $[P]_t$, we use the Glu-C assay to measure fluorescence associated with four conditions (see Figure 5A for an example): substrate (S) incubated with both esterase and Glu-C ($F_t^{\text{esterase + Glu-C}}$), substrate incubated with esterase (F_t^{esterase}), substrate incubated with Glu-C ($F_t^{\text{Glu-C}}$), and **Opt** incubated with Glu-C ($F_t^{\max}$). Note that $F_t^{\text{esterase + Glu-C}}$, F_t^{esterase}, $F_t^{\text{Glu-C}}$, and $F_t^{\max}$ refer to already blank-subtracted (blank: buffer alone) fluorescence values. We assume that these controls are independent of each other (PLE and Glu-C combined are assumed to behave the same way as they would do when incubated with peptides separately). Under these assumptions, the four controls can be physically thought of as follows:

(1) $F_t^{\text{esterase + Glu-C}}$ refers to fluorescence turn-on from product formation and other cleavage events that could lead to the loss of FRET. At early time points, background fluorescence of the substrate (or phenolic intermediate, I; we assume that substrate and intermediate have the same background fluorescence) also contributes to $F_t^{\text{esterase + Glu-C}}$. If all substrate and/or intermediate is consumed, their background fluorescence stops contributing to $F_t^{\text{esterase + Glu-C}}$. Background substrate and/or intermediate fluorescence contribution to $F_t^{\text{esterase + Glu-C}}$ is thus time dependent.
(2) F_t^{esterase} is the background fluorescence of the substrate and any proteolytic activity of the esterase that contributes to fluorescence turn on (we do not observe the latter in any experiments; F_t^{esterase} in our experiments is constant).
(3) $F_t^{\text{Glu-C}}$ accounts for the loss of FRET due to aqueous hydrolysis of the esterified substrate and partially accounts for proteolysis of the esterified substrate by Glu-C that leads to fluorescence turn-on. However, most fluorescence in $F_t^{\text{Glu-C}}$ comes from the background fluorescence of the substrate. We assume that the substrate background fluorescence contribution to $F_t^{\text{Glu-C}}$ is pretty much constant because we do not observe substantial turn on in any experiments. A small increase in $F_t^{\text{Glu-C}}$ that we observe over time in some cases (see Figure 5A) is likely from Glu-C proteolysis of a small amount of substrate.
(4) $F_t^{\max}$ reflects the maximal turn-on from complete loss of FRET. Note that, because we assume that Glu-C action on **Opt** is nearly instantaneous, we assume that background fluorescence of **Opt** does not contribute to $F_t^{\max}$ at any point.

After thinking about the physical meaning of the four controls and assuming that they are independent, we made a second assumption: that the fluorescence generated by esterase (via **Opt→Std** in the presence of Glu-C) is *directly proportional* to $[P]_t$. In other words, we take the ratio of product fluorescence to maximal possible fluorescence (once all substrate is consumed, $F_t^{\max}$) and scale it by the initial substrate concentration, $[S]_0$, obtaining:

$$[P]_t = \frac{F_t^{\text{esterase + Glu-C}} - \left(F_t^{\text{Glu-C}} - F_t^{\text{esterase}}\right) - fF_t^{\text{esterase}}}{F_t^{\max}}[S]_0 \tag{S3}$$

and

$$f = \frac{[\mathrm{S}]_t}{[\mathrm{S}]_0} = \frac{[\mathrm{S}]_0 - [\mathrm{P}]_t}{[\mathrm{S}]_0} \tag{S4}$$

where f is the fraction of reaction species (*e.g.,* substrate and/or intermediate) that is not yet product. We assume that the substrate and intermediate have the same background fluorescence. Hence, intuitively, fF_t^{esterase} can be thought of as the change in background fluorescence from reaction spaces that are not product (large at the beginning of the reaction, small at later time points). Now, $F_t^{\text{Glu-C}}$–F_t^{esterase} is change in fluorescence that stems from Glu-C proteolysis of the substrate and/or substrate hydrolysis. We subtract constant F_t^{esterase} from $F_t^{\text{Glu-C}}$ because very little substrate gets consumed in the Glu-C alone control during our assays. Finally, we subtract fF_t^{esterase} and $F_t^{\text{Glu-C}}$–F_t^{esterase} from $F_t^{\text{esterase + Glu-C}}$ to cleanly isolate the fluorescence due to fluorescence of **Opt→Std** caused by esterase (in the presence of Glu-C). Plugging eq S4 into eq S3 and solving for $[\mathrm{P}]_t$ we obtain the final formula that we use throughout this manuscript for converting fluorescence of four blank-subtracted controls into $[\mathrm{P}]_t$:

$$[\mathrm{P}]_t = \frac{F_t^{\text{esterase + Glu-C}} - F_t^{\text{Glu-C}}}{F_t^{\max} - F_t^{\text{esterase}}}[\mathrm{S}]_0 \tag{S5}$$

Conditions required for using eq S5:

1. Glu C-mediated cleavage of **Opt** into **Std** is nearly instantaneous ($[\mathrm{P}]_t \approx [\mathbf{Std}]_t$) (see Figure 4A for confirmation).
2. PLE does not observably cleave the esterified substrate ($F_t^{\text{esterase}} \approx F_t^{\text{substrate}}$, or F_t^{esterase} is constant, as we confirm in all our experiments; see Figure 5A for an example).
3. All reaction species upstream of product have the same background fluorescence (*i.e.,* the background fluorescence of intermediate is the same as that of the substrate; in other words, in eq S4, $[\mathrm{S}]_0 - [\mathrm{P}]_t \approx [\mathrm{S}]_t + [\mathrm{I}]_t$, since $[\mathrm{S}]_0 \approx [\mathrm{S}]_t + [\mathrm{I}]_t + [\mathrm{P}]_t$).
4. PLE and Glu-C combined behave the same way as they do when incubated with peptides separately (the four controls are independent).

Using eq S5, $[\mathrm{P}]_t$ was calculated for each esterified substrate using fluorescence data in Figure 5A. The resultant plots are shown in Figure S18. See "Statistical Analysis: Computing Errors" for details on data analysis.

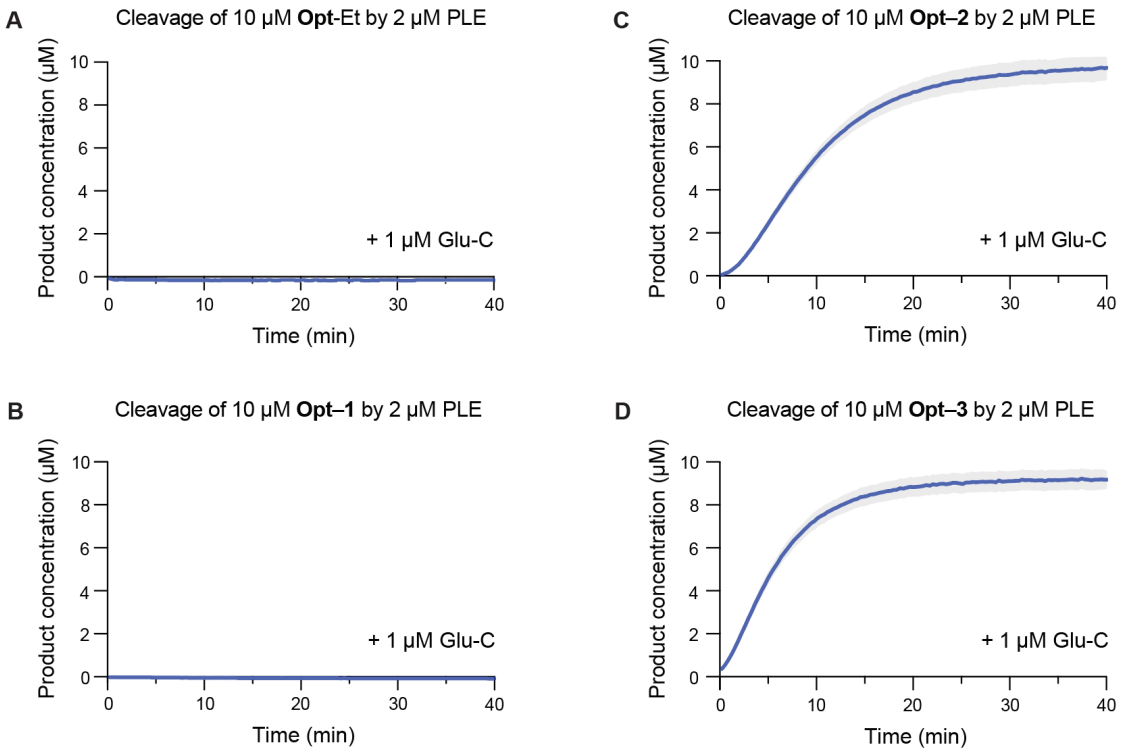

Figure S18. $[P]_t$ formed as a result of PLE-mediated cleavage of esters in (A) **Opt**-Et, (B) **Opt**–**1**, (C) **Opt**–**2**, and (D) **Opt**–**3** in 10 mM HEPES–NaOH buffer, pH 7.4, containing DMF (1.5% v/v) and Triton X-100 (0.8% w/v) in the presence of Glu-C. Gray areas represent the SD. n = 1 independent replicates, n = 3 technical replicates. For parent fluorescence data, see Figure 5A.

VII-3a. Ruling out Glu-C Inhibition by Opt–1, a Phenolic Intermediate Mimetic

To rule out Glu-C inhibition by **Opt**–**1** and the phenolic intermediate, we evaluated the ability of Glu-C to cleave **Opt** in the presence of **Opt**–**1** (a stable structural mimetic of the phenolic intermediate with the OH group replaced by CH_3). We performed this experiment using 1 µM Glu-C, 5 µM **Opt**, and 5 µM **Opt**–**1**. A 2× solution (10 µM) of **Opt** and a 4× solution of **Opt**–**1** (20 µM) were prepared in 10 mM HEPES–NaOH buffer, pH 7.4, containing 3% v/v DMF and 0.8% w/v Triton X-100 by diluting the stock solution in DMF. A 4× solution of Glu-C (4 µM) was prepared in 10 mM HEPES–NaOH buffer, pH 7.4, containing 0.8% w/v Triton X-100 from the stock solution in water and placed on ice. See "Preparation of Stock Solutions of Glu-C and Peptides" for more details. To wells of a 96-well plate were added 50 µL of the 2× solution of **Opt**. The plate was placed into a pre-warmed plate reader for 10 min to pre-equilibrate it to 37 °C. The following two strips of 9 PCR tubes were prepared: (1) strips containing 35 µL of 4× **Opt**–**1** solution or buffer (10 mM HEPES–NaOH buffer, pH 7.4, containing 0.8% w/v Triton X-100), and (2) strips containing 45 µL of 4× solution of Glu-C. Using a multichannel pipet, 35 µL of PCR strip 2 was added to PCR strip 1 (the resultant solutions contained either 2 µM Glu-C, 2 µM Glu-C and 10 µM **Opt**–**1**, or 10 µM **Opt**–**1**). The 70 µL solutions along with a set of pipet tips were placed into an incubator to equilibrate them to 37 °C for 10 min and to give **Opt**–**1** the time to bind

Glu-C if Glu-C inhibition by phenolic intermediate was going to be a problem. After 10 min, using a multichannel pipet, 50 µL of the 70 µL solution was rapidly added to the 50 µL solution of **Opt** in the 96-well plate. The plate was rapidly returned into the plate reader and shaken for 15 s at 37 °C to allow for proper mixing and temperature equilibration. The measurements were taken every 20 s for 10 min post-shaking (see "Instrumentation" for details on plate-reader setup). Fluorescence values were averaged and blank (fluorescence of 10 mM HEPES–NaOH buffer, pH 7.4, containing 0.8% w/v Triton X-100) subtracted. See "Statistical Analysis: Computing Errors" for details. Fluorescence progress curves of **Opt** (5 µM) in the presence of Glu-C (1 µM), **Opt**–**1** (5 µM) in the presence of Glu-C (1 µM), and both **Opt** (5 µM) and **Opt**–**1** (5 µM) in the presence of Glu-C (1 µM) are shown in Figure S19. The results of this experiment show that **Opt**–**1** is not a Glu-C inhibitor under the tested conditions.

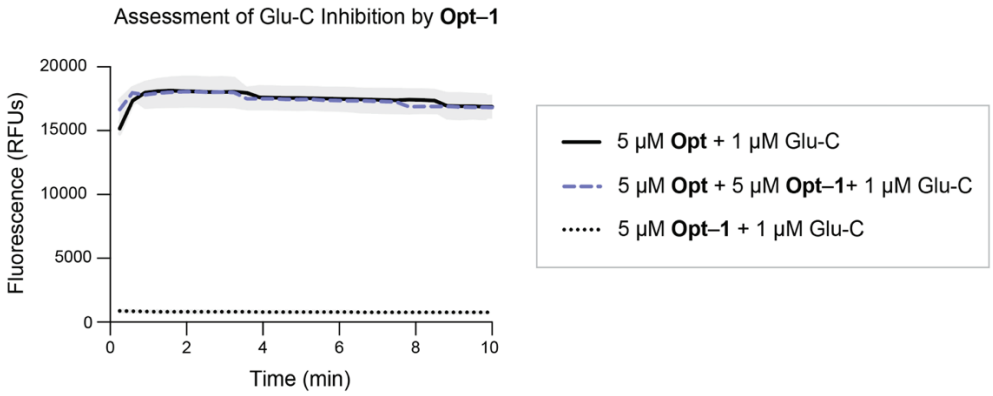

Figure S19. Fluorescence progress curves of **Opt** (5 µM) in the presence of Glu-C (1 µM), **Opt**–**1** (5 µM) in the presence of Glu-C (1 µM), and both **Opt** (5 µM) and **Opt**–**1** (5 µM) in the presence of Glu-C (1 µM). Assays were performed in 10 mM HEPES–NaOH buffer, pH 7.4, containing DMF (1.5% v/v) and Triton X-100 (0.8% w/v). Gray areas represent the SD. Progress curves were fitted from data points spaced apart by 20 s. $n = 2$ independent replicates, $n = 3$ technical replicates.

VII-3b. Ruling out PLE Inhibition by Opt–1, a Phenolic Intermediate Mimetic

We tested whether PLE gets inhibited by **Opt**–**1** for two reasons: (1) to provide evidence that **Opt**–**1** does not get cleaved because it does not bind the active site of PLE (*i.e.,* it is not an inhibitor), and (2) to rule out PLE inhibition by the phenolic intermediate, which **Opt**–**1** structurally resembles. We choose to access inhibition by comparing PLE-mediated cleavage of **Opt**–**3** in the absence and in the presence of **Opt**–**1**. Solutions (4× 20 µM) of **Opt**–**1** and **Opt**–**3** (a confirmed PLE substrate) were prepared in 10 mM HEPES–NaOH buffer, pH 7.4, containing DMF (3% v/v) and Triton X-100 (0.8% w/v) by diluting the stock solution in DMF. See "Preparation of Stock Solutions of Glu-C and Peptides" for more details. 4× solutions of PLE (16 µM and 100 nM) and Glu-C (4 µM) were prepared in 10 mM HEPES–NaOH buffer, pH 7.4, containing Triton X-100 (0.8% w/v). See "Absorbance-Based Concentration Measurements" for preparation of the PLE stock (lot activity: 62.6 U/mg). In wells of a 96-well plate were added 50 µL of buffer alone, 25 µL of **Opt**–**1** and 25 µL of buffer, 25 µL of **Opt**–**3** and 25 µL of buffer, or 25 µL of both **Opt**–**1** and

Opt–3. The plate was placed into a pre-warmed plate reader for 10 min to pre-equilibrate it to 37 °C. The following strips of PCR tubes each were prepared: (1) strips containing 45 µL of 4× Glu-C solution, and (2) strips containing 35 µL of 4× PLE solution. The PCR tubes together with a set of pipet tips were placed into an incubator to equilibrate them to 37 °C for 10 min. After 10 min, using a multichannel pipet, 35 µL of PCR strips containing Glu-C were added to PCR tubes containing PLE. Then, 50 µL of the resulting solutions were rapidly added to the 50 µL peptide solutions in the 96-well plate using a multichannel. The plate was rapidly returned into the plate reader and shaken for 15 s at 37 °C to allow for proper mixing and temperature equilibration. The measurements were taken every 20 s for ~40 min post-shaking (see "Instrumentation" for plate-reader setup). The final concentrations were: 5 µM of peptides, 4 µM or 25 nM of PLE, and 1 µM of Glu-C. Fluorescence values were averaged and blank (fluorescence of 10 mM HEPES–NaOH buffer, pH 7.4, containing 1.5% v/v DMF and 0.8% w/v Triton X-100) subtracted. See "Statistical Analysis: Computing Errors" for details on data analysis. The results of the experiment are shown in Figure S20. We did not observe any inhibition of PLE-mediated cleavage of **Opt–3** in the presence of **Opt–1**, which means that **Opt–1** does not compete for binding to the active site of PLE.

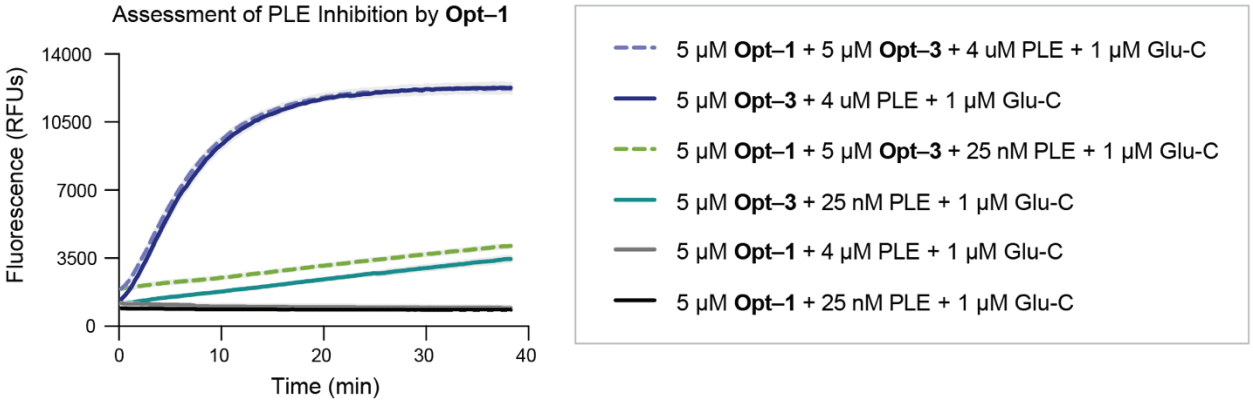

Figure S20. Fluorescence progress curves associated with the assessment of PLE inhibition by **Opt–1** using **Opt–3** as a cleavable control. Assays were performed in 10 mM HEPES–NaOH buffer, pH 7.4, containing DMF (1.5% v/v) and Triton X-100 (0.8% w/v). Gray areas represent the SD. Progress curves were fitted from data points spaced apart by 20 s. $n = 1$ independent replicates, $n = 3$ technical replicates.

VII-4. Primer: Evaluating k_I (Rate Constant of Intermediate Decay) and Esterase k_{cat} and K_M

VII-4a. The SIP (Substrate, Intermediate, Product) Model

As demonstrated in Figures 5B and S13B, esterase-mediated cleavage of **Opt–3** and **Opt–2** results in the generation of a phenolic intermediate that eventually collapses to **Opt** through 1,6-quinone methide elimination. Our assay directly reports on $[P]_t$, or the formation of **Opt** (as **Opt** is instantaneously cleaved to **Std**, producing fluorescence). Data in Figures 5B and S13B further indicate that, in the presence of 2 μM PLE, the rate-limiting step of **Opt** formation is quinone methide elimination, not esterase cleavage. Because of the intermediate, we cannot use the traditional Michaelis–Menten equation to calculate k_{cat} and K_M, as we first need to measure the rate constant (k_I) of intermediate decay to **Opt**. This rate constant is also important in itself, as it can provide insights into the rate, significance, and tunability of quinone methide elimination in biological settings. To account for the formation of the intermediate in our experiments, we updated the traditional Michaelis–Menten model, constructing a new model called SIP (substrate → intermediate → product). The key steps of SIP are shown in Figure 6 and in Figure S21. "E" refer to the esterase, and "E·S" refers to the esterase·substrate complex. SIP relies on the assumption that quinone methide elimination follows first-order kinetics due to irreversible quinone methide quenching by water, as has been assumed previously in a similar model without enzyme.[26]

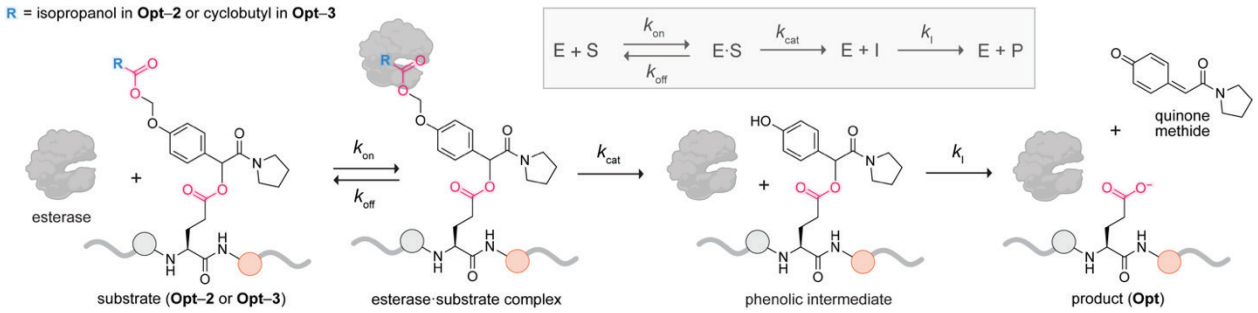

Figure S21. The substrate → intermediate → product (SIP) model that describes our system. This figure is identical to Figure 6 of the main text.

Upon constructing the SIP model (Figures 6 and S21), we can write out all the differential equations describing the rates of change of reaction species in this model

$$\frac{\mathrm{d}[\mathrm{P}]}{\mathrm{d}t} = k_\mathrm{I}[\mathrm{I}]_t \tag{S6}$$

$$\frac{\mathrm{d}[\mathrm{I}]}{\mathrm{d}t} = k_\mathrm{cat}[\mathrm{ES}]_t - k_\mathrm{I}[\mathrm{I}]_t \tag{S7}$$

$$\frac{\mathrm{d}[\mathrm{S}]}{\mathrm{d}t} = k_\mathrm{off}[\mathrm{ES}]_t - k_\mathrm{on}[\mathrm{E}]_t[\mathrm{S}]_t$$

(S8)

$$\frac{\mathrm{d[E]}}{\mathrm{d}t} = k_{\mathrm{off}}[\mathrm{ES}]_t + k_{\mathrm{cat}}[\mathrm{ES}]_t - k_{\mathrm{on}}[\mathrm{E}]_t[\mathrm{S}]_t$$

(S9)

$$\frac{\mathrm{d[ES]}}{\mathrm{d}t} = k_{\mathrm{on}}[\mathrm{E}]_t[\mathrm{S}]_t - k_{\mathrm{off}}[\mathrm{ES}]_t - k_{\mathrm{cat}}[\mathrm{ES}]_t$$

(S10)

and define K_M in the traditional manner

$$K_{\mathrm{M}} = \frac{k_{\mathrm{off}} + k_{\mathrm{cat}}}{k_{\mathrm{on}}}$$

(S11)

These equations are useful when thinking of regimes where the SIP model can be simplified to first solve for k_I and then for k_{cat} and K_M. In the following sections, we will discuss two enzyme regimes of SIP model: large (Figures 7B and S22A) and small $[E]_0$ (Figures 7C and S22B).

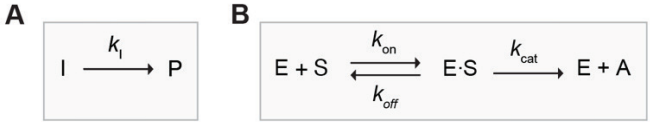

Figure S22. (A) Large $[E]_0$ regime of the SIP model, which enables k_I measurement. (B) Small $[E]_0$ regime of the SIP model, which allows k_{cat} and K_M measurement once k_I is known.

VII-4b. Evaluating k_I as well as Intermediate and Substrate Evolution Curves

When $[E]_0$ is sufficiently large, we expect the kinetic barrier between E + I and E + P to control the rate of product formation in the SIP model (Figures 6 and 7A), enabling k_I isolation. Thus, in the regime of sufficiently large $[E]_0$, our SIP model would reduce to first-order kinetics (Figures 7B and S22A). We choose a time t_x such that $[S]_{tx} \approx 0$ for $t > t_x$ (see later discussion on how to ensure that this constraint holds via self-consistency checks). At $t > t_x$, the relationship

$$[\mathrm{P}]_t + [\mathrm{I}]_t = [\mathrm{P}]_\infty$$

(S12)

holds, where $[P]_\infty$ is [P] at late times (*i.e.,* the plateau of the $[P]_t$ curve). Integrating eq S12 from t_x to t, we obtain

$$[\mathrm{I}]_t = [\mathrm{I}]_{t_x} e^{-k_I(t-t_x)}$$

(S13)

which is virtually the equation that is used to describe first-order kinetics. Next, we can combine eq S12 with eq S13 and write a formula for $[P]_t$:

$$[P]_t = [P]_\infty - [I]_{t_x} e^{-k_I(t-t_x)} \tag{S14}$$

Numerically, eq S14 can be fitted to experimental $[P]_t$ data from an esterase assay with sufficiently large $[E]_0$ with three free parameters: $[P]_\infty$, $[I]_{t_x}$, and k_I. $[P]_t$ is obtained from $F_t^{\text{esterase + Glu-C}}$, F_t^{esterase}, $F_t^{\text{Glu-C}}$, and $F_t^{\max}$ for an individual esterase substrate using eq S5. Note that t_x does not need to be at the very start of the experiment; there just needs to eventually exist a time window for fitting, $t_x < t < t_y$, where S has already decayed to zero before P has come to completion. To choose the right time window, we perform several self-consistency checks. First, we fit eq S14 in a few time windows and choose one in which k_I does not significantly change. We perform the fitting by feeding $[P]_t$ data into the curve_fit function (scipy library) in Python. Second, we later verify that $[I]_{t_x}$, $[S]_{t_x}$, is indeed very close to zero (see discussion accompanying eq S20). To find the half-life of the phenolic intermediate, we use the well-known equation from first-order kinetics:

$$t_{1/2} = \frac{\ln 2}{k_I} \tag{S15}$$

Once k_I is known, we can compute $[I]_t$ by re-writing eq 6 as

$$[I]_t = \frac{1}{k_I}\frac{d[P]}{dt} \tag{S16}$$

The derivative $d[P]/dt$ can be approximated as a discrete derivative

$$\frac{d[P]}{dt} = \frac{[P]_{(t+n_r\Delta t)} - [P]_{(t-n_l\Delta t)}}{(n_r + n_l)\Delta t} \tag{S17}$$

for a suitable choice of integer n_r and n_l. For instance, $n_r = 1$ and $n_l = 0$ gives the usual discrete derivative whereas $n_r = 1$ and $n_l = 1$ is the more numerically stable central difference approximation. In our analysis, we set $n_r = n_l = 2$, but we have confirmed that the results are not sensitive to this particular choice. In summary,

$$[I]_t = \frac{1}{k_I}\frac{[P]_{(t+n_r\Delta t)} - [P]_{(t-n_l\Delta t)}}{(n_r + n_l)\Delta t} \tag{S18}$$

As an additional self-consistency check, we ensure that $[\mathrm{I}]_{t_x}$ obtained from the fit of eq S14 matches the value of $[\mathrm{I}]_{t_x}$ obtained from eq S18. If these two values are very close, $t_x < t < t_y$ was likely determined correctly. Using the conservation law

$$[\mathrm{S}]_0 = [\mathrm{S}]_t + [\mathrm{I}]_t + [\mathrm{P}]_t \tag{S19}$$

we can compute

$$[\mathrm{S}]_t = [\mathrm{S}]_0 - [\mathrm{I}]_t - [\mathrm{P}]_t \tag{S20}$$

from known values of $[\mathrm{I}]_t$ and $[\mathrm{P}]_t$. As an extra self-consistency check, it is important to verify that at time t_x, $[\mathrm{S}]_{tx}$ is indeed close to zero. An example of evaluating k_I, $t_{1/2}$, $[\mathrm{I}]_t$, and $[\mathrm{S}]_t$ corresponding to Opt–**3** cleaved by PLE is described in the "Evaluating k_I Using the Optimal PLE Concentration". The results are displayed in Figure 8. The datasets and Python code used to find k_I, $t_{1/2}$, $[\mathrm{I}]_t$, and [S]t shown in Figure 8 are freely available via the following GitHub link: https://github.com/yana-d-petri/Finding-kI-and-kcat-KM-using-fluorescence-data-from-Glu-C-assay. For a description of statistical analysis used to compute errors in Python, see "Statistical Analysis: Computing Errors".

How to ensure that $[E]_0$ used in the experiment for evaluating k_I is sufficiently large? A few things need to be considered here. First, experimentally, once $[\mathrm{E}]_0$ is increased sufficiently, the rate of product formation becomes independent of the concentration of esterase. In our particular case, when $[\mathrm{E}]_0$ is "sufficiently large", the rates of product formation due to **Opt**–**2** and **Opt**–**3** cleavage by PLE should become the same, since, upon cleavage, these esterified substrates can transition through the same phenolic intermediate. Second, theoretically, for accessing the first-order regime of the SIP model (Figures 7B and S22A) and using eq S14 to measure k_I, the constraint $k_I < k_{cat}$ needs to hold (since, in contrast to the first step, the second step cannot be arbitrarily sped up by solely tuning $[\mathrm{E}]_0$, see Figures 6 and S21). When $k_I \geq k_{cat}$, k_I cannot be measured experimentally because the intermediate decay occurs after the rate-limiting step. (Fortunately, k_I then also becomes unimportant and can be disregarded in assessing esterase kinetics.) Hence, $k_I < k_{cat}$ is necessary to measure k_I. Mathematically, in the particular scenario when

$$k_\mathrm{I} \ll k_\mathrm{cat} \tag{S21}$$

we can prove that "sufficiently large" $[\mathrm{E}]_0$ to measure such k_I would be:

$$[\mathrm{E}]_0 > \frac{k_\mathrm{I}(K_\mathrm{M} + [\mathrm{S}]_0)}{k_\mathrm{cat}} \tag{S22}$$

Proving that relationships in eq S21 and eq S22 are sufficient for accessing the first-order kinetics regime of the SIP model. Let us introduce the notation $E' = (k_I/k_{cat})(K_M + [S]_0)$ for convenience (see eq 22). We will now show that if $k_I \ll k_{cat}$ and $[E]_0 > E'$, then S will have decayed into the intermediate before the intermediate has decayed into product, giving us a large enough window for fitting eq S14 (see Figure 8 for an example; the window refers to the separation between the green curve and the red curve). The idea will be to show that these two conditions imply that $k_S > k_I$, where k_S is the effective rate describing the speed at which S decays (in our case into I). When $k_S > k_I$, our SIP model reduces to first-order kinetics (*i.e.*, I still decays into P while S is close to 0). Our approach will be to show that $k_S = k_I$ holds if $[E]_0 = E'$, directly implying that $k_S > k_I$ if $[E]_0 > E'$ because k_S increases as we increase enzyme concentration for a fixed substrate concentration (indeed, increasing enzyme concentration cannot slow down the decay of S). Let us thus set $[E]_0 = E'$, which implies that $[E]_0/(K_M + [S]_0) = k_I/k_{cat} \ll 1$, where we used $k_I \ll k_{cat}$ in the last step. Intriguingly, this relationship implies that for $[E]_0 = E'$, the quasi-steady-state approximation (qSSA) holds (*i.e.,* $[E]_0 \ll K_M + [S]_0$), from which one can derive[29,30] that $k_S = k_{cat}[E]_0/(K_M + [S]_0) = k_I[E]_0/E'$. This k_S is the timescale for the whole process of converting S into I; it is not reflecting an instantaneous rate, which would have dependent on [S] rather than $[S]_0$. Because $[E]_0 = E'$, we indeed obtain $k_S = k_I$. To summarize, $k_S > k_I$ if $[E]_0 > E' = (k_I/k_{cat})(K_M + [S]_0)$, completing our proof.

Note Note that the larger is the enzyme concentration above the threshold in eq S22, the larger is k_S relative to k_I. A larger enzyme concentration would enlarge the fitting window for determining k_I (using eq S14), hence making the fit more accurate. However, as can be seen from a simple RIP model (see link to the code below), which is a simplistic approximation of our model in the large $[E]_0$ regime, even when $k_S \approx k_I$ we can still find a fitting window, $t_x < t < t_y$, where the fit is relatively accurate. However, to ensure the accuracy of the fit, the users would need to perform the self-consistency checks that we previously mentioned. Specifically, they need to (1) ensure that the value of k_I does not strongly depend on the chosen $t_x < t < t_y$, (2) check, after k_I is fit, that $[S]_{tx}$ is indeed close to 0, and (3) verify that the fitted $[I]_{tx}$ closely match the one plotted using eq S18 and the fitted k_I.

The GitHub link to Python code containing plots of the RIP model, variable input k_S and k_I, as well as fitted k_I and its error are freely available via this link: https://github.com/yana-d-petri/ki-fitting-window-relative-to-ks-and-ki-magnitude. The equation form the RIP model can be found in the review by Schmidt and Jullien.[26]

VII-4c. Defining a New Term, "A", and Evaluating Esterase k_{cat} and K_M

Once k_I is known (see the section above for accessing a sufficiently large $[E]_0$ regime to evaluate k_I), we can define a new term

$$[A]_t = [P]_t + [I]_t \tag{S23}$$

which allows us to "re-package" the tradition Michaelis–Menten equation[31] in familiar terms (Figures 7C and S22B). The transformed Michaelis–Menten equation then becomes

$$\frac{d[A]}{dt} = \frac{k_{cat}[E]_0[S]_t}{K_M + [S]_t} \tag{S24}$$

By combining eqs S6 and S17, we can re-write $[A]_t$ in terms of known quantities

$$[A]_t = [P]_t + \frac{1}{k_I}\frac{[P]_{(t+n_r\Delta t)} - [P]_{(t-n_l\Delta t)}}{(n_r + n_l)\Delta t} \tag{S25}$$

making $[A]_t$ and $d[A]/dt$ solvable. Equation S24 then also becomes solvable for k_{cat} and K_M under the traditional Michaelis–Menten experimental conditions when the qSSA is valid (*i.e.,* $[E]_0 \ll K_M + [S]_0$, or what we call the "low enzyme regime"). In our particular setup, we will work in the linear regime (when $[A]_t$ is linear with t) where $[S]_t$ can be replaced by $[S]_0$ in eq S24, yielding

$$\frac{d[A]}{dt} = \frac{k_{cat}[E]_0[S]_0}{K_M + [S]_0} \tag{S26}$$

Experimentally, solving for kinetic constants of esterase requires evaluating $[P]_t$ as a function of time for various $[S]_0$. Using eq 25, known k_I, and $[P]_t$, we computed $[A]_t$ for each $[S]_0$ and plotted it as a function of t. Then, to find $d[A]/dt$ for each $[S]_0$, we used the curve_fit function in Python to fit $[A]_t$ evolution to a function $y = ax + b$, where $a = d[A]/dt$, and b is not forced to be 0. Note that, to ensure that $[A]_t$ is within the initial-rates regime, we used only $[A]_t$ values <10% of $[S]_0$ for the linear fitting. To calculate k_{cat} and K_M separately, $d[A]/dt$ versus $[S]_0$ can then be plotted and the resultant graph can be fitted to eq S26 if the tested $[S]_0$ reaches $\geq 10 \times K_M$[32] or the integrated LambertW function can be used if the tested $[S]_0$ is on the order of K_M.[33] However, in our specific case, the largest tested $[S]_0$ was $\ll K_M$, as indicated by a linear relationship between $d[A]/dt$ and $[S]_0$ (see Figure 9C). We tested $[S]_0$ up to 10 μM due to inner filter effect constrains (see "Inner Filter Effect Characterization and Limit of Detection (LOD)"). To find k_{cat}/K_M for our specific

case, we found the slope of the d[A]/dt versus $[S]_0$ graph ($y = ax + b$, where b is not forced to be 0) using the curve_fit function (scipy library) in Python. The value of k_{cat}/K_M was computed from the slope of the resultant line using the equation:

$$\frac{k_{cat}}{K_M} = \frac{\text{slope}}{[E]_0} \tag{S27}$$

An example of evaluating k_{cat}/K_M associated with Opt–**2** cleavage by PLE is described in the section "Evaluating k_{cat}/K_M of PLE with **Opt**–**2**". The results are displayed in Figure 9. The corresponding datasets and Python code used to find k_{cat}/K_M are freely available via the following GitHub link: https://github.com/yana-d-petri/Finding-kI-and-kcat-KM-using-fluorescence-data-from-Glu-C-assay. For a description of statistical analysis used to compute errors with Python, see section "Statistical Analysis: Computing Errors".

What is the experimental setup sufficient for using this "re-packaged" eq 24 to find k_{cat}/K_M? To be in the quasi-steady-state regime, we need to satisfy $[E]_0 \ll K_M + [S]_0$ (what we call the "low enzyme regime"). In our specific case, we used eq 26 because we used the liner portion of the $[A]_t$ versus t plot (assuming that $[S]_t \approx [S]_0$ for the linear portion).

VII-5. Evaluating k_I of Opt–2 and Opt–3 Upon Ester Cleavage by PLE

VII-5a. Identifying a "Sufficiently Large" PLE Concentration for Evaluating k_I

To find k_I, we first needed to identify a PLE concentration at which the rates of **Opt**–**2** and **Opt**–**3** conversion into product were (1) independent of PLE, and (2) identical (since **Opt**–**2** and **Opt**–**3** can transition through the same phenolic intermediate upon esterase cleavage). For detailed description of evaluating k_I, see "Evaluating k_I as well as Intermediate and Substrate Evolution Curves". Solutions (2× 20 μM) of **Opt**–**2** and **Opt**–**3** were prepared in 10 mM HEPES–NaOH buffer, pH 7.4, containing DMF (3% v/v) and Triton X-100 (0.8% w/v) by diluting the stock solution in DMF. 4× solutions of PLE (64 μM, 32 μM, 16 μM, and 8 μM) and Glu-C (4 μM) were prepared in 10 mM HEPES–NaOH buffer, pH 7.4, containing Triton X-100 (0.8% w/v). See "Absorbance-Based Concentration Measurements" for the preparation of the PLE stock (lot activity: 62.6 U/mg) and "Preparation of Stock Solutions of Glu-C and Peptides" for more details. Aliquots (50 μL) of 20 μM peptide solutions were added to wells of a 96-well plate. The plate was placed into a pre-warmed plate reader for 10 min to pre-equilibrate it to 37 °C. The following 2 strips of 12 PCR tubes each were prepared: (1) strips containing 45 μL of 4× Glu-C solution, and (2) strips containing 35 μL of 4× PLE solutions. The 2 strips of PCR tubes together with a set of pipet tips were placed into an incubator to equilibrate them to 37 °C for 10 min. After 10 min, using a multichannel pipet, 35 μL of PCR strip 1 was added to PCR strip 2 (resulting in a solution containing 32 μM, 16 μM, 8 μM, or 4 μM PLE and 2 μM Glu-C). Then, 50 μL of these solutions were rapidly added to the 50 μL peptide solutions in the 96-well plate using a multichannel. The plate was rapidly returned into the plate reader and shaken for 15 s at 37 °C to allow for proper mixing and temperature equilibration. The measurements were taken every 20 s for 40 min post-shaking (see "Instrumentation" for plate-reader setup). The final concentrations were: 10 μM of esterified peptides; 2, 4, 8, or 16 μM of PLE; and 1 μM of Glu-C. Fluorescence values were averaged and blank (fluorescence of 10 mM HEPES–NaOH buffer, pH 7.4, containing 1.5% v/v DMF and 0.8% w/v Triton X-100) subtracted. See "Statistical Analysis: Computing Errors" for details on data analysis. Progress curves of **Opt**–**2** (Figure S23A) and **Opt**–**3** (Figure S23B) cleavage in the presence of various concentrations of PLE (read out by Glu-C fluorescence) suggested that, for both esterified peptides, the rate of product formation was maximal in the presence of 4 μM PLE. Higher concentrations of PLE resulted in fluorescence suppression artifacts (as suggested by a decreased fluorescence intensity of the plateau), potentially related to the loss of active Glu-C or some competition effect resulting in decreased ability of Glu-C to bind the de-esterified peptide. As a consistency check, we ensured that, at higher concentrations of PLE, the rates of product formation for **Opt**–**2** and **Opt**–**3** become similar (see Figure S24 for an alternative data representation).

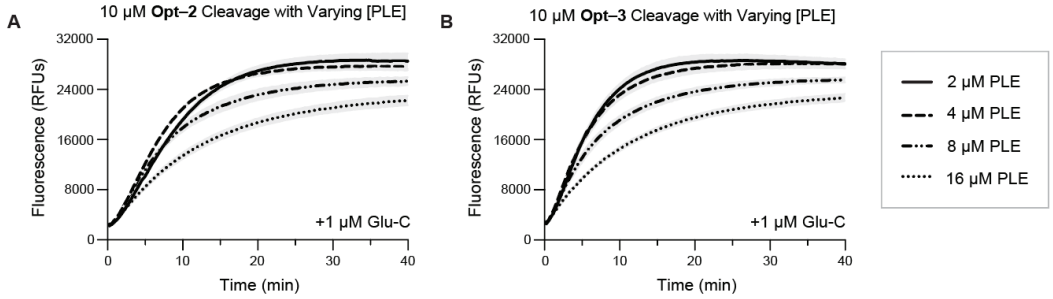

Figure S23. Fluorescence progress curves related to assaying cleavage of (A) **Opt**–**2**, and (B) **Opt**–**3** esters in the presence of various concentrations of PLE. Assays were performed in 10 mM HEPES–NaOH buffer, pH 7.4, containing DMF (1.5% v/v) and Triton X-100 (0.8% w/v). Gray areas represent the SD. Progress curves were fitted from data points spaced apart by 20 s. $n = 1$ independent replicates, $n = 3$ technical replicates.

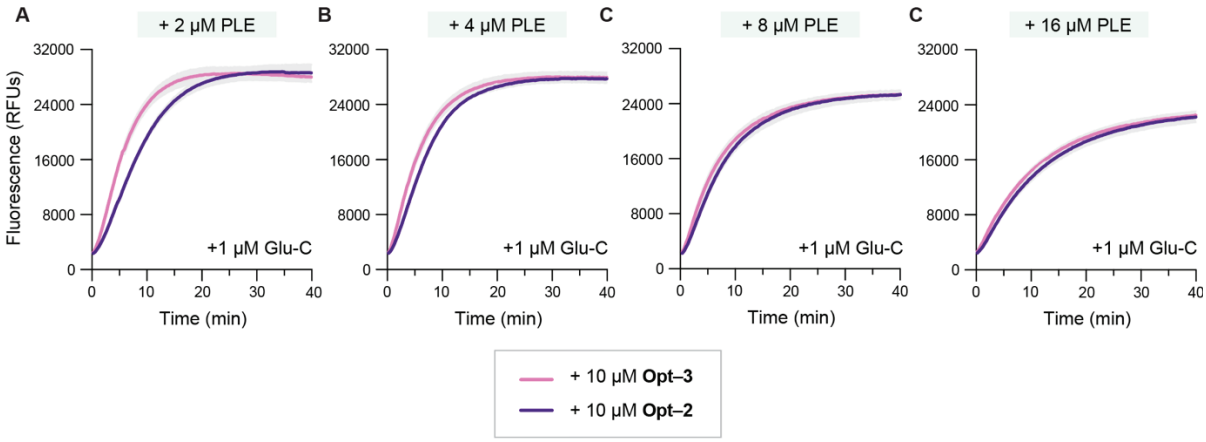

Figure S24. Another representation of the data presented in Figure S23 emphasizing that the rates of product formation for **Opt**–**2** and **Opt**–**3** become similar at higher [PLE].

VII-5b. Evaluating k_I Using the Optimal PLE Concentration

The experiment described in "Assaying Esterified Peptides for Cleavage by PLE" was repeated with **Opt** and **Opt**–**3** except the final concentration of PLE in the assay was changed from 2 μM to 4 μM (see the section above for the reasoning behind the selection of 4 μM as the optimal PLE concentration). The final concentrations of **Opt** and **Opt**–**3** in the assay was 10 μM and the final concentration of Glu-C was 1 μM. The fluorescence of the buffer (10 mM HEPES–NaOH buffer, pH 7.4, containing 1.5% v/v DMF and 0.8% w/v Triton X-100) was subtracted from each experimental fluorescence curve. See "Statistical Analysis: Computing Errors" for details on blank subtraction, averaging, error propagation methods, and statistical analysis used to compute errors with Python. Progress curves of **Opt**–**3** cleavage by PLE (read out by Glu-C fluorescence) are shown in Figure S25A with all corresponding controls. Using eq S5, the fluorescence(t) values were converted into product concentration(t) values and plotted in Figure 25B. (This figure also appears as Figure 8 of the main text.) Using the method described in "Evaluating k_I as well as Intermediate and Substrate Evolution Curves", $[P]_t$ versus t data were fitted with Python to eq S14 with three free parameters (k_I, $[P]_\infty$, and $[I]_{t_x}$). For fitting, we selected a time window $t_x < t < t_y$, where t_x = 250 s and t_y = 1500 s, and checked that the obtained value of k_I was not strongly dependent on this particular choice. As a further self-consistency check, we ensured that, at the chosen t_x, $[S]_t$ was close to 0 (Figure 8), and the value of $[I]_{tx}$ obtained from the fit matched the one plotted (Table S2). The calculated exponential fit (dashed line) was overlaid with the experimental $[P]_t$ versus t data in Figure S25B and showed a good overlap, suggesting that the chosen model is suitable. The three free fitting parameters obtained from the fit, $t_{1/2}$ of the phenolic intermediate (calculated using eq S15), and their 95% confidence interval (1.96 × SD), are reported in Table S2. In Figure S25B, we also plotted $[I]_t$ and $[A]_t = [I]_t + [P]_t$ evolution, as these progress curves could be easily computed from eqs S18 and S25, respectively. The corresponding datasets and Python code used for data plotting, evaluating the free parameters (k_I, $[P]_\infty$, and $[I]_{t_x}$), $[I]_t$, $[A]_t = [I]_t + [P]_t$, and computing errors are freely available via this GitHub link: https://github.com/yana-d-petri/Finding-kI-and-kcat-KM-using-fluorescence-data-from-Glu-C-assay.

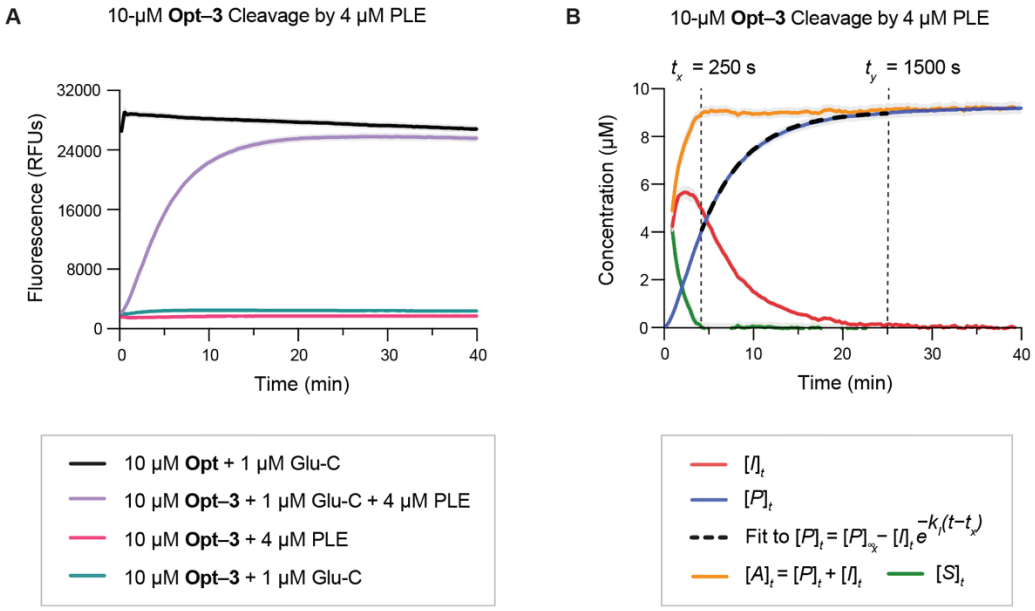

Figure S25. (A) Fluorescence progress curves related to assaying PLE (4 μM) cleavage of **Opt–3** (10 μM). (B) $[P]_t$, $[I]_t$, and $[A]_t$ formed as a result of PLE-mediated cleavage of **Opt–3** computed from the Glu-C assay dataset in (A). Assays were performed in 10 mM HEPES–NaOH buffer, pH 7.4, containing DMF (1.5% v/v) and Triton X-100 (0.8% w/v). Gray areas represent the SD. Progress curves were fitted from data points spaced apart by 20 seconds. $n = 2$ independent replicates, $n = 3$ technical replicates. Figure S25B also appears as Figure 8 in the main text.

Table S2. Parameters and half-life (eq S15) of the quinone methide intermediate obtained upon fitting eq S14 to $[P]_t$ data.

Parameter	Fit output (eq S14)	95% confidence interval
k_I	0.00325 s^{-1}	± 0.00020 s^{-1}
$t_{1/2}$	3.55 min	± 0.22 min
$[P]_\infty$	9.08 μM	± 0.10 μM
$[I]_{tx}$	5.04 μM	± 0.11 μM

VII-6. Evaluating k_{cat}/K_M of PLE with Opt–2

Once k_I was calculated from experimental data (Figures 8 and S25B), we proceeded to apply the method described in "Defining a New Term, "A", and Evaluating Esterase k_{cat} and K_M") to find the k_{cat}/K_M of one of the cleavable, intermediate-forming esterase substrates, **Opt**–**2**, with enzyme PLE as a proof-of-concept. **Opt**–**2** is a slightly worse PLE substrate than **Opt**–**3**, hence the k_{cat}/K_M value of **Opt**–**2** would be a lower bound of the k_{cat}/K_M value of **Opt**–**3**. To assume $[S]_t \approx [S]_0$ in eq S26, we needed to operate under experimental conditions where $[E]_0 \ll K_M + [S]_0$. Literature data for PLE and small-molecule substrates indicated that reported K_M values on the lower end of the spectrum are in the 0.5–50 μM range.[34-36] We assumed that, since **Opt**–**2** is a bulkier esterase substrate than a small molecule, the K_M of **Opt**–**2** is unlikely to be lower than 1 μM. Based on this logic, we chose $[E]_0$ = 25 nM. Next, we proceeded to choose $[S]_0$ concentrations to test with 25 nM PLE. We chose eight $[S]_0$ (10×0.7^0, 10×0.7^1, 10×0.7^2, 10×0.7^3, 10×0.7^4, 10×0.7^5, 10×0.7^6, and 10×0.7^7 μM) within the 0–10 μM range of the Glu-C assay wherein inner filter effect was deemed negligible (Figure S10). The experiment detailed in "Assaying Esterified Peptides for Cleavage by PLE" was repeated with **Opt** and **Opt**–**2** except: (1) the final concentration of PLE in the assay was changed from 2 μM to 25 nM, (2) measurements were collected for 1 h, and (3) instead of testing a single final concentration of 10 μM for both **Opt** and **Opt**–**2**, a broader range of final concentrations was tested (10×0.7^0, 10×0.7^1, 10×0.7^2, 10×0.7^3, 10×0.7^4, 10×0.7^5, 10×0.7^6, and 10×0.7^7 μM). Note that [**Opt**] = [**Opt**–**2**] for each of the 8 tested final concentrations. The final concentration of Glu-C in the assay was 1 μM. The fluorescence of the buffer (10 mM HEPES–NaOH buffer, pH 7.4, containing 1.5% v/v DMF and 0.8% w/v Triton X-100) was subtracted from each experimental fluorescence curve. See "Statistical Analysis: Computing Errors" for details on blank subtraction, averaging, error propagation methods, and statistical analysis used to compute errors with Python. Using eq S5, the recorded fluorescence(t) values (n = 3 of each of blank-subtracted $F_t^{\text{esterase + Glu-C}}$, F_t^{esterase}, $F_t^{\text{Glu-C}}$, and $F_t^{\max}$ progress curves at a single final $[S]_0$ for a single experiment; 8 total experiments for 8 tested $[S]_0$, n = 2 independent replicates) were converted into product concentration(t) values and plotted in Figure 9A. Next, using the previously calculated value of k_I (Table S2), $[A]_t$ values were computed using eq S25. Note that, to ensure that $[A]_t$ is within the initial rates regime, we only used $[P]_t$ values <10% of $[S]_0$ for computing $[A]_t$. The plot of $[A]_t$ versus t for each of the final concentrations of $[S]_0$ is shown in Figure 9B. In contrast to $[P]_t$ progress curves, $[A]_t$ progress curves are strikingly linear. The linearity of $[A]_t$ progress curves is highly dependent on the value of k_I used to calculate them (we tested 3× higher and 3× lower k_I values than the k_I reported in Table S2 and noticed that $[A]_t$ versus t plots begin to lose linearity). These observations served as a self-consistency check, suggesting that k_I was determined correctly. Using the curve_fit function (scipy library) in Python, $d[A]/dt$ was calculated for each of the $[A]_t$ versus t plots assuming a linear fit and the resultant values of $d[A]/dt$ versus $[S]_0$ were plotted in Figure 9C. The plot in Figure 9C is linear, suggesting that the tested $[S]_0$ values are less than the K_M of **Opt**–**2**. Hence, the K_M value of **Opt**–**2** is $\gg$ 10 μM. Using the curve_fit function (scipy library) in Python, the slope of $d[A]/dt$ versus $[S]_0$ was calculated using a linear fit and from it the value of k_{cat}/K_M of **Opt**–**2** and its 95% confidence

interval (1.96 × SD) was obtained (see the table in Figure 9C for the values). The corresponding datasets and Python code used for data plotting, evaluating k_{cat}/K_M, and computing errors are freely available via this GitHub link along with code outputs: https://github.com/yana-d-petri/Finding-kI-and-kcat-KM-using-fluorescence-data-from-Glu-C-assay.

VIII. Assaying Esterified Peptides for Cleavage by Human Carboxylesterases

VIII-1. Cleavage Assays with Human Carboxylesterase 2 (CES2)

A 4× solution (200 nM) of recombinant CES2 (50 μg from MedChemExpress, see "Biological Reagents and Supplies" for product specifications) was prepared by dissolving the solid in 4.17 mL of cold 10 mM HEPES–NaOH buffer, pH 7.4, assuming the molecular weight of 60 kDa. In our hands, only CES2 expressed in HEK293 cells was active in the Glu-C assay. According to the manufacturer, CES2 solid was lyophilized from a solution of 50 mM sodium acetate buffer, pH 5.5, containing NaCl (150 mM), glycerol (10% v/v), trehalose and mannitol (5–8% w/v), and Tween 80 (0.01% v/v). Triton X-100 was avoided in the 4× solution of CES2 as it has been reported to have an inhibitory effect[37] on CES2. In the assay buffer, Triton X-100 was included to minimize peptide sticking to plastic surfaces. (We observed that a final concentration of 0.7% w/v of Triton X-100 in the assay was tolerated by CES2.) Solutions (2× 10 μM) of **Opt**, **Opt**-Et, **Opt**–**1**, **Opt**–**2**, and **Opt**–**3** were prepared in 10 mM HEPES–NaOH buffer, pH 7.4, containing DMF (3% v/v) and Triton X-100 (0.8% w/v) by diluting the stock solution in DMF. A 4× solution of Glu-C (2 μM) was prepared in 10 mM HEPES–NaOH buffer, pH 7.4, containing Triton X-100 (0.8% w/v). See "Preparation of Stock Solutions of Glu-C and Peptides" for more details. Note that, in this experiment, our goal was to determine qualitatively whether a human esterase CES2 can cleave members of the ester panel rather than measure specific kinetic parameters. To avoid artifacts related to Glu-C-mediated cleavage of CES2, we used Glu-C concentration of 0.5 μM in the assay (as instantaneous Glu-C-mediated cleavage of **Opt** is only required for quantitative measurements). Aliquots (50 μL) of 10 μM peptide solutions were added to wells of a 96-well plate. The plate was placed into a pre-warmed plate reader for 10 min to pre-equilibrate it to 37 °C. The following 6 strips of 12 PCR tubes each were prepared: (1) strips containing 45 μL of 4× Glu-C solution, (2) strips containing 35 μL of 4× CES2 solution, (3) strips containing 45 μL of reaction buffer without DMF, (4) strips containing 35 μL of 4× Glu-C solution, (5) strips containing 45 μL of reaction buffer without DMF, and (6) strips containing 35 μL of 4× CES2 solution. The 6 strips of PCR tubes together with a set of pipet tips were placed into an incubator to equilibrate them to 37 °C for 10 min. After 10 min, using a multichannel pipet, 35 μL of PCR strip 1 was added to PCR strip 2 (resulting in a solution containing 100 nM CES2 and 1 μM Glu-C); 35 μL of PCR strip 3 was added to PCR strip 4 (resulting in a solution containing 1 μM Glu-C); 35 μL of PCR strip 5 was added to PCR strip 6 (resulting in a solution containing 100 nM CES2). Then, 50 μL solutions of either 100 nM CES2 and 1 μM Glu-C, 1 μM Glu-C, or 100 nM PLE were rapidly added to the 50 μL peptide solutions in the 96-well plate using a multichannel. The plate was rapidly returned into the plate reader and shaken for 15 s at 37 °C to allow for proper mixing and temperature equilibration. The measurements were taken every 20 s for 40 min post-shaking (see "Instrumentation" for more details). The final concentrations were: 5 μM of **Opt** or esterified peptides, 50 nM of CES2, and 0.5 μM of Glu-C. Fluorescence values were averaged and blank (fluorescence of 10 mM HEPES–NaOH buffer, pH 7.4, containing 5% v/v DMF and 0.8% w/v Triton X-100.) subtracted. Progress curves of **Opt**-Et, **Opt**–**1**, **Opt**–**2**, and **Opt**–**3** cleavage by CES2 (read out by Glu-C fluorescence) are shown in Figure S26 with all corresponding controls.

Sodium acetate and other chemicals contained within the lyophilized CES2 solid were not present in the Glu-C only control and the cleaved **Opt** control. Due to these considerations, we did not convert fluorescence values into product concentrations. Nevertheless, Figure S26 qualitatively indicates that whereas **Opt**–**2** and **Opt**–**3** can get cleaved by 50-nM CES2, **Opt**-Et and **Opt**–**1** do not get cleaved by CES2 under the same conditions.

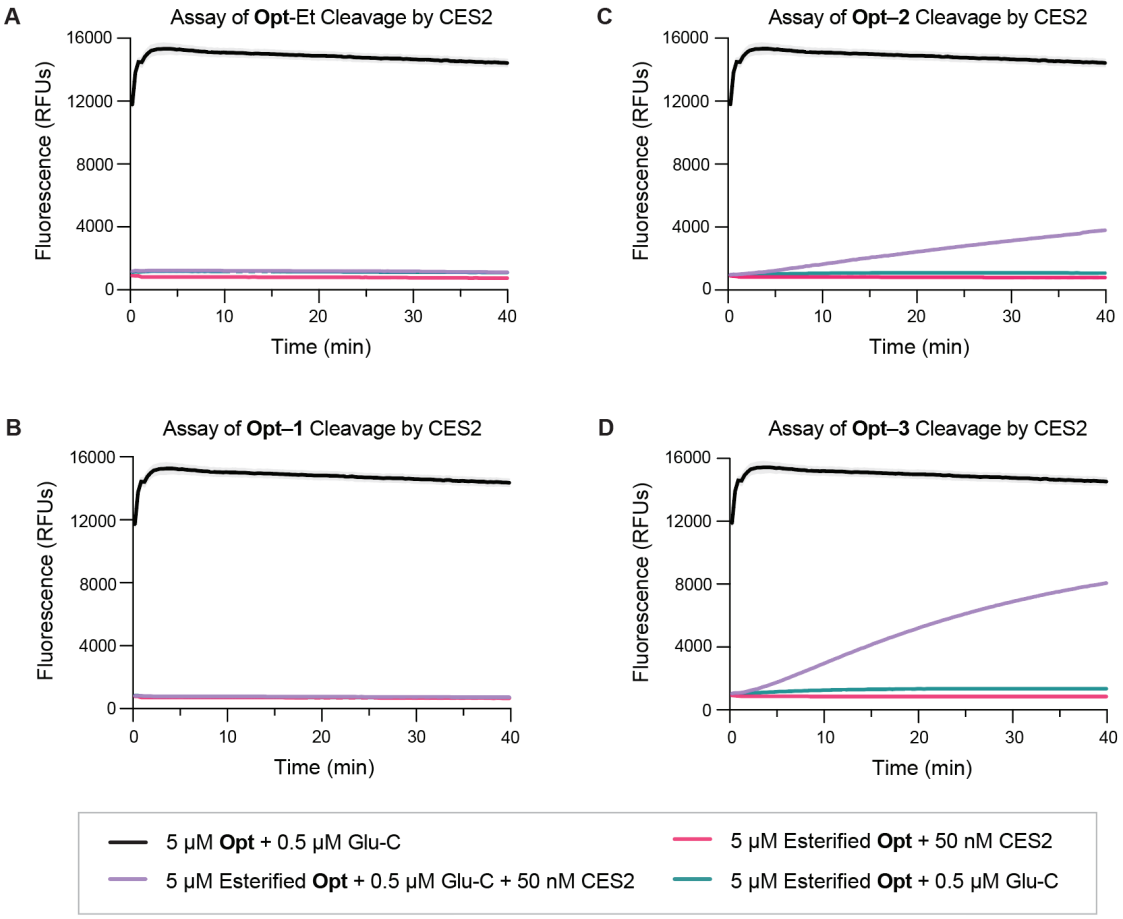

Figure S26. Fluorescence progress curves related to assaying human CES2 cleavage of (A) **Opt**-Et, (B) **Opt**–**1**, (C) **Opt**–**2**, and (D) **Opt**–**3**. Assays were performed in 10 mM HEPES–NaOH buffer, pH 7.4, containing DMF (1.5% v/v) and Triton X-100 (0.7% w/v). Gray areas represent the SD. Progress curves were fitted from data points spaced apart by 20 s. n = 2 independent replicates, n = 3 technical replicates.

VIII-2. Cleavage Assays with Human Carboxylesterase 1 (CES1)

A 4× solution (200 nM) of recombinant CES1 (50 µg from Sino Biological, see "Biological Reagents and Supplies" for product specifications) was prepared by dissolving the solid in 4.03 mL of cold 10 mM HEPES–NaOH buffer, pH 7.4, assuming the molecular weight of 62 kDa. In our hands, only CES1 expressed in HEK293 cells was active in the Glu-C assay. According to the manufacturer, CES1 solid was lyophilized from a solution of PBS, pH 7.4, containing 5–8% trehalose, mannitol, and 0.01% Tween 80. Triton X-100 was avoided in the 4× solution of CES1 as it has been reported to have an inhibitory effect[37] on CES1. We also had to avoid using Triton X-100 in the assay as virtually all activity of CES1 was inhibited by 0.8% w/v Triton X-100. Note that, whereas both CES1 and CES2 are sensitive to Triton X-100 concentrations, the inhibitory effect of Triton X-100 on CES1 is stronger than that on CES2.[37] Solutions (2× 10 µM) of **Opt**, **Opt**-Et, **Opt**–**1**, **Opt**–**2**, and **Opt**–**3** were prepared in 10 mM HEPES–NaOH buffer, pH 7.4, containing DMF (3% v/v) by diluting the stock solution in DMF. A 4× solution of Glu-C (2 µM) was prepared in 10 mM HEPES–NaOH buffer, pH 7.4. Note that, in this experiment, our goal was to determine qualitatively whether a human esterase CES1 can cleave members of the ester panel rather than measure specific kinetic parameters. To avoid artifacts related to Glu-C-mediated cleavage of CES1, we used Glu-C concentration of 0.5 µM in the assay (as instantaneous Glu-C-mediated cleavage of **Opt** is only required for quantitative measurements). See "Preparation of Stock Solutions of Glu-C and Peptides" for more details. Aliquots (50 µL) of 10 µM peptide solutions were added to wells of a 96-well plate. The plate was placed into a pre-warmed plate reader for 10 min to pre-equilibrate it to 37 °C. The following 6 strips of 12 PCR tubes each were prepared: (1) strips containing 45 µL of 4× Glu-C solution, (2) strips containing 35 µL of 4× CES1 solution, (3) strips containing 45 µL of reaction buffer without DMF, (4) strips containing 35 µL of 4 Glu-C solution, (5) strips containing 45 µL of reaction buffer without DMF, and (6) strips containing 35 µL of 4× CES1 solution. The 6 strips of PCR tubes, together with a set of pipet tips, were placed into an incubator to equilibrate them to 37 °C for 10 min. After 10 min, using a multichannel pipet, 35 µL of PCR strip 1 was added to PCR strip 2 (resulting in a solution containing 100 nM CES1 and 1 µM Glu-C); 35 µL of PCR strip 3 was added to PCR strip 4 (resulting in a solution containing 1 µM Glu-C); 35 µL of PCR strip 5 was added to PCR strip 6 (resulting in a solution containing 100 nM CES1). Then, 50 µL solutions of either 100 nM CES1 and 1 µM Glu-C, 1 µM Glu-C, or 100 nM PLE were rapidly added to the 50 µL peptide solutions in the 96-well plate using a multichannel. The plate was rapidly returned into the plate reader and shaken for 15 s at 37 °C to allow for proper mixing and temperature equilibration. The measurements were taken every 20 s for 36 min post-shaking (see "Instrumentation" for more details). The final concentrations were: 5 µM of **Opt** or esterified peptides, 50 nM of CES2, and 0.5 µM of Glu-C. Fluorescence values were averaged and blank (fluorescence of 10 mM HEPES–NaOH buffer, pH 7.4, containing 1.5% v/v DMF) subtracted. Progress curves of **Opt**-Et, **Opt**–**1**, **Opt**–**2**, and **Opt**–**3** cleavage by CES1 (read out by Glu-C fluorescence) are shown in Figure S27 with all corresponding controls. Because 0.8% w/v Triton X-100 was not used to fully solubilize the peptides, we did not convert fluorescence values into concentrations (**Opt** is likely more

soluble in the absence of detergent than esterified **Opt** peptides, hence using its fluorescence to convert fluorescence values of esterified peptides into concentrations of cleaved product might not be accurate). Nevertheless, Figure S27 qualitatively indicates that, whereas **Opt**–**2** and **Opt**–**3** are cleaved in the presence of 50-nM CES1, **Opt**-Et and **Opt**–**1** are not.

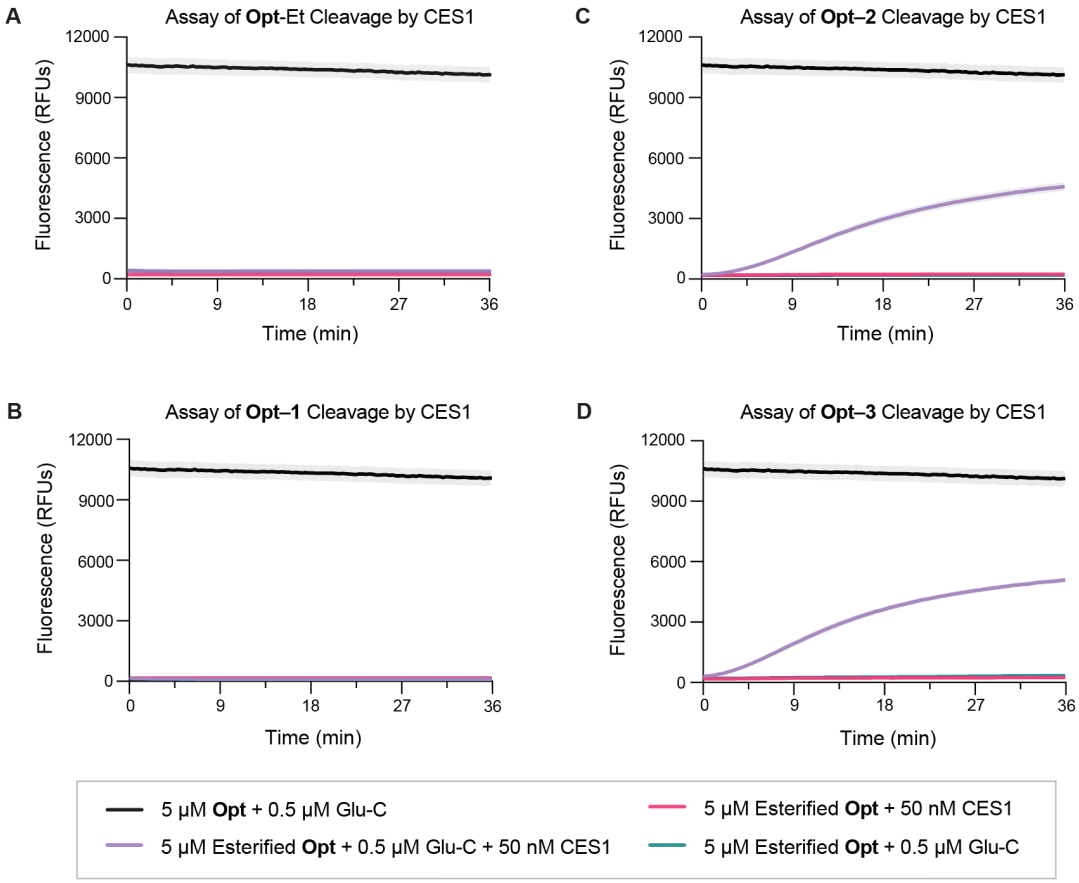

Figure S27. Fluorescence progress curves related to assaying human CES1 cleavage of (A) **Opt**-Et, (B) **Opt**–**1**, (C) **Opt**–**2**, and (D) **Opt**–**3**. Assays were performed in 10 mM HEPES–NaOH buffer, pH 7.4, containing DMF (1.5% v/v). Gray areas above and below progress curves represent the SD. Progress curves were fitted from data points spaced apart by 20 s. $n = 2$ independent replicates, $n = 3$ technical replicates.

IX. Assaying Esterified Peptides for Cleavage by Human Intestine S9 Fraction

A 4× solution (1.6 mg protein/mL) of human intestine S9 fraction (1 mL of 4 mg protein/mL suspension in 50 mM Tris-HCl, 150 mM KCl, 1 mM EDTA, 20% glycerol, heparin, leupeptin, DTT, aprotinin from XenoTech, see "Biological Reagents and Supplies" for product specifications) was prepared by diluting 1 mL of the 4 mg protein/mL suspension with 1.5 mL of cold 10 mM HEPES–NaOH buffer, pH 7.4, containing Triton X-100 (0.8% w/v). Note that XenoTech has validated that an ester prodrug, 6α-methylprednisolone 21-hemisuccinate, gets cleaved by the human intestine S9 fraction (see product information). Furthermore, in written communication with XenoTech, we obtained confirmation that the human intestine S9 fraction contains active CES2. Since we previously observed that CES2 exhibits activity in the presence of Triton X-100 (even though Triton X-100 is known to inhibit it[37]), we included Triton X-100 in the assay buffer. Solutions (2× 10 μM) of **Opt**, **Opt**-Et, **Opt**–**1**, **Opt**–**2**, and **Opt**–**3** were prepared in 10 mM HEPES–NaOH buffer, pH 7.4, containing DMF (3% v/v) and Triton X-100 (0.8% w/v) by diluting the stock solution in DMF. A 4× solution of Glu-C (4 μM) was prepared in 10 mM HEPES–NaOH buffer, pH 7.4, containing Triton X-100 (0.8% w/v). See "Preparation of Stock Solutions of Glu-C and Peptides" for more details. The goal of this experiment was to validate that our Glu-C assay can detect the activity of esterases in a complex mixture from human tissues. Aliquots (50 μL) of 10 μM peptide solutions were added to wells of a 96-well plate. The plate was placed into a pre-warmed plate reader for 10 min to pre-equilibrate it to 37 °C. The following 6 strips of 12 PCR tubes each were prepared: (1) strips containing 45 μL of 4× Glu-C solution, (2) strips containing 35 μL of 4× intestinal fraction solution, (3) strips containing 45 μL of reaction buffer without DMF, (4) strips containing 35 μL of 4× Glu-C solution, (5) strips containing 45 μL of reaction buffer without DMF, and (6) strips containing 35 μL of 4× intestinal fraction. The 6 strips of PCR tubes together with a set of pipet tips were placed into an incubator to equilibrate them to 37 °C for 10 min. After 10 min, using a multichannel pipet, 35 μL of PCR strip 1 was added to PCR strip 2 (resulting in a solution containing 0.8 mg/mL intestinal fraction and 2 μM Glu-C); 35 μL of PCR strip 3 was added to PCR strip 4 (resulting in a solution containing 2 μM Glu-C); 35 μL of PCR strip 5 was added to PCR strip 6 (resulting in a solution containing 0.4 mg/mL intestinal fraction). Then, 50 μL solutions of either 0.8 mg/mL intestinal fraction and 2 μM Glu-C, 2 μM Glu-C, or 0.8 mg/mL intestinal fraction were rapidly added to the 50 μL peptide solutions in the 96-well plate using a multichannel. The plate was rapidly returned into the plate reader and shaken for 15 s at 37 °C to allow for proper mixing and temperature equilibration. The measurements were taken every 20 s for 56 min post-shaking (see "Instrumentation" for more details). The final concentrations were: 5 μM of **Opt** or esterified peptides, 0.4 mg/mL intestinal fraction, and 1 μM of Glu-C. Fluorescence values were averaged and blank (fluorescence of 10 mM HEPES–NaOH buffer, pH 7.4, containing 1.5% v/v DMF and 0.8% w/v Triton X-100) subtracted. Progress curves of **Opt**-Et, **Opt**–**1**, **Opt**–**2**, and **Opt**–**3** cleavage by intestinal fraction (read out by Glu-C fluorescence) are shown in Figure S28 with all corresponding controls. Tris–HCl and other chemicals contained within the intestinal fraction were not present in the Glu-C

only control and the cleaved **Opt** control. Due to these considerations, we did not convert fluorescence values into product concentrations. Nevertheless, Figure S28 qualitatively indicates that, whereas **Opt**–**3** gets cleaved by 0.4 mg/mL of the intestinal fraction, **Opt**-Et, **Opt**–**1,** and **Opt**–**2** do not. Figure S28 also shows that our assay can enable the detection of esterified substrate cleavage in a complex mixture.

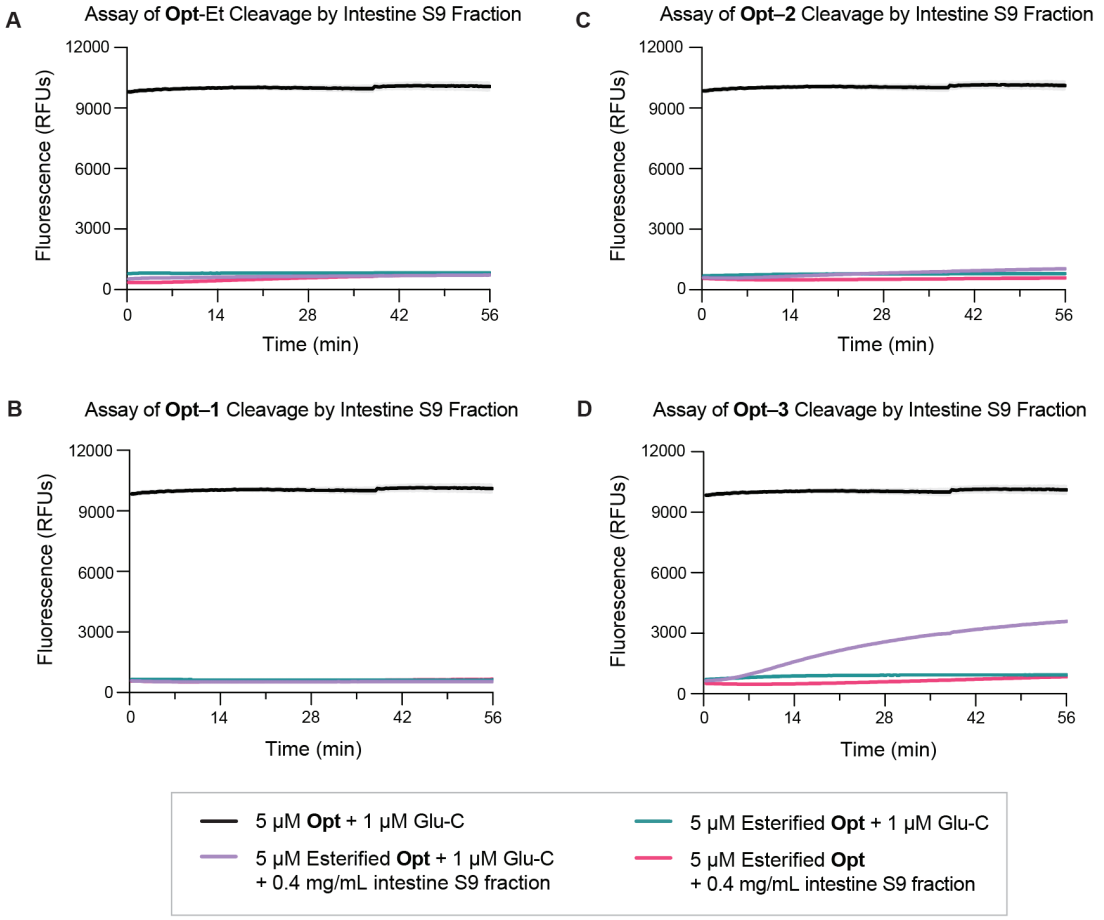

Figure S28. Fluorescence progress curves related to assaying human intestine S9 cleavage of (A) **Opt**-Et, (B) **Opt**–**1**, (C) **Opt**–**2**, and (D) **Opt**–**3**. Assays were performed in 10 mM HEPES–NaOH buffer, pH 7.4, containing DMF (1.5% v/v) and Triton X-100 (0.8% w/v). Gray areas above and below progress curves represent the SD. Progress curves were fitted from data points spaced apart by 20 s. n = 2 independent replicates, n = 3 technical replicates.

X. Statistical Analysis: Computing Errors

Code with Examples of Error Estimation and Error Propagation

For examples of applying error analysis methods described below with our datasets, see the Python code freely available via this GitHub link: https://github.com/yana-d-petri/Finding-kI-and-kcat-KM-using-fluorescence-data-from-Glu-C-assay.

Formulas Employed for Error Estimation and Error Propagation

The mean and standard deviation associated with one independent measurement with technical replicates were computed using standard formulas

$$\mu = \frac{\sum x_i}{N} \tag{S28}$$

$$\sigma = \sqrt{\frac{\sum (x_i - \mu)^2}{N}} \tag{S29}$$

where x_i is each value from the population, μ is the population mean, N is the size of the population, and σ is the population standard deviation. To propagate error for computed parameters that encompass multiple sources of uncertainty, the following error propagation formulas were applied:

For $x = A + B$ or $x = A - B$: $$\sigma_X = \sqrt{(\sigma_A)^2 + (\sigma_B)^2} \tag{S30}$$

For $x = A/B$ or $x = A \times B$: $$\sigma_X = x\sqrt{\left(\frac{\sigma_A}{A}\right)^2 + \left(\frac{\sigma_B}{B}\right)^2} \tag{S31}$$

For $x = A^y$: $$\sigma_X = xy\frac{\sigma_A}{A} \tag{S32}$$

For $x = A/y$: $$\sigma_X = \frac{\sigma_A}{y} \tag{S33}$$

Error Associated with Plotted Fluorescence Values

For data with $n = 1$ independent measurements (with $n = 3$ technical replicates), μ and σ were reported (as in Figure 5A). For data with $n = 2$ independent measurements (with $n = 3$ technical replicates each) (as in Figure S28), the μ of 6 technical replicates was reported along with standard deviation (σ_F):

$$\sigma_F = \frac{\sqrt{(\sigma_1)^2 + (\sigma_2)^2}}{2} \tag{S34}$$

derived from eq S30, where σ_1 and σ_2 are standard deviations of the technical replicate populations within independent measurements 1 and 2, respectively. Note that pipetting and enzyme preparation are the largest contributors to variability within independent replicates and within technical replicates associated with the Glu-C assay.

Error Associated with Plotted $[P]_t$ in Figure S18

Error associated with $[P]_t$ reported in Figure S18 was computed by (1) evaluating μ and σ associated with each of the fluorescence progress curves ($F_t^{\text{esterase + Glu-C}}$, F_t^{esterase}, $F_t^{\text{Glu-C}}$, $F_t^{\max}$) as described above, (2) substituting respective μ values into eq S5 to find $[P]_t$, and (3) computing SD associated with $[P]_t$ by applying the standard error propagation formulas for subtraction (eq S30) and division (eq S31).

Error Associated with Plotted $[P]_t$ in Figures 8 (same as Figure S25B) and 9A

The goal of evaluating $[P]_t$ in Figures 8 and 9A was to calculate the derivative d[P]/dt, which was used for computing several useful downstream parameters. Propagating error on d[P]/dt from standard deviation associated with an average value of $[P]_t$ is a rather mathematically challenging task. Therefore, in cases where $[P]_t$ is used for evaluating d[P]/dt, we resorted to the following approach:

1) $F_t^{\text{esterase + Glu-C}}$, F_t^{esterase}, $F_t^{\text{Glu-C}}$, $F_t^{\max}$ values within each of the two independent measurements were randomly paired with each other and eq S5 was applied on the pairings. Using this approach, 81 possible values of $[P]_t$ were generated for each set of independent measurements with n = 3 technical replicates.
2) $[P]_t$ values across two independent replicates were averaged and the σ associated with $[P]_t$ values of each of the two independent replicates was found.
3) Equation S34 was applied to find the total standard deviation of $[P]_t$ values across two independent replicates.

Error Associated with k_I, $[P]_\infty$, $[I]_{t_x}$, and $t_{1/2}$

The average value of $[P]_t$ and the associated σ were fed into the curve_fit function (scipy library) in Python for fitting eq S14 with three free fitting parameters. The output covariance matrix was examined and it was ensured that the diagonal elements were larger than the off-diagonal elements by accordingly re-scaling the input parameters for ensuring the stability of the fit. The σ associated with k_I, $[P]_\infty$, and $[I]_{t_x}$ was computed by taking the square root of their covariance. The σ associated with $t_{1/2}$ was computed by using the error propagation formula for exponents (eq S33). The 95% confidence intervals were calculated using

$$95\%\ \text{Confidence Interval} = 1.96 \times \sigma \quad \text{(S35)}$$

Error Associated with Plotted $[I]_t$ and $[A]_t$

Using the random pairings approach, 81 possible values of d[P]/dt were generated for each set of independent measurements with $n = 3$ technical replicates. Average d[P]/dt value was computed from 162 resultant values and the associated standard deviation was calculated using eq S34. The value of Σ associated with $[I]_t$ was computed using error propagation formula for division (eq S31) from the standard deviation associated with averaged d[P]/dt value. The value of σ associated with $[A]_t$ values <10% of $[S]_0$ was computed using error propagation formula for addition (eq S30).

Error Associated with Plotted dA/dt

The $[A]_t$ values for each $[S]_0$ and the associated σ were fed into the curve_fit function (scipy library) in Python for fitting a straight line, where the slope is d[A]/dt. The output covariance matrix was examined, and it was ensured that the diagonal elements were larger than the off-diagonal elements by accordingly re-scaling the input parameters for ensuring the stability of the fit. The δ associated with the slope (or each resultant d[A]/dt value) was computed by taking the square root of the respective variance found in the covariance matrix.

Error Associated with k_{cat}/K_M

d[A]/dt values for each $[S]_0$ and the associated σ were fed into curve_fit function (scipy library) in Python for fitting a straight line, where the slope equated to $k_{cat}/K_M[E]_0$. The output covariance matrix was examined, and it was ensured that the diagonal elements were larger than the off-diagonal elements by accordingly re-scaling the input parameters for ensuring the stability of the fit. The σ associated with the slope was computed by taking the square root of the respective variance found in the covariance matrix. Error propagation for division (eq S31) was applied to the slope to obtain the σ associated with k_{cat}/K_M. The respective 95% confidence interval computed for k_{cat}/K_M using eq S35.

XI. NMR Spectra

^{1}H NMR (400 MHz) spectrum of **S1** in $CDCl_3$

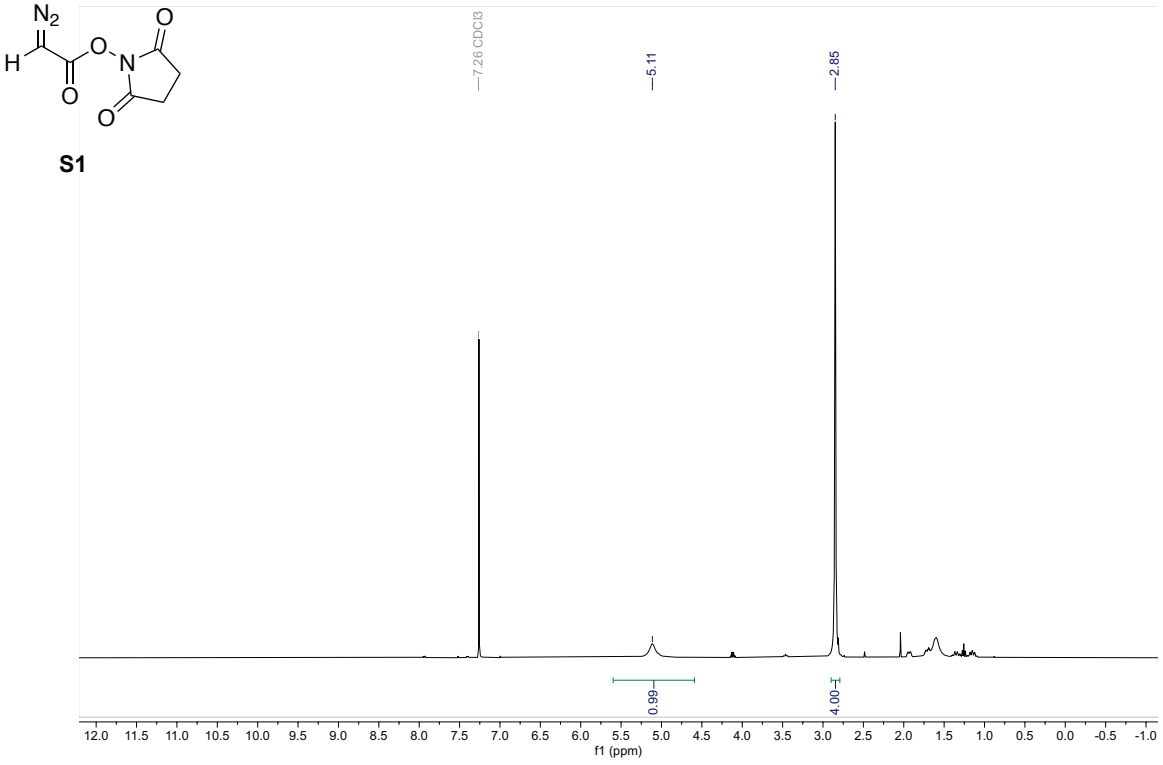

^{1}H NMR (500 MHz) spectrum of **1** in CD_3CN

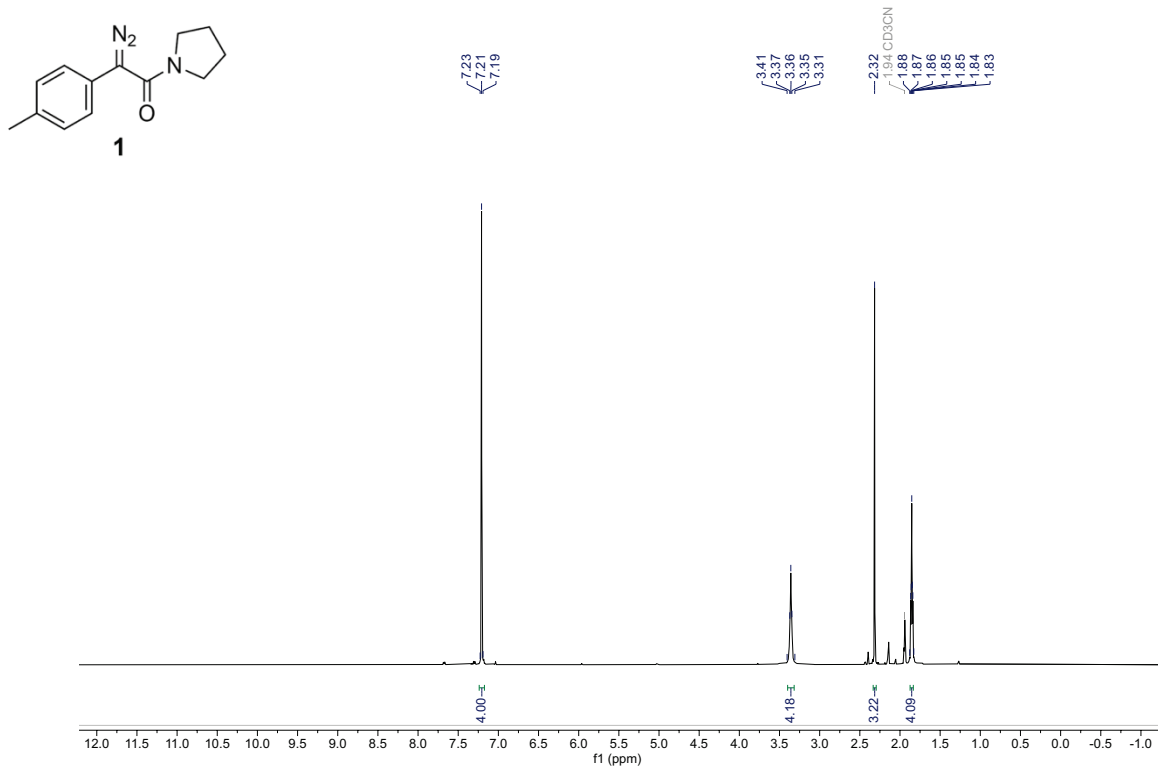

^{1}H NMR (400 MHz) spectrum of **S2** in CD_3CN

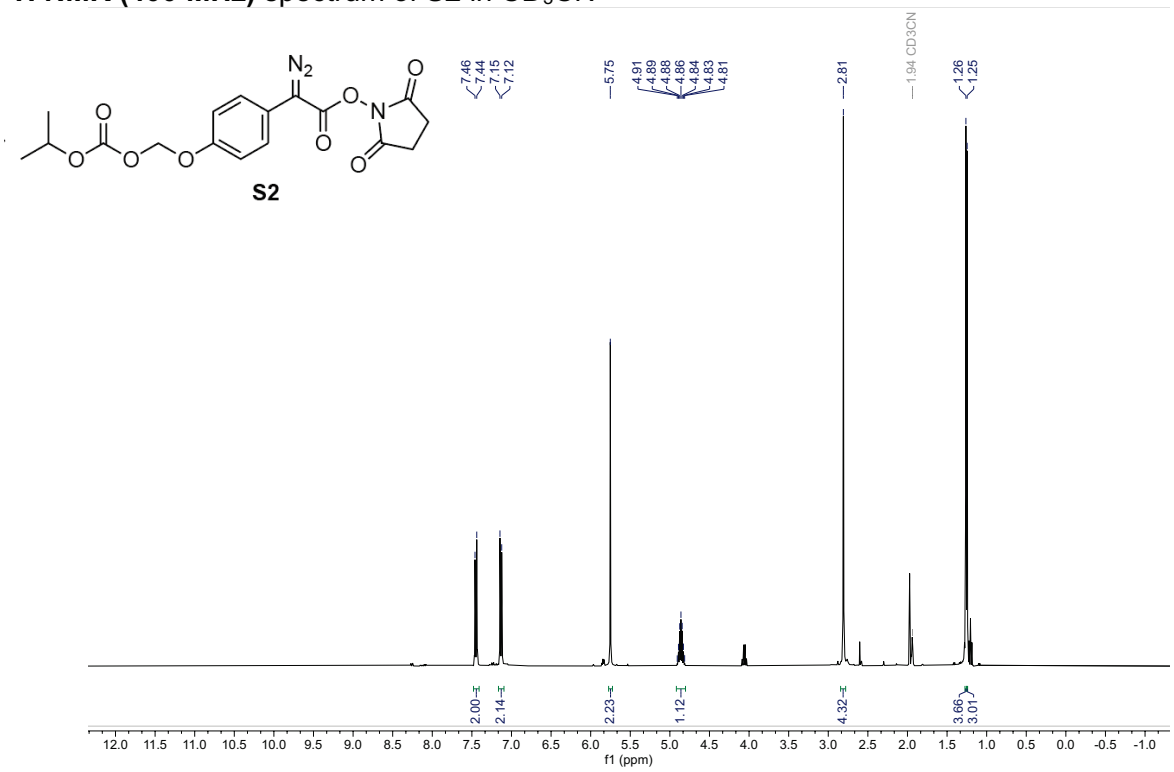

^{1}H NMR (500 MHz) spectrum of **2** in CD_3CN

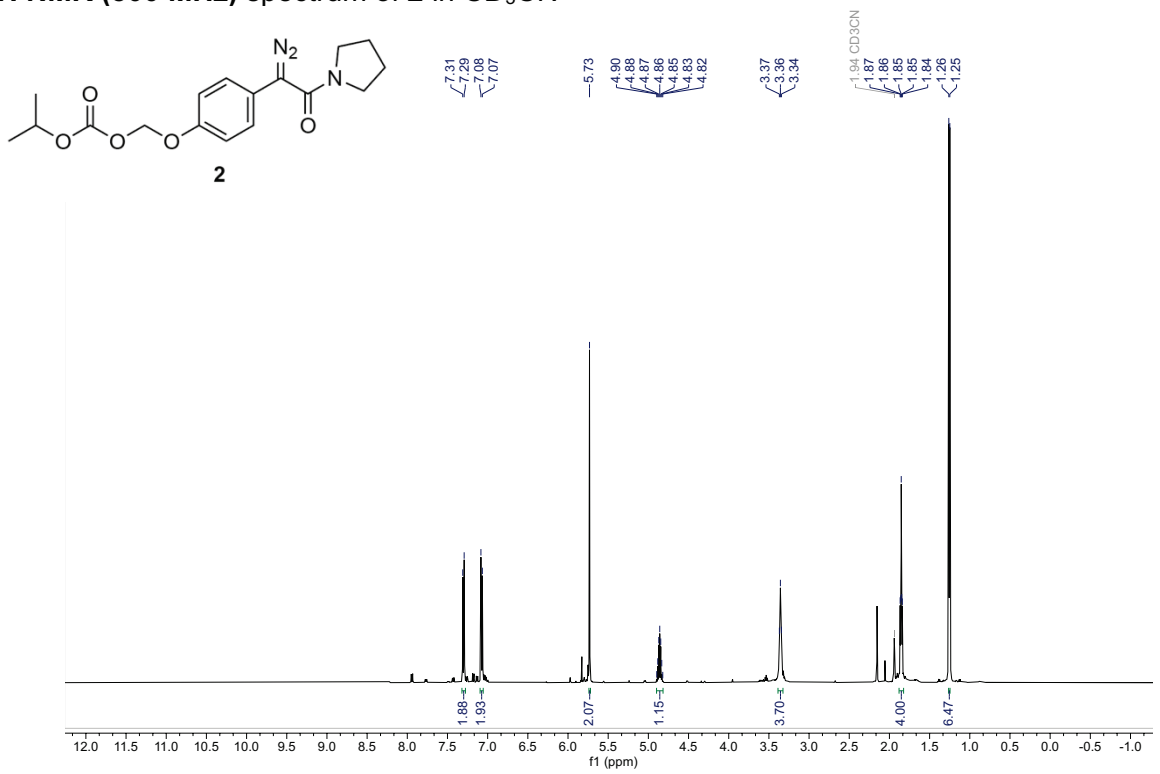

^{13}C NMR (500 MHz) spectrum of **2** in CD_3CN

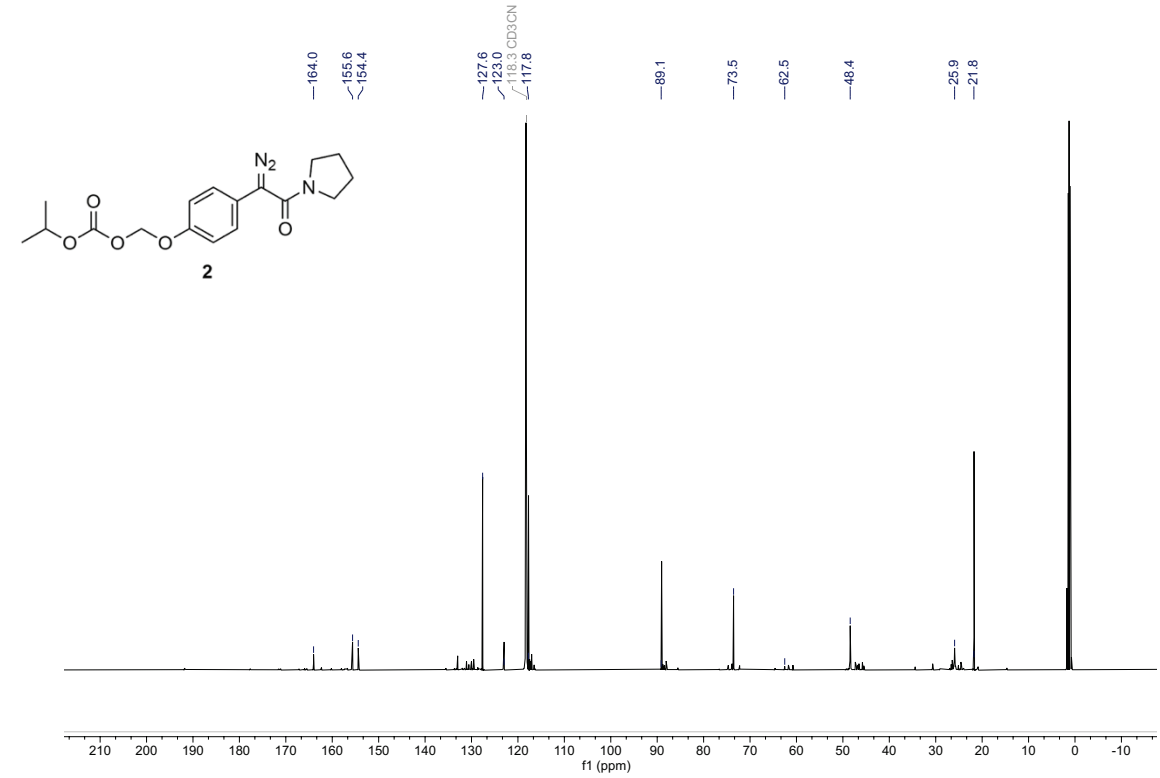

HSQC NMR (500 MHz) spectrum of **2** in CD_3CN

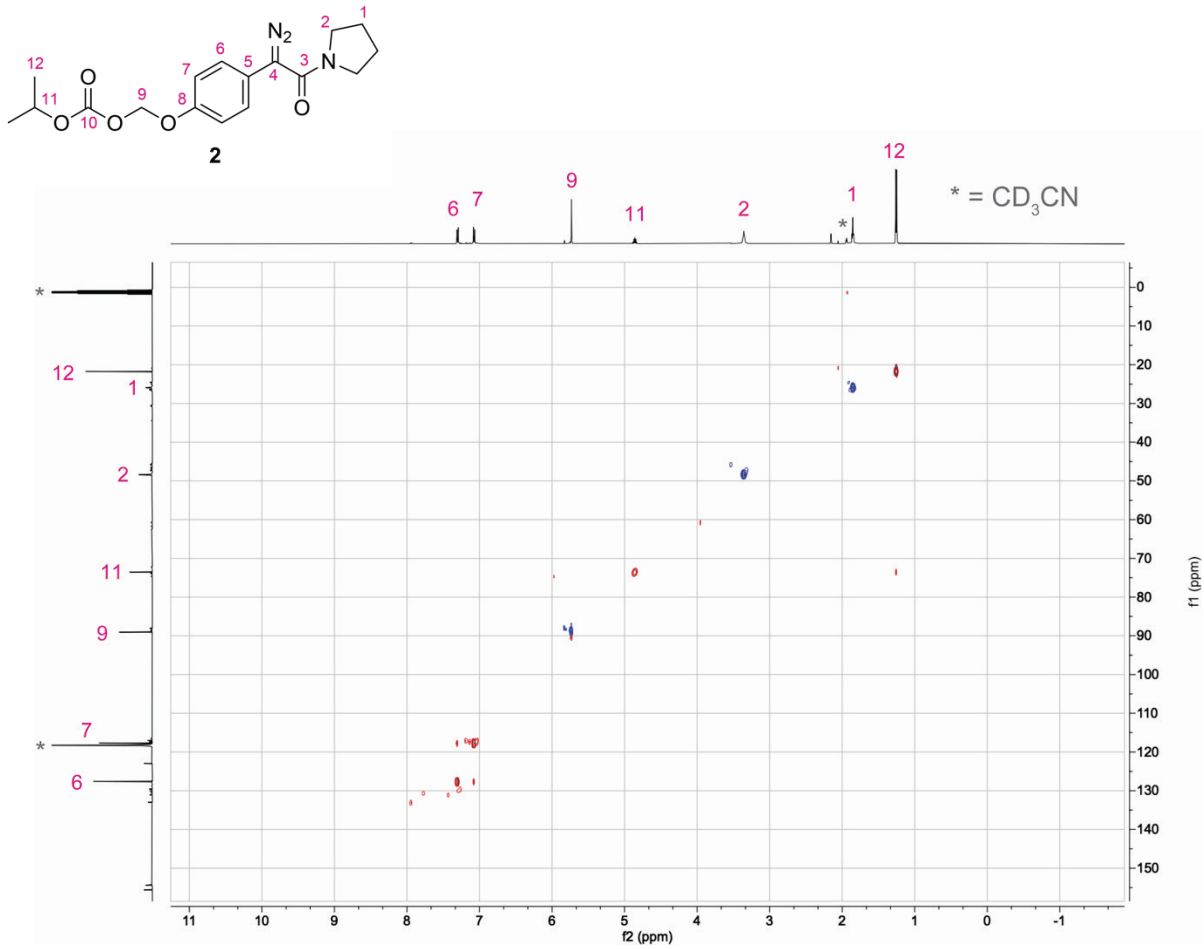

HMBC NMR (500 MHz) spectrum of **2** in CD_3CN

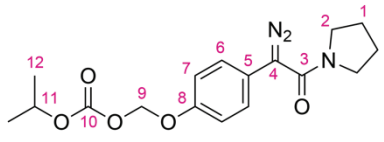

2

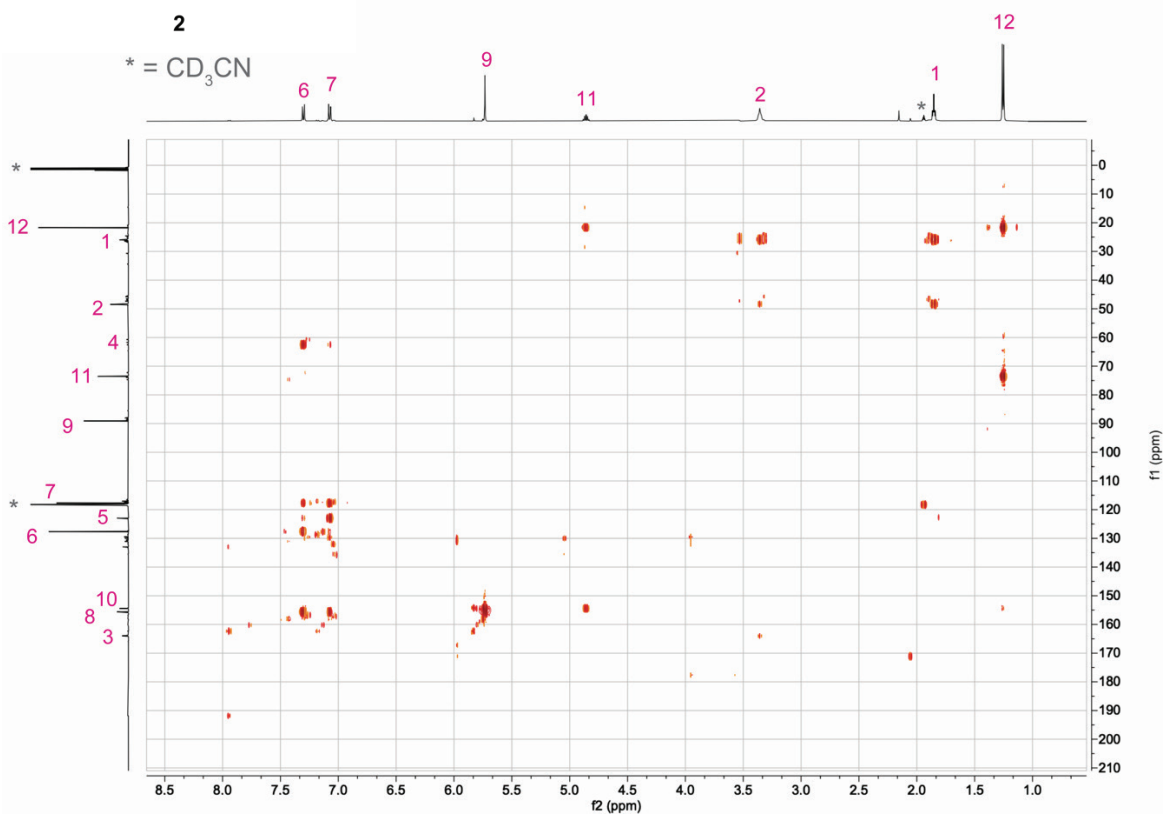

Zoom-in on the diazo carbon 4 (62.5 ppm) correlation:

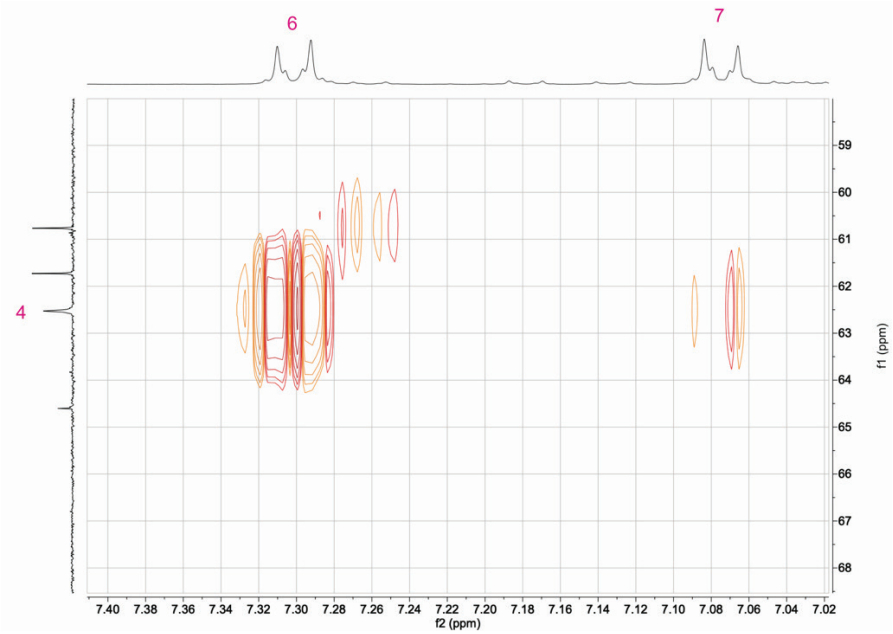

^{1}H NMR (400 MHz) spectrum of **S4** in $CDCl_3$

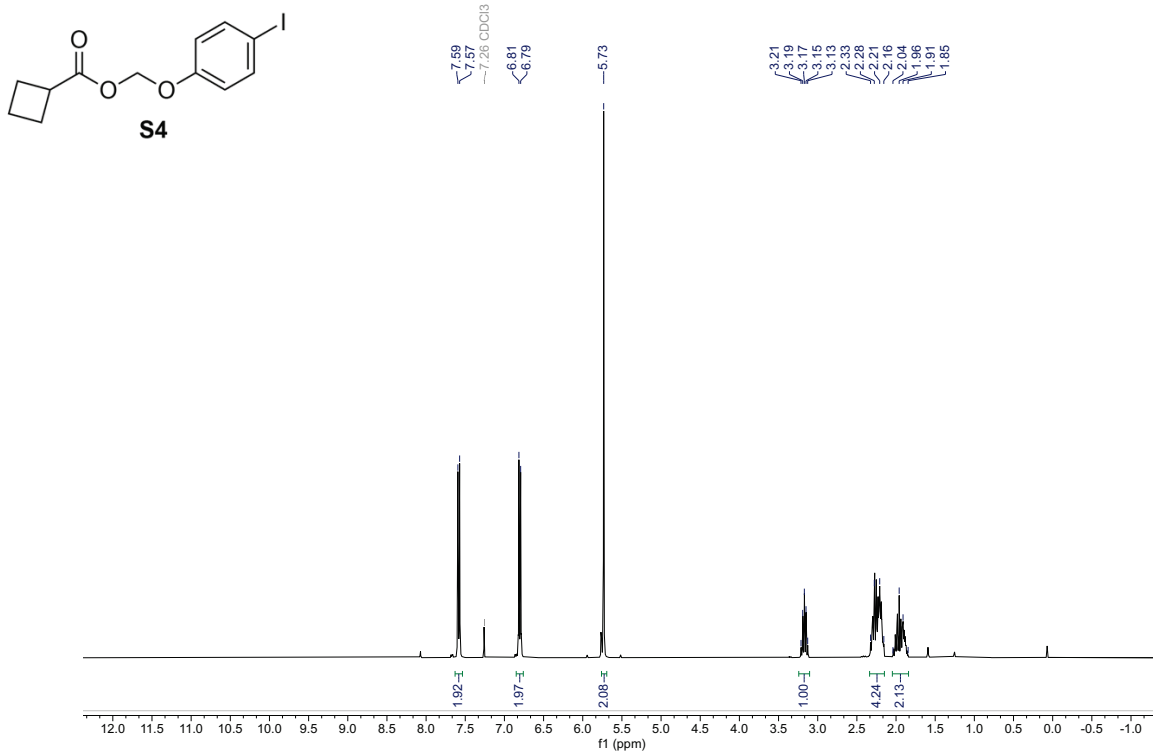

^{13}C NMR (400 MHz) spectrum of **S4** in $CDCl_3$

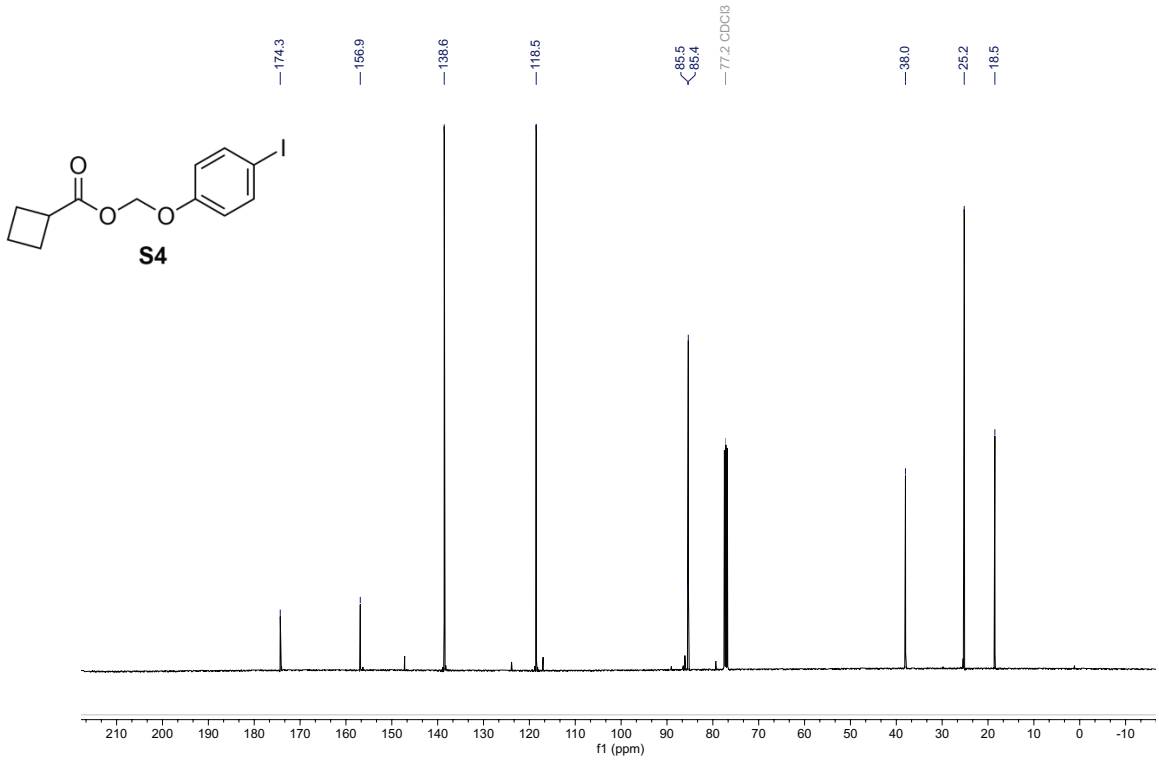

HSQC (500 MHz) spectrum of **S4** in $CDCl_3$

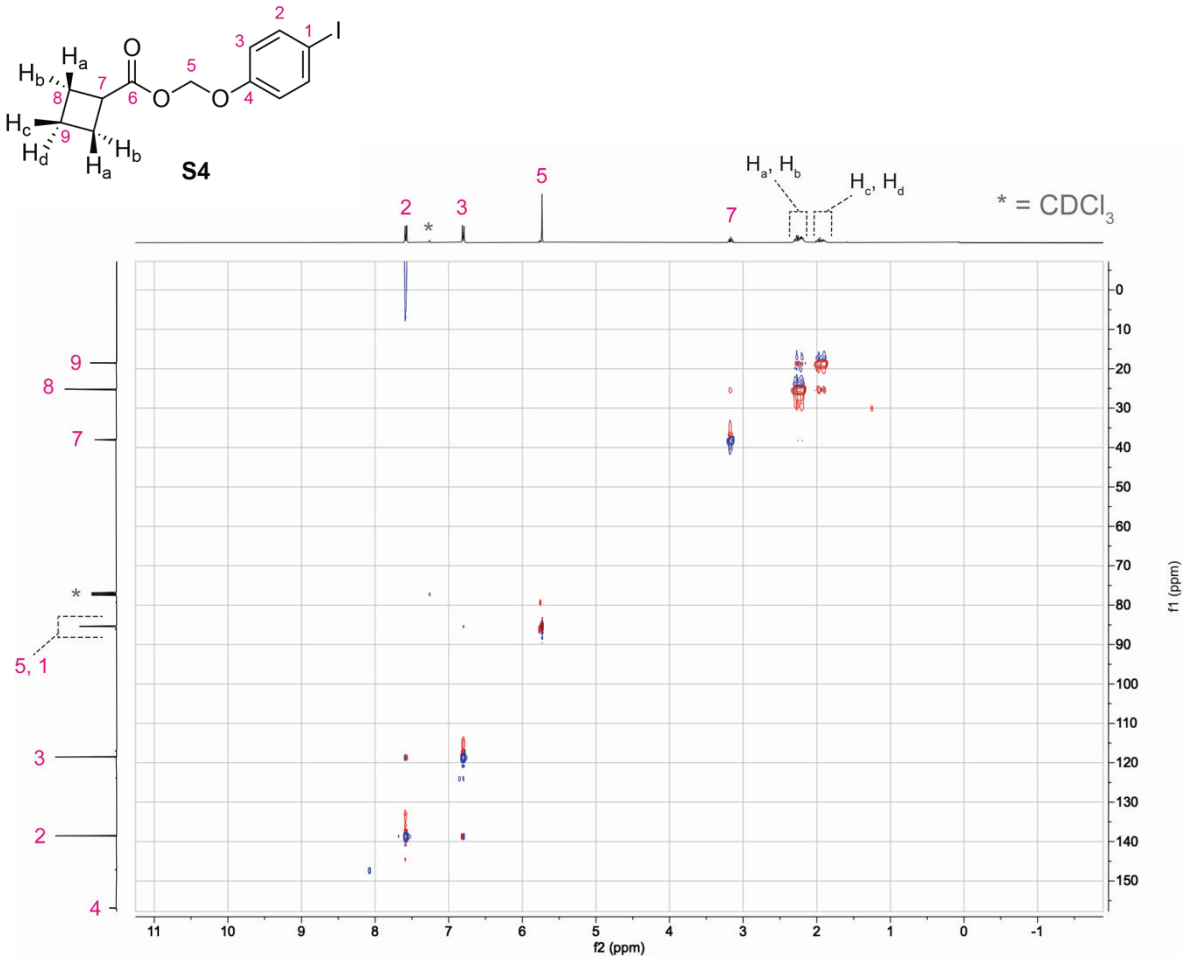

HMBC (500 MHz) spectrum of **S4** in $CDCl_3$

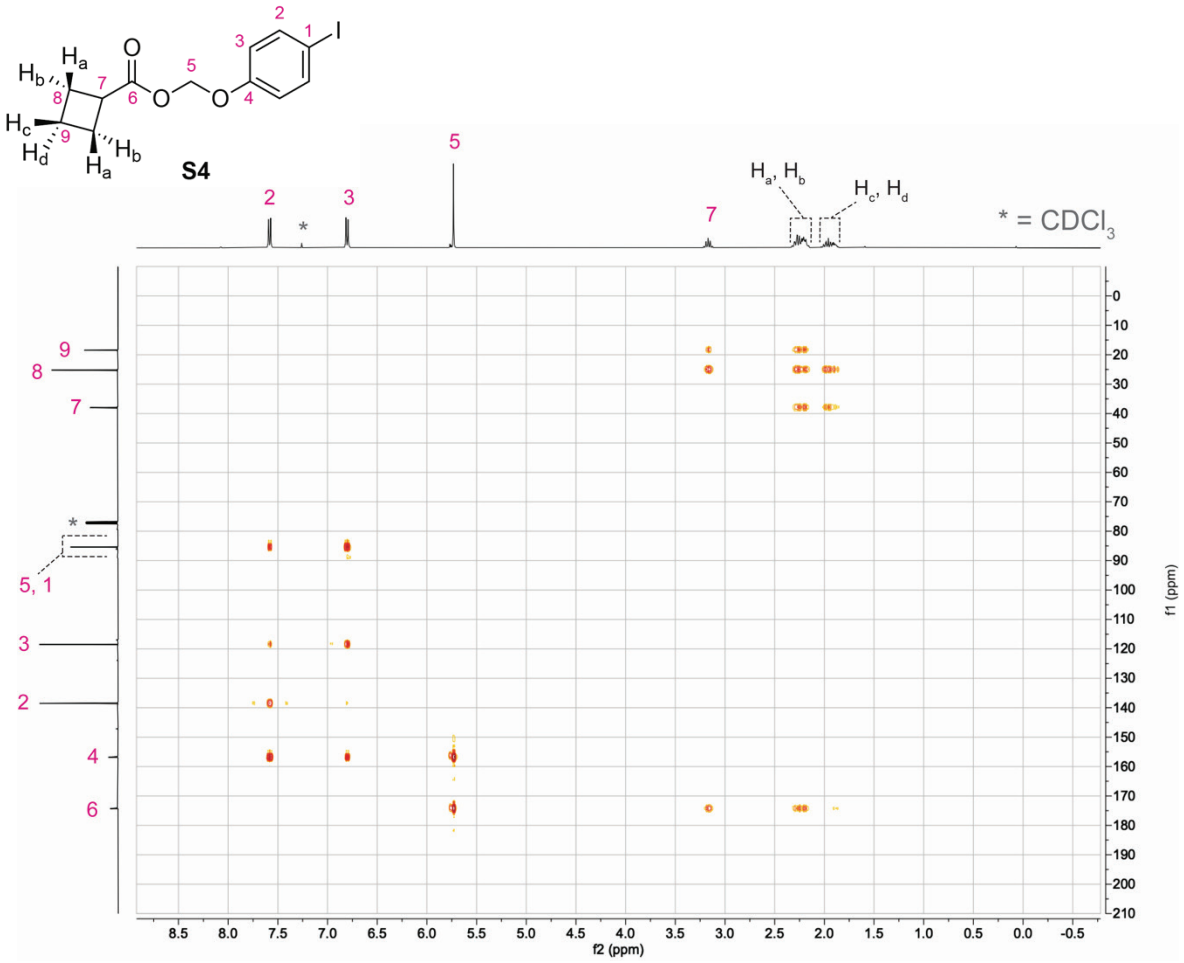

Zoom-in on the correlation of carbon 1:

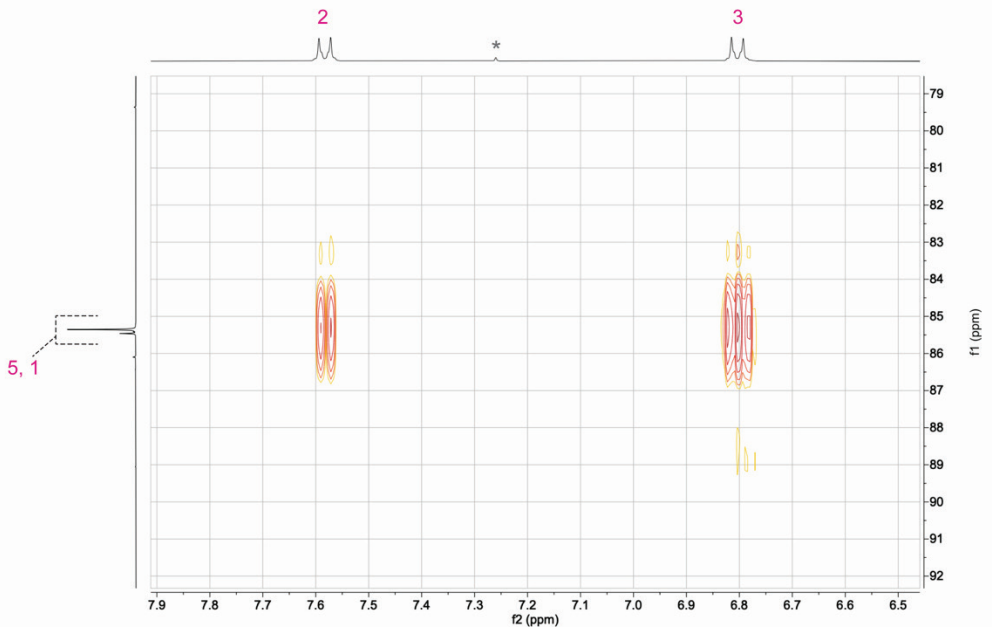

^{1}H NMR (500 MHz) spectrum of **3** in CD_3CN

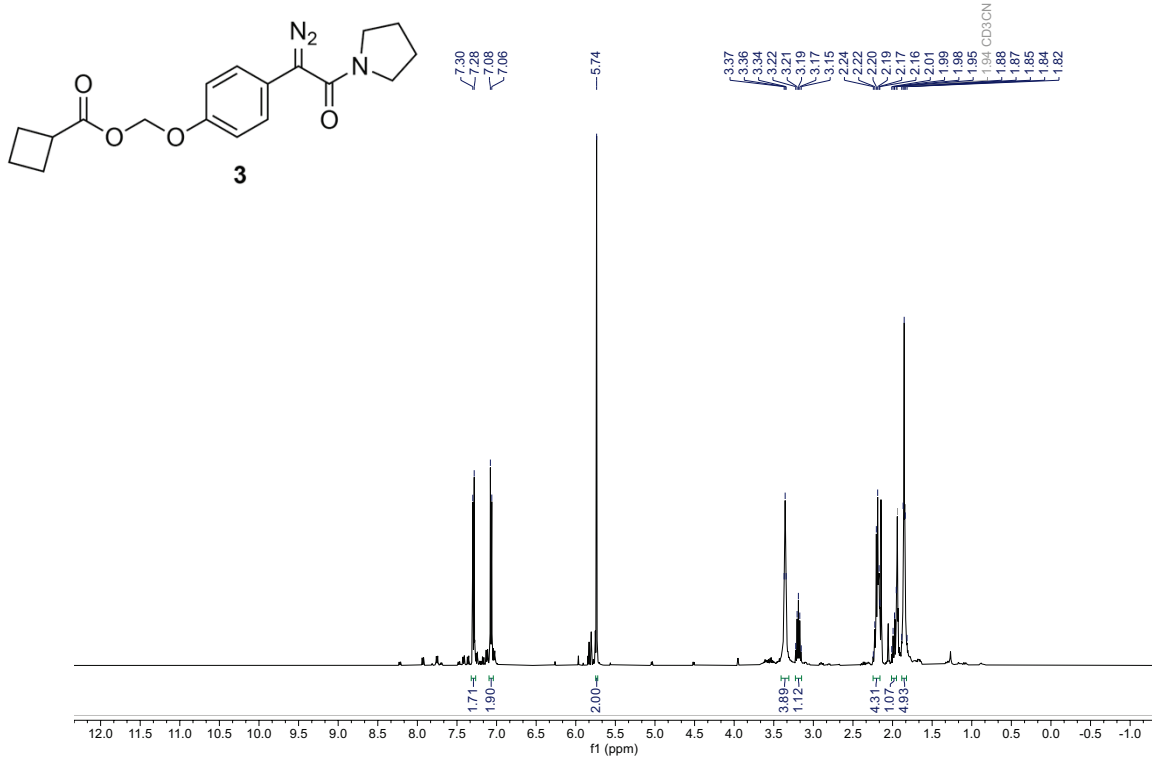

^{13}C NMR (500 MHz) spectrum of **3** in CD_3CN

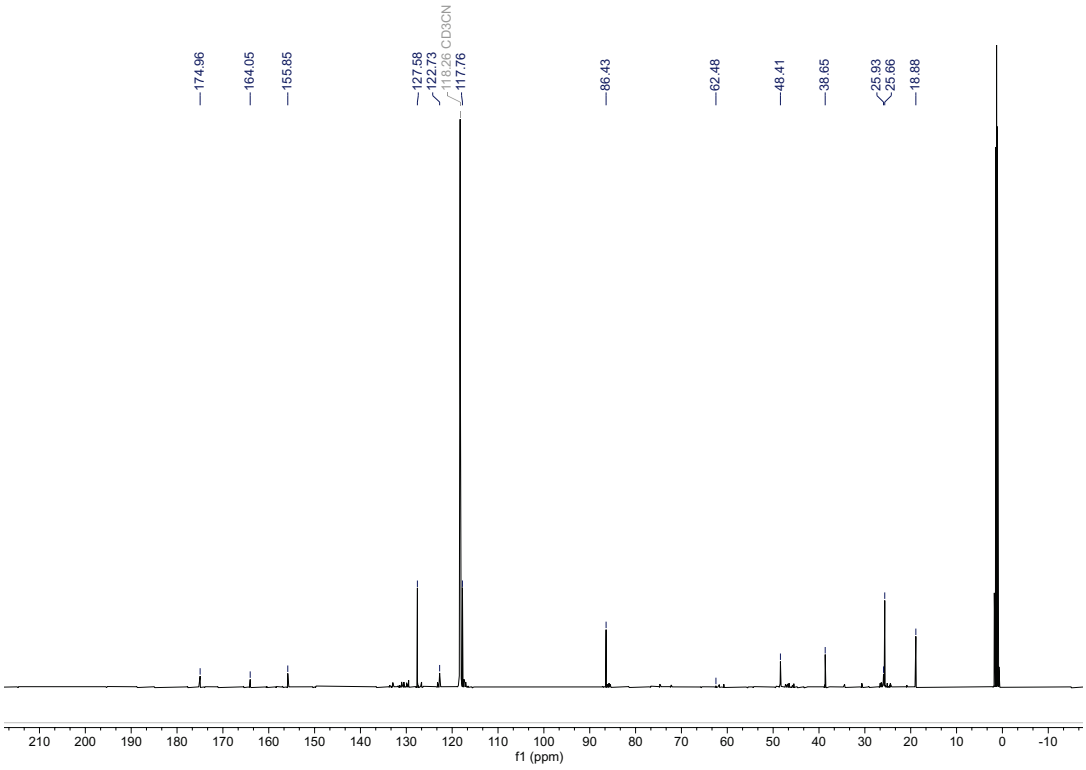

HSQC (500 MHz) spectrum of **3** in CD_3CN

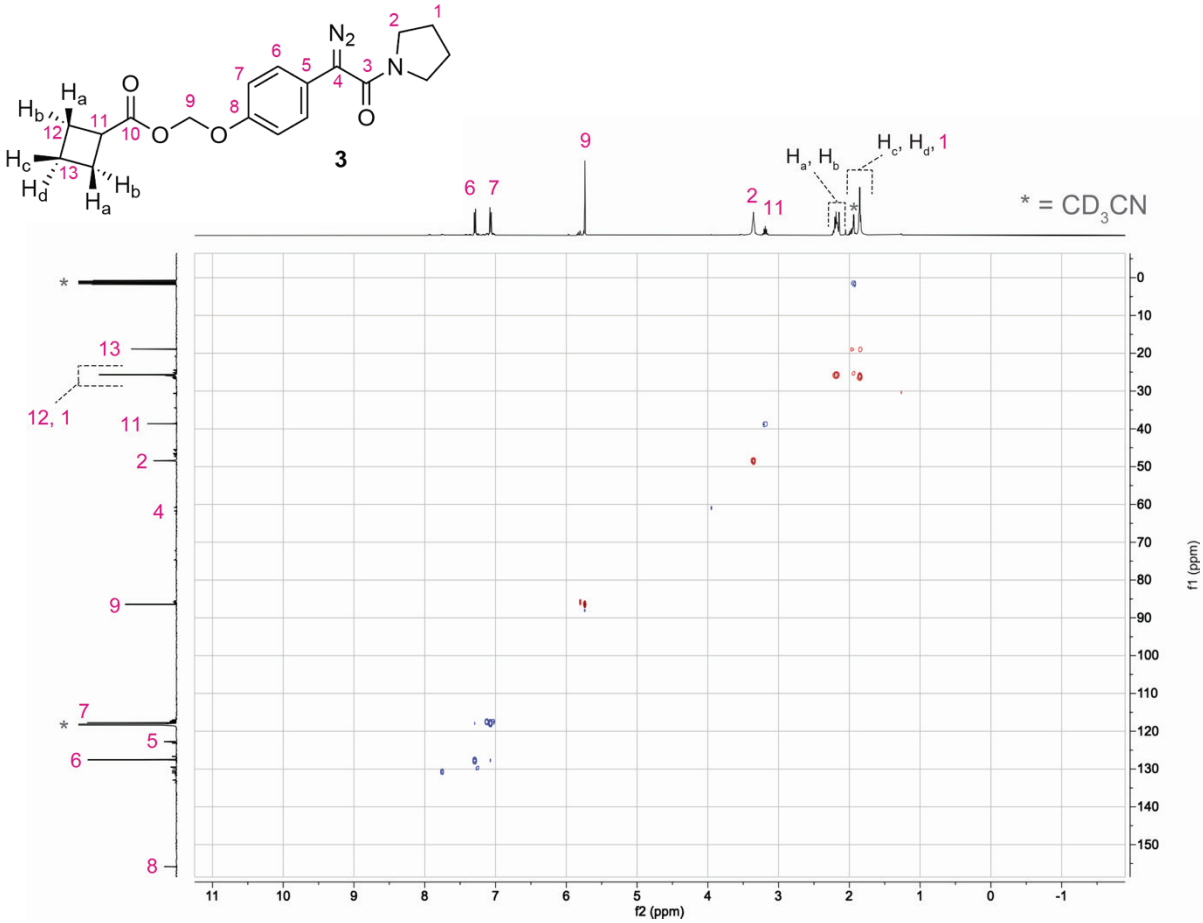

Zoom-in on the correlations of carbon 12 and 1:

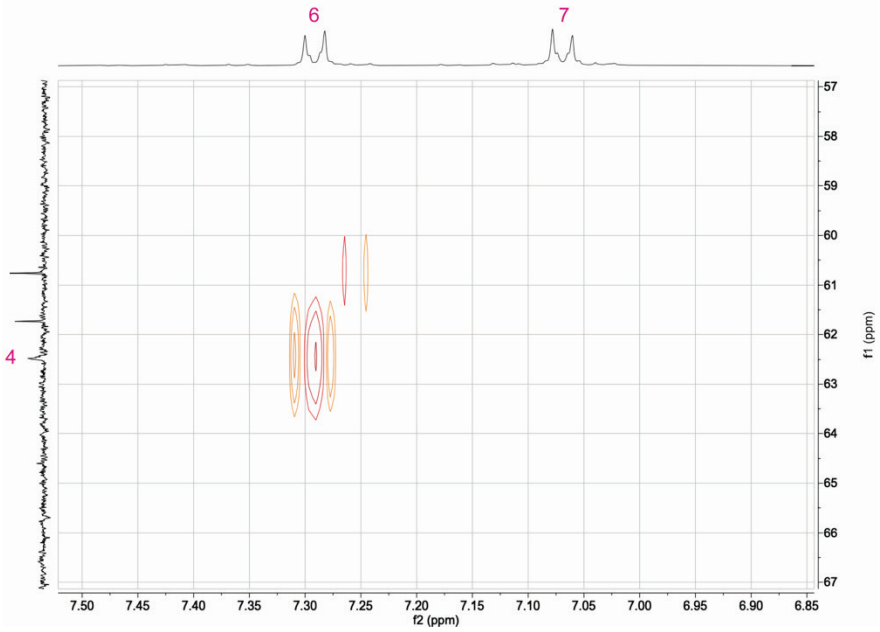

HMBC (500 MHz) spectrum of **3** in CD_3CN

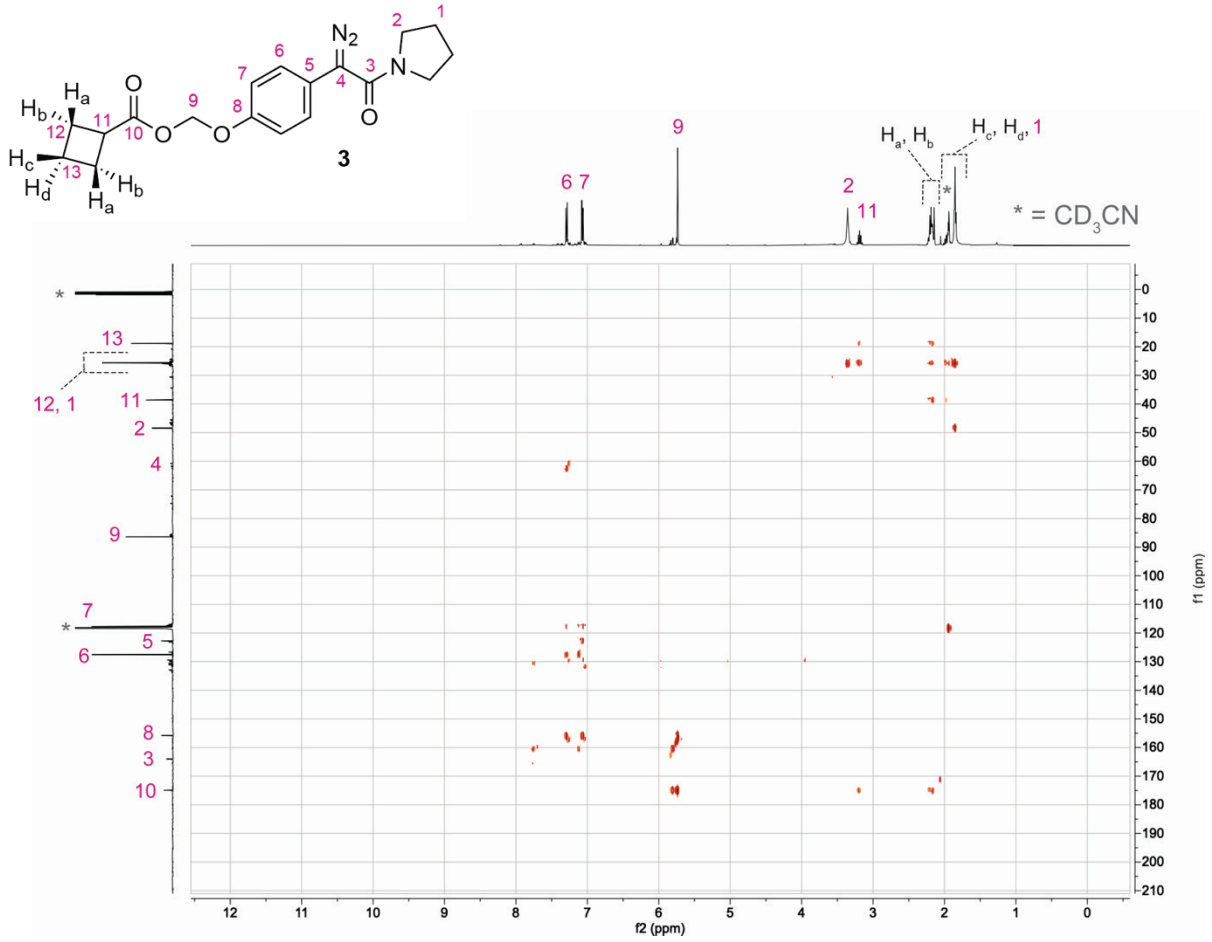

Zoom-in on the diazo carbon 4 (62.5 ppm) correlation:

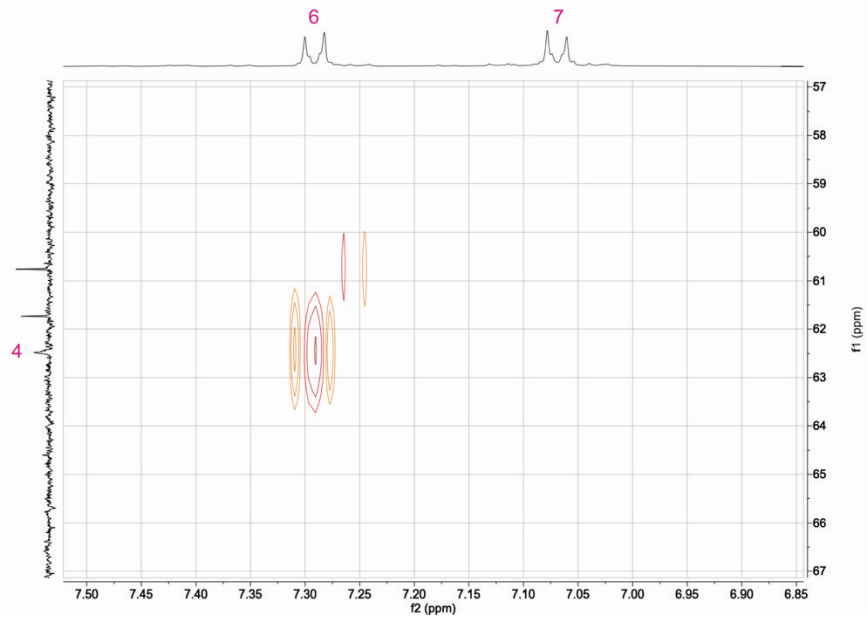

XII. References

(1) Ouihia, A.; Rene, L.; Guilhem, J.; Pascard, C.; Badet, B. A new diazoacylating reagent: Preparation, structure, and use of succinimidyl diazoacetate. *J. Org. Chem.* **1993**, *58*, 1641–1642.

(2) Green, S. P.; Wheelhouse, K. M.; Payne, A. D.; Hallett, J. P.; Miller, P. W.; Bull, J. A. Thermal stability and explosive hazard assessment of diazo compounds and diazo transfer reagents. *Org. Process Res. Dev.* **2020**, *24*, 67–84.

(3) Jun, J. V.; Raines, R. T. Two-step synthesis of α-aryl-α-diazoamides as modular bioreversible labels. *Org. Lett.* **2021**, *23*, 3110–3114.

(4) Matayoshi, E. D.; Wang, G. T.; Krafft, G. A.; Erickson, J. Novel fluorogenic substrates for assaying retroviral proteases by resonance energy transfer. *Science* **1990**, *247*, 954–958.

(5) Gasteiger, E.; Hoogland, C.; Gattiker, A.; Duvaud, S.; Wilkins, M. R.; Appel, R. D.; Bairoch, A., Protein identification and analysis tools on the Expasy server. In *The Proteomics Handbook*, Walker, J., Ed. Humana Press: Totowa, NJ, 2005.

(6) Windsor, I. W.; Raines, R. T. Fluorogenic assay for inhibitors of HIV-1 protease with sub-picomolar affinity. *Sci. Rep.* **2015**, *5*, 11286.

(7) Trott, O.; Olson, A. J. AutoDock Vina: Improving the speed and accuracy of docking with a new scoring function, efficient optimization, and multithreading. *J. Comput. Chem.* **2010**, *31*, 455–461.

(8) Zhao, Y.; Truhlar, D. G. Density functionals with broad applicability in chemistry. *Acc. Chem. Res.* **2008**, *41*, 157–167.

(9) Zhao, Y.; Truhlar, D. G. The M06 suite of density functionals for main group thermochemistry, thermochemical kinetics, noncovalent interactions, excited states, and transition elements: Two new functionals and systematic testing of four M06-class functionals and 12 other functionals. *Theor. Chem. Acc.* **2008**, *120*, 215–241.

(10) Frisch, M. J.; Trucks, G. W.; Schlegel, H. B.; Scuseria, G. E.; Robb, M. A.; Cheeseman, J. R.; Scalmani, G.; Barone, V.; Petersson, G. A.; Nakatsuji, H.; Li, X.; Caricato, M.; Marenich, A. V.; Bloino, J.; Janesko, B. G.; Gomperts, R.; Mennucci, B.; Hratchian, H. P.; Ortiz, J. V.; Izmaylov, A. F.; Sonnenberg, J. L.; Williams; Ding, F.; Lipparini, F.; Egidi, F.; Goings, J.; Peng, B.; Petrone, A.; Henderson, T.; Ranasinghe, D.; Zakrzewski, V. G.; Gao, J.; Rega, N.; Zheng, G.; Liang, W.; Hada, M.; Ehara, M.; Toyota, K.; Fukuda, R.; Hasegawa, J.; Ishida, M.; Nakajima, T.; Honda, Y.; Kitao, O.; Nakai, H.; Vreven, T.; Throssell, K.; Montgomery Jr., J. A.; Peralta, J. E.; Ogliaro, F.; Bearpark, M. J.; Heyd, J. J.; Brothers, E. N.; Kudin, K. N.; Staroverov, V. N.; Keith, T. A.; Kobayashi, R.; Normand, J.; Raghavachari, K.; Rendell, A. P.; Burant, J. C.; Iyengar, S. S.; Tomasi, J.; Cossi, M.; Millam, J. M.; Klene, M.; Adamo, C.; Cammi, R.; Ochterski, J. W.; Martin, R. L.; Morokuma, K.; Farkas, O.; Foresman, J. B.; Fox, D. J. *Gaussian 16 Rev. C.01*, Wallingford, CT, 2016.

(11) Prasad, L.; Leduc, Y.; Hayakawa, K.; Delbaere, L. T. J. The structure of a universally employed enzyme: V8 protease from *Staphylococcus aureus*. *Acta Crystallogr. D Biol. Crystallogr.* **2003**, *60*, 256–259.

(12) Gupta, A. K.; Yin, X.; Mukherjee, M.; Desai, A. A.; Mohammadlou, A.; Jurewicz, K.; Wulff, W. D. Catalytic asymmetric epoxidation of aldehydes with two VANOL-derived chiral borate catalysts. *Angew. Chem., Int. Ed.* **2019**, *58*, 3361–3367.

(13) Jun, J. V.; Petri, Y. D.; Erickson, L. W.; Raines, R. T. Modular diazo compound for the bioreversible late-stage modification of proteins. *J. Am. Chem. Soc.* **2023**, *145*, 6615–6621.

(14) Wralstad, E. C.; Sayers, J.; Raines, R. T. Bayesian inference elucidates the catalytic competency of the SARS-CoV-2 main protease 3CL^{pro}. *Anal. Chem.* **2023**, *95*, 14981–14989.

(15) Li, J.; Sha, Y. A convenient synthesis of amino acid methyl esters. *Molecules* **2008**, *13*, 1111–1119.

(16) Chen, B.-C.; Skoumbourdis, A. P.; Guo, P.; Bednarz, M. S.; Kocy, O. R.; Sundeen, J. E.; Vite, G. D. A facile method for the transformation of *N*-(*tert*-butoxycarbonyl) α-amino acids to *N*-unprotected α-amino methyl esters. *J. Org. Chem.* **1999**, *64*, 9294–9296.

(17) Takaishi, T.; Izumi, M.; Ota, R.; Inoue, C.; Kiyota, H.; Fukase, K. Product selectivity of esterification of L-aspartic acid and L-glutamic acid using chlorotrimethylsilane. *Nat. Prod. Commun.* **2017**, *12*, 247–249.

(18) Fei, N.; Sauter, B.; Gillingham, D. The pK_a of Brønsted acids controls their reactivity with diazo compounds. *Chem. Commun.* **2016**, *52*, 7501–7504.

(19) Petri, Y. D.; Gutierrez, C. S.; Raines, R. T. Chemoselective caging of carboxyl groups for on-demand protein activation with small molecules. *Angew. Chem., Int. Ed.* **2023**, *62*, e202215614.

(20) Guthrie, J. P. Hydrolysis of esters of oxy acids: pK_a values for strong acids; Brønsted relationship for attack of water at methyl; free energies of hydrolysis of esters of oxy acids; and a linear relationship between free energy of hydrolysis and pK_a holding over a range of 20 pK units. *Can. J. Chem.* **2011**, *1*, 2342–2354.

(21) Drapeau, G. R. The primary structure of staphylococcal protease. *Can. J. Biochem.* **1978**, *56*, 534–544.

(22) Folkers, E.; Runquist, O. Correlation of base strengths of aliphatic and *N*-substituted anilines. *J. Org. Chem.* **1964**, *29*, 830–832.

(23) Liu, Y.; Kati, W.; Chen, C.-M.; Tripathi, R.; Molla, A.; Kohlbrenner, W. Use of a fluorescence plate reader for measuring kinetic parameters with inner filter effect correction. *Anal. Biochem.* **1999**, *267*, 331–335.

(24) Palmier, M. O.; Van Doren, S. R. Rapid determination of enzyme kinetics from fluorescence: Overcoming the inner filter effect. *Anal. Biochem.* **2007**, *371*, 43–51.

(25) Borman, P.; Elder, D., Q2(R1) Validation of analytical procedures. In *ICH Quality Guidelines*, 2017; pp 127–166.

(26) Alouane, A.; Labruère, R.; Le Saux, T.; Schmidt, F.; Jullien, L. Self-immolative spacers: Kinetic aspects, structure–property relationships, and applications. *Angew. Chem., Int. Ed.* **2015**, *54*, 7492–7509.

(27) Wang, H.; Wahi, M. S.; Rokita, S. E. Immortalizing a transient electrophile for DNA cross-linking. *Angew. Chem., Int. Ed.* **2008**, *47*, 1291–1293.

(28) Fakhari, F.; Rokita, S. E. A walk along DNA using bipedal migration of a dynamic and covalent crosslinker. *Nat. Commun.* **2014**, *5*, 5591.

(29) Schnell, S.; Mendoza, C. Closed form solution for time-dependent enzyme kinetics. *J. Theor. Biol.* **1997**, *187*, 207–212.

(30) Segel, L. A.; Slemrod, M. The quasi-steady-state assumption: A case study in perturbation. *SIAM Review* **1989**, *31*, 446–477.

(31) Johnson, K. A.; Goody, R. S. The original Michaelis constant: Translation of the 1913 Michaelis–Menten paper. *Biochemistry* **2011**, *50*, 8264–8269.

(32) Bisswanger, H. Enzyme assays. *Perspect. Sci.* **2014**, *1*, 41–55.

(33) Goličnik, M. On the Lambert *W* function and its utility in biochemical kinetics. *Biochem. Eng. J.* **2012**, *63*, 116–123.

(34) Tian, L.; Yang, Y.; Wysocki, L. M.; Arnold, A. C.; Hu, A.; Ravichandran, B.; Sternson, S. M.; Looger, L. L.; Lavis, L. D. Selective esterase–ester pair for targeting small molecules with cellular specificity. *Proc. Natl. Acad. Sci. U. S. A.* **2012**, *109*, 4756–4761.

(35) Hetrick, K. J.; Aguilar Ramos, M. A.; Raines, R. T. Terbium(III) luminescence-based assay for esterase activity. *Anal. Chem.* **2019**, *91*, 8615–8621.

(36) Lan, L.; Ren, X.; Yang, J.; Liu, D.; Zhang, C. Detection techniques of carboxylesterase activity: An update review. *Bioorg. Chem.* **2020**, *94*, 103388.

(37) Zhang, C.; Xu, Y.; Zhong, Q.; Li, X.; Gao, P.; Feng, C.; Chu, Q.; Chen, Y.; Liu, D. In vitro evaluation of the inhibitory potential of pharmaceutical excipients on human carboxylesterase 1A and 2. *PLoS One* **2014**, *9*, e93819.